Icelandic
Meteorological Office

Veðurstofa
Íslands

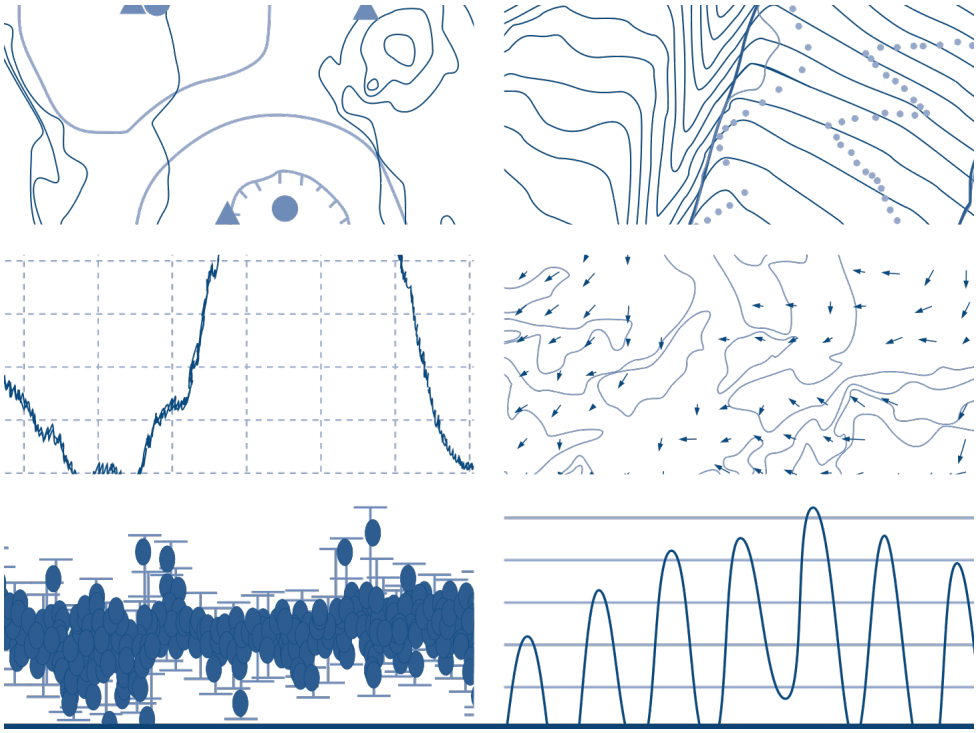

# The wind energy potential of Iceland

Nikolai Nawri
Guðrún Nína Petersen
Halldór Björnsson
Kristján Jónasson

**Report**

VÍ 2013-001

Icelandic
Meteorological Office

Veðurstofa Íslands

# The wind energy potential of Iceland

Nikolai Nawri, Icelandic Met Office
Guðrún Nína Petersen, Icelandic Met Office
Halldór Björnsson, Icelandic Met Office
Kristján Jónasson, University of Iceland

**Report**

Veðurstofa Íslands
Bústaðavegur 7–9
150 Reykjavík

+354 522 60 00
vedur@vedur.is

VÍ 2013-001
ISSN 1670-8261

**Keypage**

Veðurstofa Íslands

| Report no.: | Date.: | ISSN: | Public ☒ Restricted ☐ |
|---|---|---|---|
| VÍ 2013-001 | March 2013 | 1670-8261 | Provision: |

| Report title / including subtitle | No. of copies: 20 |
|---|---|
| The wind energy potential of Iceland | Pages: 72 |
| | Managing director: Jórunn Harðardóttir |
| **Author(s):** Nikolai Nawri, Guðrún Nína Petersen, Halldór Björnsson, Kristján Jónasson | Project manager: Halldór Björnsson |
| | Project number: 5813-0-0004 |
| Project phase: | Case number: 2012-333 |

**Report contracted for:**
IceWind Project

**Prepared in cooperation with:**


**Summary:**
In this study, Weather Research and Forecasting (WRF) Model simulations, performed by Reiknistofa í veðurfræði, are used to determine the wind energy potential of Iceland. This allows regional comparisons and an identification of suitable wind farm sites. Based on these results, 14 test sites were selected for more detailed analyses using the Wind Atlas Analysis and Application Program (WAsP) developed by Risø National Laboratory. The wind energy potential of Iceland is within the highest class as defined in the European Wind Atlas. Also, even modest wind farms are capable of producing as much energy over the course of the year as the smallest currently operational hydro- and geothermal power plants in Iceland.



**Keywords:**
Wind energy potential
Wind atlas
Weather Research and Forecasting Model
Wind Atlas Analysis and Application Program
Iceland


**Managing director's signature:**

**Project manager's signature:**

**Reviewed by:**

# Contents

# List of Figures

# 1 Introduction

Wind power is an important source of low-impact renewable energy, especially if used in combination with glacial river hydro-electric power, as would be the case in Iceland. In winter the highest average wind speeds coincide with reduced stream flow and sunshine hours. Unlike solar energy, wind power can therefore be used throughout the year, and reduces the need for water regulation.

As described in more detail in this report, wind power varies with the cube of wind speed, and is therefore strongly dependent on the intensity of the wind. Amongst several criteria, such as icing, accessibility, and environmental concerns, the local wind climate must crucially be taken into account when choosing locations for the installation of wind turbines. However, an accurate assessment of the climatological wind conditions at a given location is complicated by the fact that the motion of the atmosphere is highly variable in space and time. Several geographical effects and atmospheric phenomena are responsible for generating this variability, and to different degrees contribute to the wind climate of a given region. The goal of this study is to develop a wind atlas for Iceland, to provide an overview across the entire island of those wind statistics relevant to wind energy assessments. This allows regional comparisons of wind energy potential, and an identification of suitable wind farm sites.

The research was conducted by the Icelandic Meteorological Office (Veðurstofa Íslands; IMO) and the University of Iceland (Háskóli Íslands; UI) in the context of Work Package 2 of the project "Improved Forecast of Wind, Waves and Icing" (IceWind), funded primarily by the Nordic Top-level Research Initiative (Toppforskningsinitiativet; TFI), including national and private organisations. This report is the fifth in a series of IMO reports produced for IceWind, the others being Nawri et al. (2012d,a,b,c).

The present study consists of three parts: 1) a statistical correction of the numerical model input data using surface weather station measurements; 2) an estimation of statistical parameters describing local wind speed distributions over Iceland, based on the corrected numerical model data; 3) more detailed analyses of the wind climates at 14 test sites, using a parameterised boundary-layer model.

The methodology of the statistical correction of model data employed in Part 1 is described in detail in the earlier reports. In short, the original model wind speeds are transformed linearly such that at station locations, separately for individual months and for different categories of the geostrophic wind speed and direction, averages and standard deviations are identical to the measured values. For Part 2, data files describing the local wind statistics on the regular model grid covering Iceland are made available through an online wind atlas (follow the link from http://www.vedur.is/vedur/vedurfar/vindorka/). The files contain estimates of Weibull parameters at each grid point, for twelve wind direction sectors, five heights (10, 25, 50, 100, 200 m above ground level (mAGL)), and five surface roughness lengths (0, 3, 10, 40 and 150 cm). The wind statistics are calculated for locally flat terrain. For Part 3, the locations of the 14 test sites (see Figure 1) were chosen based on either particularly high wind energy potential at a given elevation, or due to their proximity to existing power plants, making it easier to integrate locally generated wind energy into the electricity grid.

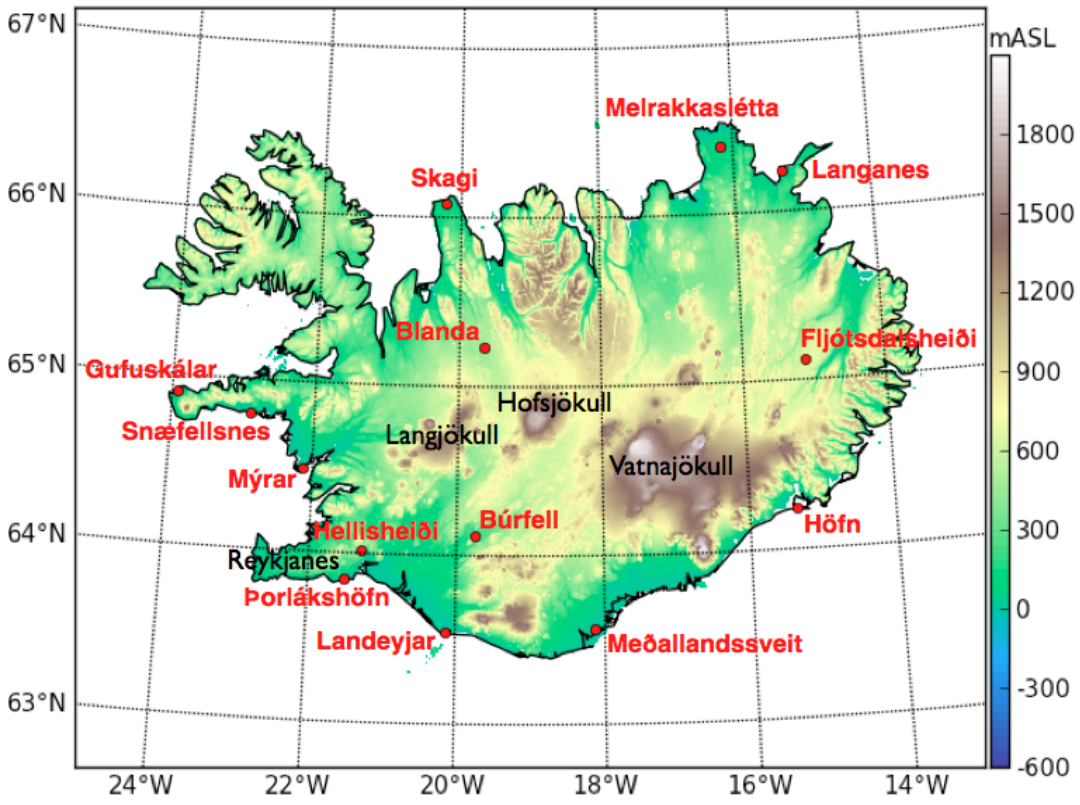


*Figure 1. Topographic map of Iceland, with the locations of test sites, for which detailed analyses were performed.*

This report is organised as follows. Section 2 gives a short introduction to the forces that govern low level winds over Iceland and their variability with space and time. Section 3.1 describes the numerical model data on which the wind energy assessments are based, as well as the parameterised boundary-layer model used to perform more detailed analyses. Section 3.2 describes the approximation of local wind climates by the Weibull distribution. Also discussed are critical wind speeds for wind turbines. The effects of air density on wind energy production are discussed in Section 3.3. Section 4 discusses the evaluation and correction of the numerical model data based on station measurements. Section 5.1 provides an overview of the wind statistics across Iceland, such as annual and seasonal average wind speeds at 50 and 100 mAGL, as well as Weibull parameters. Section 5.2 discusses wind power density over Iceland, in comparison with the recent Norwegian reanalysis project (NORA10). More detailed analyses for the 14 test sites are discussed in Section 6 and the appendices. Finally, Section 7 contains the conclusions.

# 2 Spatial and temporal variability of low-level wind

Atmospheric motion near the ground, especially over complex terrain, is highly variable, both in space and time. Therefore, several geographical and atmospheric forcing mechanisms need to be taken into account for a reliable assessment of any regional wind climate.

The spatial variability of wind, over a relatively small area such as Iceland, is primarily due to changes in surface characteristics. Of these, changes in terrain elevation are among the most important. An increase in elevation of a few hundred metres or more increases the effect of large-scale forcing by reducing the land area at or above that level, and thereby reducing the effect of surface drag on momentum transfer from the overlying flow. However, even with small elevation changes of only a few tens of metres, terrain can have a significant impact by causing boundary-layer winds to deflect horizontally and vertically. Slopes create barriers which, up to a certain height, horizontally deflect the motion of air. This effect tends to be strongest in winter, when the atmosphere is most stably stratified. Above that level, vertical displacement of air occurs as well, resulting in dynamically induced speed-up over crests and mountain tops, whereas sheltering and a reduction in wind speed tends to occur in valleys. Changes in surface roughness, such as between forests (high) and lakes (low), also have a strong impact on low-level wind by changing the magnitude of viscous dissipation. The resulting changes in wind speed, which are not related to the large-scale pressure field, create a temporary imbalance in the flow. Under those conditions, significant changes in wind direction may occur even over flat terrain. Changes in the thermal properties of the earth's surface create horizontal inhomogeneity in surface heating of the atmosphere. The specific heat capacity, a measure of the energy required to change the temperature of a substance by a given amount, differs greatly between common natural surfaces. For example, the thermal inertia of liquid water is about twice as high as that of ice or snow; which in turn may be more than twice as high as that of sand and soil, depending on the water content. With the same energy input from the sun, significant small-scale temperature gradients can quickly develop, causing horizontal differences in the stability of the boundary-layer stratification, and through that, differences in the rate of turbulent momentum transfer, as well as differences in the intensity of convection. Over the ocean surrounding Iceland, independent of thermal properties, differences in water temperatures are due to warm currents in the south and west, and cold currents in the north and east. Additionally, the variable presence of sea ice, primarily northwest of Iceland during the winter months, introduces variations in surface heating of the atmosphere, as well as in the aerodynamic roughness of the ocean surface. Given these surface-related effects, vertical changes with increasing height above ground are due to the reduced impact of the underlying surface, and the adjustment of the wind to the free atmospheric conditions above the boundary layer.

Temporal variability of the atmosphere is linked to processes with a wide range of dominant timescales. Seasonal and diurnal cycles are directly related to the planet's motion within the solar system. The seasonal cycle in wind speed at mid- and high-latitudes is due to the intensification of the thermal gradient across the polar front of the winter hemisphere, whereas the diurnal cycle is related to the differential heating and cooling between surfaces with significantly different thermal properties, such as water and land, or between flat and inclined land surfaces. The result of diurnal process may be land – sea (or lake) breezes, and various types of up- or downslope winds over complex terrain. On sunny and otherwise calm days, wind speeds associated with sea breezes can reach up to 10 m $s^{-1}$ at various locations around the Icelandic coast (Einarsson, 1976). Land

breezes occur less frequently and are generally weaker. On intermediate time-scales of several days, temporal variability is primarily due to the evolution and passage of cyclonic storm systems. Cyclones, being instabilities of the polar front, indirectly derive their thermal and rotational energy from the planet's motion and orientation relative to the sun. Iceland is situated just north of a region with frequent and intense cyclonic storms, referred to in climatic terms as the Icelandic Low (Einarsson, 1984). The strongest winds over Iceland are predominantly associated with these large-scale storm systems, whereby in many parts of the island low-level wind speeds in excess of 20 m $s^{-1}$ in winter are not uncommon. Small-scale convective storm systems are less important in Iceland than at mid- and low-latitudes. Unlike over mid-latitudes continental regions, thunderstorms in Iceland are most common during the winter months (Dec – Feb) (Einarsson, 1976). They typically form when cold air masses, originating in Canada, move northeastwards over the warm water south of Iceland. These air masses, made potentially unstable by surface heating, are lifted over the mountains along the south coast. This can create convective storms, which in addition to strong gusts, may be associated with snow showers, hail, ice pellets, and lightning. Afternoon thunderstorms resulting from convection through surface heating over land are most frequent in July. Both types of convective storms are most common in southern and southwestern Iceland, and are reported on fewer than 2 days per year in any given region. With a weakening of the large-scale atmospheric circulation in summer, temperature-driven downslope, or katabatic, winds from the glaciers may become important. They can develop either during the day or at night, and are most intense on the steep south-facing slopes of Vatnajökull, where wind speeds on otherwise calm days can reach up to 6 m $s^{-1}$ (Björnsson et al., 2005).

In this study, as described below, the natural variability of the low-level wind field over Iceland is estimated through the use of two models, in combination with surface station measurements.

# 3 Methodology

This section describes the numerical input data for this study and the associated wind atlas, and the parameterised boundary-layer model and statistical analyses used to process the data. It also addresses the spatial and temporal variability of air density, and its effects on wind energy potential.

## 3.1 Wind modelling

The Icelandic network of weather stations is sufficient to provide a good overview of the surface wind conditions over the low-lying parts of the island. However, it leaves several regions unobserved, which may be suitable for the installation of wind turbines. It is therefore important to augment the observational data with results from numerical simulations, which provide regularly gridded fields of atmospheric variables at different heights above the ground.

The simulated data used for this study was obtained by Reiknistofu í veðurfræði in the context of "Reikningar á veðri" (RÁV), which is a joint project of several Icelandic research institutions. The RÁV model runs were produced with the mesoscale Weather Research and Forecasting (WRF) Model (Version 3.1.1; see Skamarock et al. (2008) for details). Simulations were performed in three nested horizontal domains, all approximately centred around Iceland: the outer domain with $43\times42$ grid points spaced at 27 km ($1134\times1107$ km), the intermediate domain with $95\times90$ grid points spaced at 9 km, and the inner domain with $196\times148$ grid points spaced at 3 km. The northwest corner of the outer domain covers a part of the southeast coastal region of Greenland. Otherwise, the only landmass included in the model domain is Iceland. For a detailed description of the simulations refer to Rögnvaldsson et al. (2007, 2011). The data used here is that of the inner domain. The initial and boundary conditions for the WRF model simulations were determined by 6-hourly operational analyses obtained from the European Centre for Medium-Range Weather Forecasts (ECMWF), valid at 00, 06, 12, and 18 UTC (which is local time in Iceland throughout the year) (Courtier, 1997; Andersson and Thépaut, 2008). After initialisation of the model run, this data is only applied at the outer boundaries. WRF model output fields were produced every 3 hours. Data is available for the period 1 Sep 1994 – 2 Nov 2009, but was reduced for this study to the period 1995 – 2008, including only whole years.

WRF model results were compared with station measurements at 10 m above ground level (mAGL), as well as with the Norwegian Reanalysis at 10 km spatial resolution (NORA10) (Reistad et al., 2011). NORA10 was derived by dynamical downscaling of the ECMWF reanalyses ERA-40 (Uppala et al., 2005) until 2002, and the ECMWF operational analyses afterwards, using the High Resolution Limited Area Model (HIRLAM) version 6.4.2 (Undén et al., 2002). NORA10 data is available for the entire RÁV period. However, as explained in Nawri et al. (2012b), for the comparison of WRF model results with station data, the period was reduced to the 4 years from 1 Nov 2005 to 31 Oct 2009. Both measured and modelled wind speeds only take into account the horizontal motion of the atmosphere, ignoring any vertical displacements. With wind turbines rotating in a vertical plane, this is the component of the three-dimensional flow relevant for wind energy assessments.

The simulated data provide a good overview for the whole island. However, with a grid-point spacing of 3 km, the WRF model results are too coarse for a precise assessment of the wind conditions within a limited region, such as an individual valley or ridge, that may be appropriate for wind energy production. For this, a spatial resolution of 100 m or higher is required. It would be too computationally expensive to reduce the grid-spacing of a full prognostic numerical model to that scale. Therefore, the Wind Atlas Analysis and Application Program (WAsP) was developed by the Wind Energy and Atmospheric Physics Department at Risø National Laboratory (now the Department of Wind Energy at the Technical University of Denmark), which employs parameterised boundary-layer modelling within a geographically consistent or contained region (Troen and Petersen, 1989). The input data can be either measured or simulated time-series at one location somewhere within the domain, ideally near the centre.

In the first step of WAsP, the input data is "generalised" through a process of reverse (or "upward") modelling. This step is intended to remove effects of local terrain features and obstacles from measured wind data, or of model orography and surface type from simulated winds. The result is a regional wind climate for the entire domain, which is an approximation of the wind above the boundary layer. The main parameterisations of boundary-layer wind conditions employed in WAsP are a logarithmic profile for the vertical dependence of wind speed, with a small heat flux modification, and taking into account the response of vertical wind shear to changes in surface roughness; a geostrophic drag law, balancing pressure gradients against frictional forces; a simplified description of orographic effects, assuming potential flow, with a viscous modification in a shallow surface layer; as well as a description of sheltering for objects with sizes comparable to the height above ground of the input data, and for distances from the input data comparable to the object size.

The wind conditions at any point within the domain, at the same or different heights above the ground, are derived from the generalised wind climate through direct (or "downward") modelling, by taking into account the specific geographical conditions at the target location. The accuracy of the projected wind conditions depends on the geographical homogeneity within the domain. Due to the simplified description of boundary-layer dynamics, there are limitations. For example, measurements in one valley cannot be assumed to be correlated well with the wind conditions in a neighbouring valley. Usually, therefore, generalised wind climates do not extend beyond orographic barriers. The detailed WAsP results for 14 test sites within Iceland are discussed in Section 6.

In an alternative approach to downward modelling, the generalised wind climate is projected to standard surface roughness classes and standard height levels above ground. This method is less computationally expensive, but does not take into account variations in surface characteristics or terrain elevation in the vicinity of a potential target location. The results from this approach are presented in tabulated form, which is described in the following subsection, and are made available through an online wind atlas (follow the link from the IMO webpages on the wind energy potential of Iceland at http://www.vedur.is/vedur/vedurfar/vindorka/).

## 3.2 Weibull statistics

Whether considering specific or generalised wind climates, the basis for the statistical analyses presented here is the determination of local distributions of wind speed for separate wind direction sectors.

Within each sector, WAsP calculates averages and other relevant statistical properties from an analytical approximation of the wind speed distribution, rather than from the data directly. This reduces the amount of data that needs to be disseminated to a few parameters, that describe each wind speed distribution. Of the various probability density functions for boundary-layer wind speeds, $s$, the 2-parameter Weibull distribution,

$$f(s;A,k) = \frac{k}{A}\left(\frac{s}{A}\right)^{k-1} \exp\left[-\left(\frac{s}{A}\right)^{k}\right] , \tag{1}$$

is the one most commonly employed for wind energy studies (Morgan et al., 2011). It is determined by the scale parameter $A \geq 0$ in units of wind speed, and the non-dimensional shape parameter $k > 1$. By its definition, the Weibull distribution is only applicable to non-zero wind speeds. Calm conditions are therefore excluded from the analysis. There are different methods for determining the parameters $A$ and $k$ from a given measured distribution (e.g., Seguro and Lambert, 2000). For wind energy assessments, the interest is primarily on high wind speeds. Therefore, following the method employed by Troen and Petersen (1989), the two Weibull parameters are calculated here by: 1) matching the average wind power density in the Weibull distribution to that of the measured or modelled distribution of wind speeds; and 2) requiring the occurrence of above average wind speeds in the Weibull distribution to be equal to that of the measured or modelled distribution.

A comparison between annual modelled wind speed distributions in the regions of Hellisheiði and Skagi (see Figure 1), and their respective Weibull fits is shown in Figure 2. By definition, the agreement is better for above- than below-average wind speeds. Discrepancies between measured and analytical distributions do not necessarily imply problems with the Weibull fit. Due to measurement errors and the possibility of undersampling, a smooth Weibull distribution may be more representative of the actual longterm statistics than a given sample of measured values. Taking into account the data from all surface weather stations on Iceland with at least 95% wind speed data availability at 10 mAGL, together with WRF model data interpolated to the same locations following the procedure described in Nawri et al. (2012b), the average difference between seasonal mean wind speed calculated from the Weibull fit and that calculated directly is 0.08 m s$^{-1}$ (0.04 m s$^{-1}$) in winter (summer) for station data, and -0.10 m s$^{-1}$ (-0.02 m s$^{-1}$) in winter (summer) for WRF model data. Overall, there is therefore a small positive bias of the Weibull fits compared with measurements, and a small negative bias compared with model data. Mean absolute differences are 0.10 m s$^{-1}$ (0.05 m s$^{-1}$) in winter (summer) for station data, and 0.15 m s$^{-1}$ (0.05 m s$^{-1}$) in winter (summer) for WRF model data. This amounts to 1 – 2% of the directly calculated averages.

Once the two Weibull parameters have been determined, the average of the (wind speed) distribution is given by

$$\mu = A\,\Gamma(1+1/k) , \tag{2}$$

with gamma function, $\Gamma$, defined as usual. Wind power density, a measure of the energy flux through an area perpendicular to the direction of motion, varies not only with the cube of wind

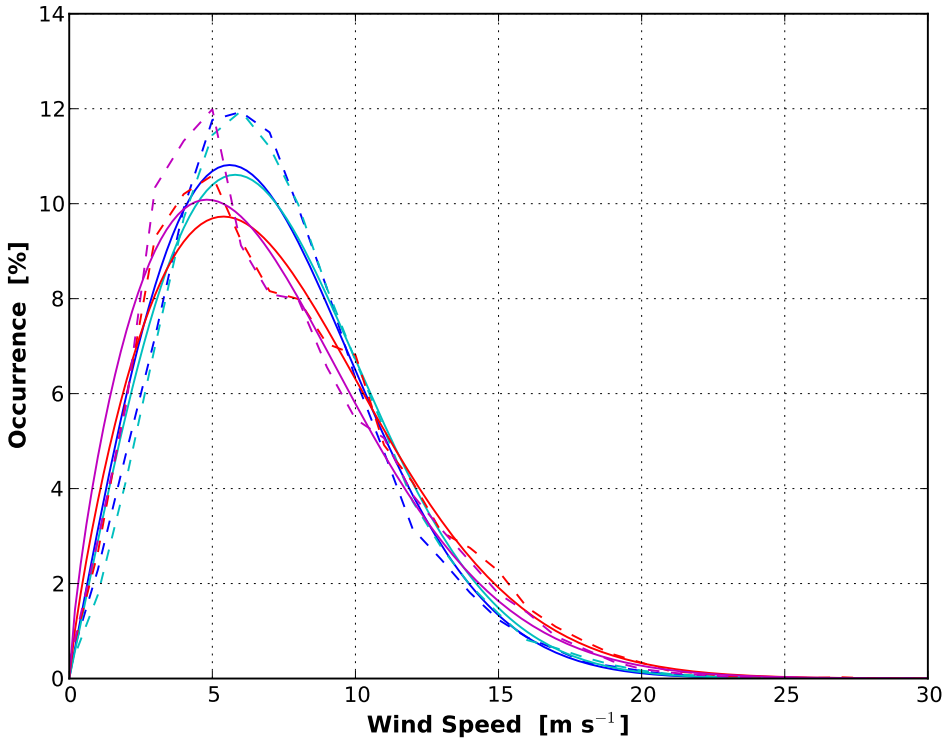


*Figure 2. Annual modelled distributions (dashed lines) and corresponding Weibull fits (solid lines) of wind speed at 50 mAGL, for two grid points on Hellisheiði (blue and cyan lines), and for two grid points on Skagi (red and magenta lines).*

speed, but also with air density. To simplify wind energy assessments, and to allow for the use of Weibull statistics, it is commonly assumed that air density, $\rho$, is not correlated in time with wind speed, at least on a seasonal basis (Hennessey, 1977). Average wind power density is then proportional to the mean cube of wind speed,

$$E = \frac{1}{2}\bar{\rho}A^3\Gamma(1+3/k) \ , \tag{3}$$

where $\bar{\rho}$ is average air density. Wind power density only depends on atmospheric variables, and is therefore most appropriate for turbine-independent evaluations of wind energy potential, such as for wind atlases. To be able to determine the actual power or energy, which can be extracted from the atmosphere, specific information about a chosen wind turbine is required. The available power not only depends on the area swept by the rotor blades, but also on aerodynamic efficiency. Since the wind is not entirely stopped by the turbine, only a certain proportion of the incoming power can be extracted, which depends on the size and shape of the blades, as well as on wind speed. This efficiency is expressed by a turbine-specific power coefficient, which has a theoretical maximum of 0.593 (Betz, 1966). Practically, however, the power coefficient of modern wind turbines typically has highest values of 0.40 – 0.50, for wind speeds between 5 and 10 m s$^{-1}$. The effective power curve, i.e., the actual power produced by a given turbine as a function of wind speed, needs to be determined empirically, and is made available by the manufacturers. For a particular turbine, the average available wind power can then be calculated by integrating over its power curve, multiplied by the probability density function for wind speed, as determined by the Weibull distribution.

*Table 1. Technical specifications of two wind turbines, for which explicit power calculations were performed. The information is provided by the manufacturers.*

| | Enercon E44 | Vestas V80 |
|---|---|---|
| Rotor diameter [m] | 44 | 80 |
| Hub height [m] | 55 | 67 |
| Rated power [kW] | 900 | 2000 |
| Cut-in speed [m $s^{-1}$] | 3 | 4 |
| Rated speed [m $s^{-1}$] | 15 | 16 |
| Cut-out speed [m $s^{-1}$] | 28 | 25 |

For any given turbine, there are three important characteristic wind speeds. The cut-in speed is the lowest wind speed at which a turbine can generate usable power. The rated speed is the lowest wind speed at which a turbine operates at its rated capacity, i.e., at maximum power output. The cut-out speed is the lowest wind speed at which there is the potential of damage to the turbine, if operation continues. At wind speeds between the rated and cut-out speed, power production is limited by rotating the blades around their own axes, to reduce aerodynamic lift and drag, while maintaining the maximum power output. The relative angle of attack by the wind on the blades can either be increased (as in stalling) or decreased (as in furling). At the cut-out speed, mechanical breaks may need to be employed in addition to furling, to bring the rotor to a standstill. Consequently, no energy is produced at this and higher wind speeds. Effectively, the available wind power does not increase with the square of blade length, since large turbines have higher cut-in speeds, and generally a lower aerodynamic efficiency. As specific examples for this study, in addition to power density, the actual power outputs for two common onshore wind turbines were calculated at 14 test sites (see Section 6). For these turbines, the rated power and characteristic wind speeds are listed in Table 1. The given hub heights are those used for the calculations here. Other tower heights are possible and would change the results. The Enercon E44 was chosen since, at the time of publication of this report, the Icelandic power company Landsvirkjun has installed two of these turbines for testing near the Búrfell hydroelectric power station (see their description at http://www.landsvirkjun.com/ResearchDevelopment/Research/WindPower/). The Vestas V80 was chosen as an example from another major manufacturer, and to determine the benefit in increased power for a significant increase in rotor diameter, together with a slight increase in hub height.

Based on the Weibull distribution, the probability of wind speed exceeding any given value, $s$, is given by

$$f_+(s;A,k) = \exp\left[-\left(\frac{s}{A}\right)^k\right] . \tag{4}$$

The percentage of time, during which at a given location wind speed exceeds the cut-out value, $s_{\max}$, is therefore given by $f_+(s_{\max};A,k)$. The percentage of time with wind speeds at or below the cut-in speed, $s_{\min}$, is given by $1 - f_+(s_{\min};A,k)$.

For the online wind atlas (follow the link from http://www.vedur.is/vedur/vedurfar/vindorka/), Weibull statistics are determined for generalised wind climates. At each WRF model grid point, Weibull parameters for five surface roughness classes (SRCs), five height levels (HLs) above ground, and twelve 30-degree wind direction sectors (WDSs) are calculated and tabulated in text

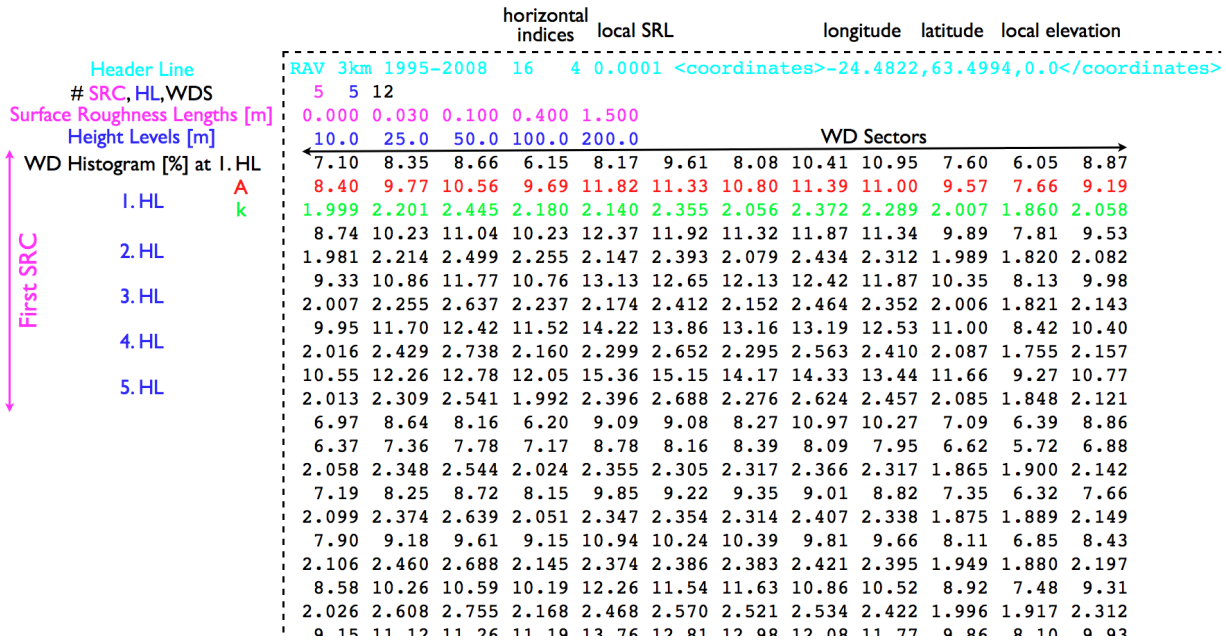


*Figure 3. Annotated example of a wind atlas (.lib) text file, following the standard developed by Risø National Laboratory.*

files with .lib extension, and with a size of about 4 KB each. The structure of these wind atlas files follows the standard developed by Risø National Laboratory (Troen and Petersen, 1989). An annotated example is shown in Figure 3. The header line contains information about the model run, the index numbers of the particular grid point, the local surface roughness length (SRL), as well as a triplet of numbers with longitude in degrees east, latitude in degrees north, and height above mean sea level in metres. The second line gives the number of surface roughness classes, height levels, and wind direction sectors, which may differ from the standard numbers used here. The third line gives the value of surface roughness length in metres for each of the roughness classes. The fourth line gives the height levels in metres above ground. The remaining part of the data file has twelve columns, one for each of the 30-degree wind direction sectors. The first sector is centred at zero degrees (north), and wind direction is defined to increase clockwise. In the vertical, the main part of the data is broken down into groups of rows for each of the surface roughness classes. The first row of each group gives the wind direction histogram. The remaining rows give the $A$ and $k$ Weibull parameter values for each of the height levels.

## 3.3 Density effects

As mentioned in the previous subsection, wind power density depends linearly on air density which, for simplicity, is assumed to be uncorrelated in time with wind speed. The standard density value used for wind energy assessments, such as in WAsP, is $\rho_0 = 1.225$ kg m$^{-3}$, which corresponds to dry air with a temperature of 15°C and a pressure of 1013.25 hPa. In the case of Iceland, the climate deviates significantly from these standard atmospheric conditions. Additionally, terrain elevation varies considerably across the island. Therefore, seasonal and annual differences in air density from the standard value, as well as spatial variability, need to be taken into account.

Approximate air density can be calculated by assuming the validity of the ideal gas law, hydrostatic balance, a piecewise linear vertical gradient of air temperature, and neglecting the effects of water vapour. Pressure, $p$, as a function of height can then be derived through vertical integration of the hydrostatic balance equation, and is given by

$$p(h(x,y),z) = p_0 \exp\left(-\frac{g}{R}\int_0^{h(x,y)+z} \frac{d\xi}{T(\xi)}\right) , \tag{5}$$

where $p_0$ is pressure at mean sea level, $T$ is absolute air temperature (in degrees Kelvin), $h$ is local terrain elevation above mean sea level (as a function of the horizontal coordinates), $z$ is height above ground, $g = 9.81$ m s$^{-2}$ is the gravitational constant, and $R = 287$ J K$^{-1}$ kg$^{-1}$ is the specific gas constant of dry air.

Nawri et al. (2012a) showed that seasonal averages of surface air temperature over Iceland decrease linearly with terrain elevation above mean sea level. Additionally, the vertical dependence of seasonally averaged temperature within the boundary layer atmosphere is well approximated by a linear profile. Temperature as a function of height, $\xi$, above mean sea level can therefore be written as

$$T(\xi) = \begin{cases} T_0 + L_T\xi & \text{for } 0 \le \xi \le h \\ T_0 + L_T h + L(\xi - h) & \text{for } h \le \xi \le h+z\,, \end{cases} \tag{6}$$

where $T_0$ is air temperature at mean sea level, $L_T$ is the constant terrain-following temperature lapse rate, and $L$ is the constant atmospheric temperature lapse rate. The integral in (5) can then be explicitly evaluated, giving

$$p(h(x,y),z) = p_0 \left(\frac{T_0}{T_0 + L_T h}\right)^{\frac{g}{L_T R}} \left(\frac{T_0 + L_T h}{T_0 + L_T h + Lz}\right)^{\frac{g}{LR}} . \tag{7}$$

The values of all atmospheric constants are given in Table 2. Based on the ideal gas law, air density is then given by

$$\rho(h(x,y),z) = \frac{p(h(x,y),z)}{RT(h(x,y)+z)} . \tag{8}$$

The results are shown in Figure 4. At a given location, seasonal changes are small, justifying the assumption of a constant air density for the calculation of average power density. For the coastal region of Iceland, the differences between winter and summer are around 2%, and smaller at higher elevations. However, given the large range in terrain elevation, spatial air density differences are around 25% between coastal regions and the highest points over the glaciers, and around 10%

*Table 2. Annual, winter (DJF), and summer (JJA) average values of mean sea level air pressure, $p_0$ (Hanna et al., 2004), mean sea level air temperature, $T_0$, terrain-following temperature lapse rate, $L_T$, and atmospheric temperature lapse rate, L (Nawri et al., 2012a).*

| | Winter | Annual | Summer |
|---|---|---|---|
| $p_0$ [hPa] | 1000 | 1006 | 1012 |
| $T_0$ [°C] | 1 | 5 | 9 |
| $L_T$ [K km$^{-1}$] | 7.1 | 6.3 | 5.1 |
| $L$ [K km$^{-1}$] | 2.6 | 5.7 | 7.9 |

within that part of the island with terrain up to 1000 m above mean sea level (mASL). The exponential decrease in pressure with height outweighs the linear decrease in temperature, leading to an effective decrease in air density with height. The standard value of 1.225 kg m$^{-3}$ is therefore only appropriate at low elevations, where the effects of reduced temperature and pressure relative to standard atmospheric conditions approximately cancel each other. The correction of wind power values calculated with standard air density is done through multiplication with the ratio $\rho(h(x,y),z)/\rho_0$. The increase in wind power with terrain elevation or turbine height, due to an increase in wind speed, is then somewhat mitigated by a decrease with height in air density.

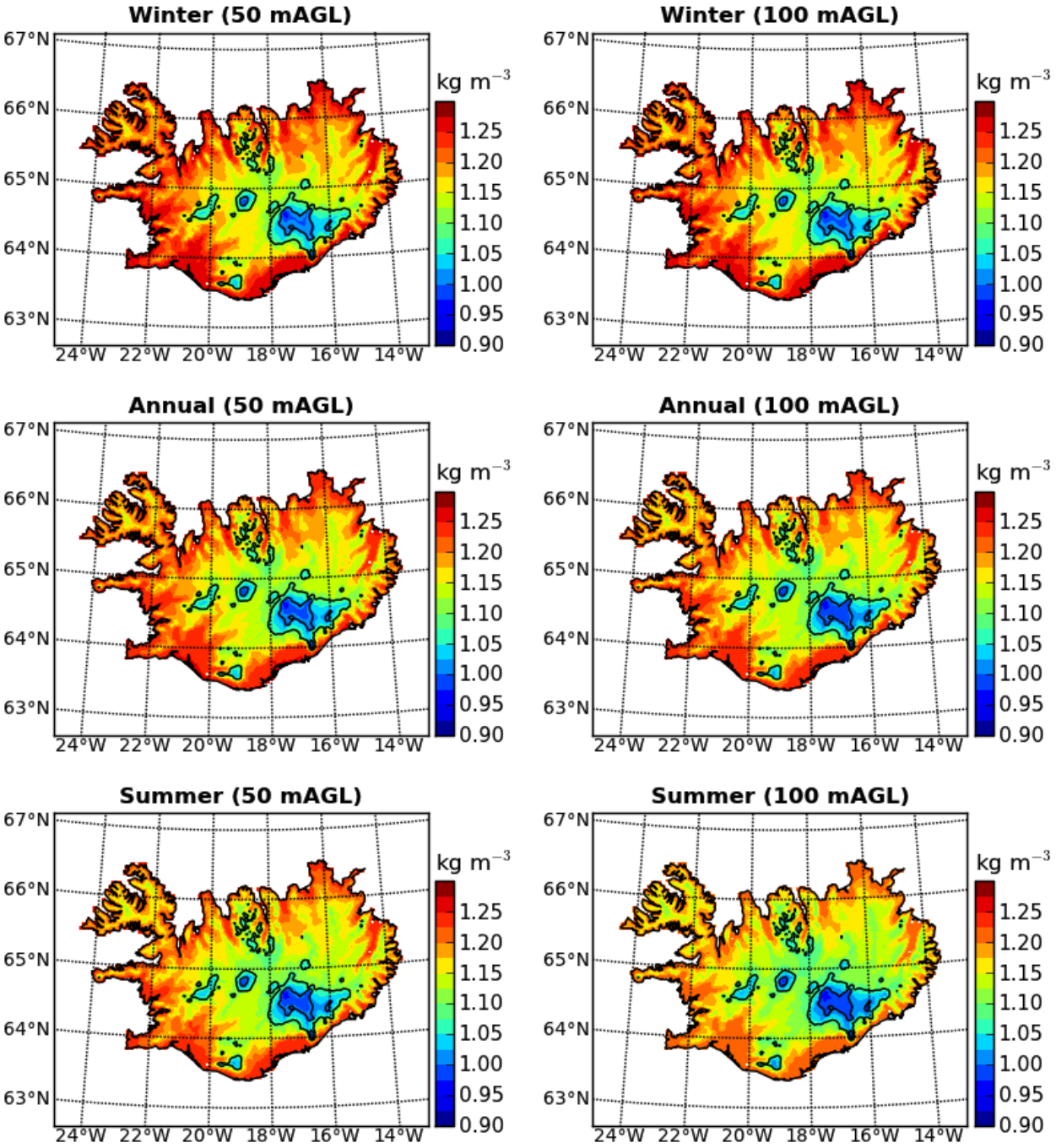


*Figure 4. Annual, winter (DJF), and summer (JJA) averages of air density at 50 (left column) and 100 mAGL (right column). Terrain elevation contour lines are drawn at 1000 and 1500 mASL.*

# 4 Evaluation of model results

As discussed in Nawri et al. (2012b), with the exception of the ocean and glaciers, surface roughness lengths in the RÁV WRF model setup are typically too large by up to an order of magnitude. This, combined with strong forcing at the model boundaries, results in a systematic spatial bias in low-level wind speed, with too strong winds in coastal regions, and too weak winds in the interior.

Figure 5 shows a comparison of average wind speed at 10 mAGL between the WRF model and station measurements. Model data is interpolated onto station locations as described in Nawri et al. (2012b). To reduce the effects from local obstacles or terrain features, which are not represented in the model simulations, at each time-step, station measurements are regionally averaged as described in Nawri et al. (2012c). In this comparison, measurements are taken into account from all surface weather stations on Iceland with at least 95% data availability for wind speed. In winter, differences along the coast range from 0 to 2.5 m $s^{-1}$. The negative bias in the interior is larger, with differences between model and station averages down to -4.5 m $s^{-1}$ at station locations, and possibly lower over the glaciers. During the rest of the year, the differences are smaller, as absolute wind speeds are reduced. Wintertime differences in average wind power density at 10 mAGL are between 0 and 750 W $m^{-2}$ along the coast, and down to -750 W $m^{-2}$ at station locations in the interior (not shown). These differences are of about half the magnitude of the absolute measured values.

Nawri et al. (2012b) and Nawri et al. (2012c) introduced a methodology for adjusting WRF model results based on surface measurements. This is done through a linear transformation of average model fields such that at station locations the model averages and standard deviations are identical to the measured values. It was shown that away from locations at which data is used for correction, the accuracy of model averages compared with independent station measurements is improved if averages and standard deviations are corrected simultaneously, rather than difference in averages alone. This amounts to minimising local normalised mean squared deviations, without changing the correlation between modelled and measured time-series. However, the linear transformation is only applicable to mean fields, with a sufficiently long averaging period, to allow for representative averages and standard deviations to be calculated. An application of the linear transformation to individual data points of local time-series can result in unphysical negative values.

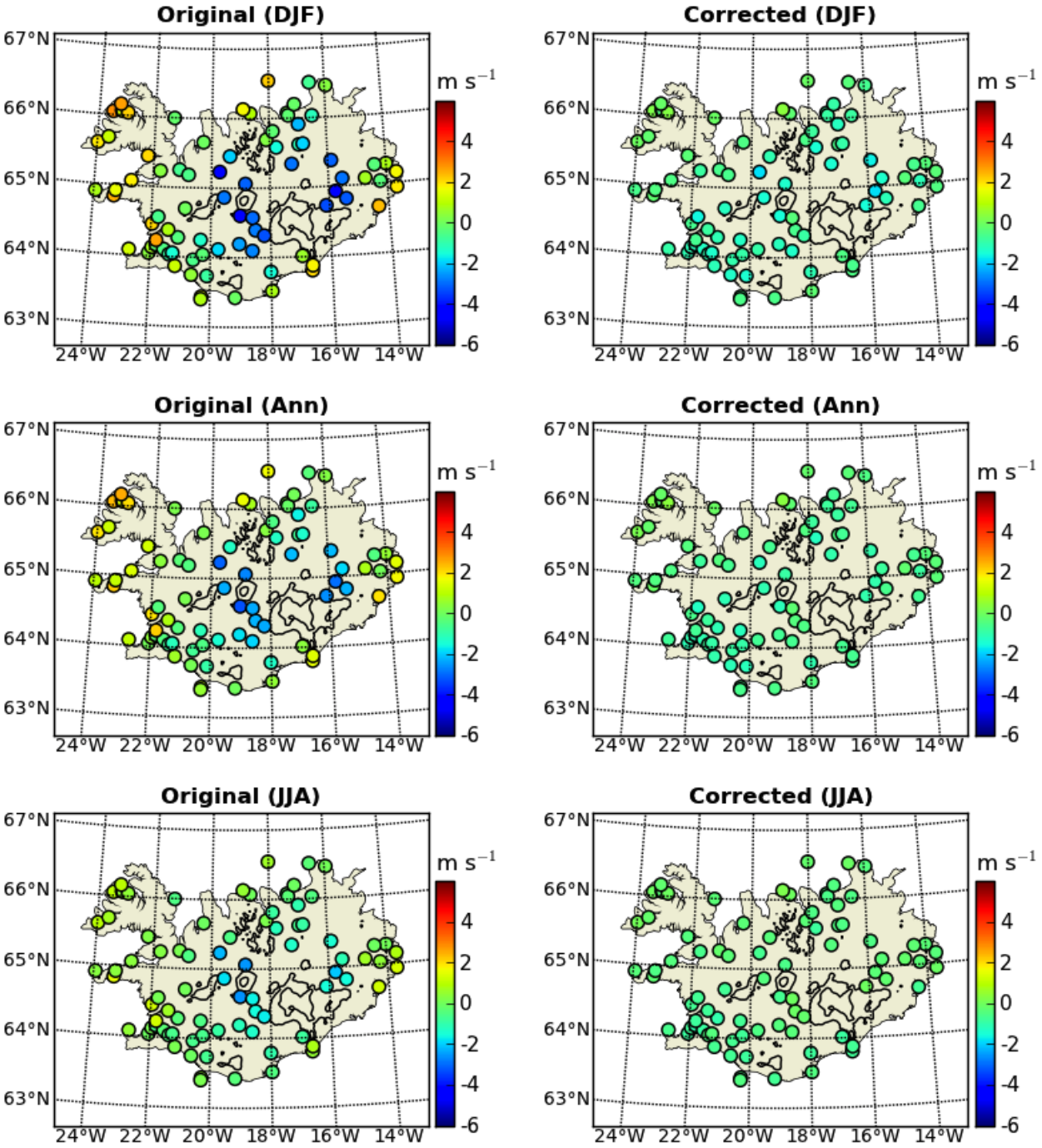


*Figure 5. Differences in annual, winter (DJF), and summer (JJA) averages of wind speed at 10 mAGL between either original or corrected WRF model data and station measurements. Terrain elevation contour lines are drawn at 1000 and 1500 mASL.*

As described in Section 3.2, the WAsP method is based on Weibull statistics of wind speed, working with the distribution of individual data points. The linear transformation of model data therefore needs to be restricted to rescaling, or the multiplication of time-series with a non-dimensional positive factor which, within each averaging period, only depends on the location in space. Negative wind speed values are then avoided, and the percentage of zero wind speeds (calms) is maintained. With one free parameter at each grid point, this only allows for the correction of a single statistical property.

One approach would be to rescale the model time-series, $S_m$, such that the slope of the regression line with the measured time-series, $S_o$, becomes equal to one. This is accomplished by multiplying the model time-series by the slope of the original regression line, $r_{om}\,\sigma_o/\sigma_m$, where $\sigma_o$ and $\sigma_m$ are the standard deviations of the measured and modelled time-series, respectively, and $r_{om}$ is the correlation coefficient between the two time-series. However, neither the rescaled model averages, $\overline{S_m} \rightarrow r_{om}\,\sigma_o/\sigma_m\,\overline{S_m}$, nor the rescaled model standard deviations, $\sigma_m \rightarrow r_{om}\,\sigma_o$, are necessarily closer to the measured values than those of the original model time-series.

For wind energy assessments, the main emphasis is on an accurate determination of average wind power density. As discussed in previous sections, average power density is approximately proportional to the mean cube of wind speed. Rescaling factors for modelled wind speed time-series, interpolated to station locations, are therefore defined here as $\sqrt[3]{\overline{S_o^3}/\overline{S_m^3}}$. Aside from this definition of the rescaling factor, and omitting the zero-speed offset, the same methodology for adjusting WRF model results is employed here, as that described in Nawri et al. (2012b) and Nawri et al. (2012c), including the same vertical projection of wind speed from elevated terrain to mean sea level, prior to the calculation of local rescaling factors, and the same horizontal interpolation of local rescaling factors at mean sea level onto the regular model grid. Although this correction is aimed at mean cubed wind speed, differences between modelled and measured mean wind speeds are significantly reduced as well (see again Figure 5). Since measurements are only available at 10 mAGL, the same rescaling factors are applied at 50 and 100 mAGL.

A comparison between average wind power density at 50 mAGL, based on the original and corrected WRF model data, is shown in Figure 6. Along the coast, with a good coverage of station data, differences between corrected and original values are of the same magnitude as the local differences between the measured and original model values at 10 mAGL. In winter, wind power density over the highest points of near-coastal terrain in the western part of the island is reduced from around 1250 to 750 W $m^{-2}$. In the interior, wind power density is effectively doubled by the correction. Over intermediate terrain, with elevations of 500 – 1000 mASL, wintertime wind power density is increased from around 500 to 1000 W $m^{-2}$, while over the highest terrain, the maximum wintertime wind power density is increased from around 1.5 to 3.0 kW $m^{-2}$ and above. However, these regions above 1000 mASL are glaciers, and are not relevant for wind energy production. The highest wintertime wind speeds at 50 mAGL over near-coastal terrain in the western part of the island are reduced from 11 – 12 m $s^{-1}$ to around 10 m $s^{-1}$, whereas over intermediate terrain in the interior, wind speed is increased from around 7 m $s^{-1}$ to around 10 m $s^{-1}$ (not shown).

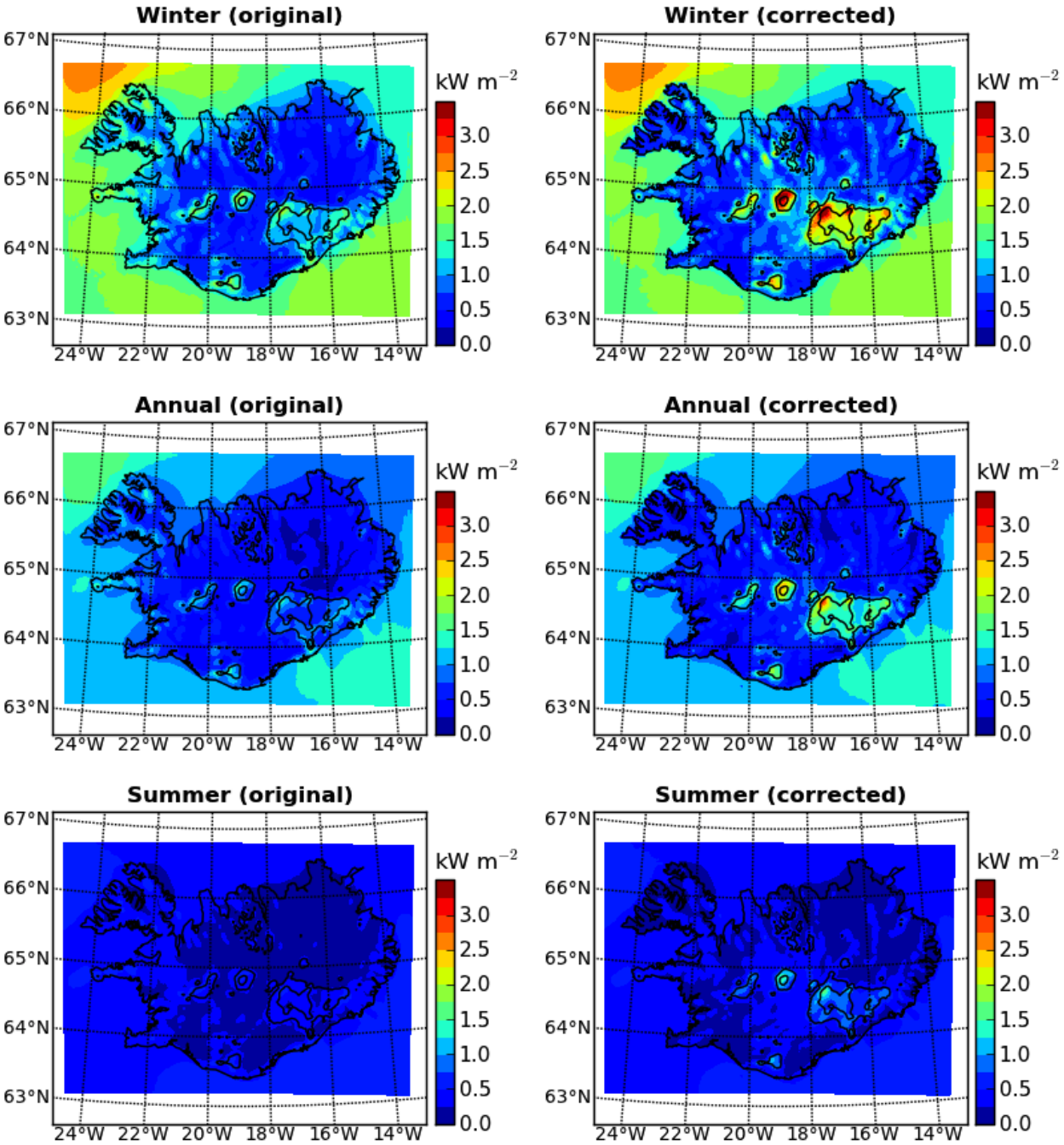


*Figure 6. Annual, winter (DJF), and summer (JJA) averages of wind power density at 50 mAGL, based on the original and corrected WRF model data. Terrain elevation contour lines are drawn at 1000 and 1500 mASL.*

# 5 Large-scale overview

This section provides an overview of the climatological wind conditions and wind power density across Iceland based on the corrected WRF model. For power density, a comparison is made with NORA10 data. High-resolution WAsP simulations for specific locations are discussed in the following section.

## 5.1 Climatological wind conditions

Annual, winter (DJF), and summer (JJA) averages of wind speeds at 50 and 100 mAGL are shown in Figure 7. The spatial variability of wind speed, especially for the corrected WRF model data, strongly depends on terrain elevation. Over intermediate terrain elevations of 500 - 1000 mASL, wind speeds at 50 mAGL vary over the course of the year between 6 – 8 m $s^{-1}$ in summer, and 10 – 11 m $s^{-1}$ in winter. The lowest wind speeds at some sheltered locations, e.g., in some valleys, range from 3 m $s^{-1}$ in summer to 5 m $s^{-1}$ in winter. At 100 mAGL, the seasonal range of wind speeds over intermediate terrain elevations is between 7 – 9 m $s^{-1}$ in summer, and 11 – 12 m $s^{-1}$ in winter.

Due to the rise in terrain, wind speed generally increases towards the interior of the island. However, away from the coast, and on higher terrain, accessibility is generally reduced, and other climate related problems such as icing may be more of an issue for wind power production. To be able to identify regions with relatively strong winds at a given elevation, average wind speed projected to 50 and 100 m above flat terrain at mean sea level is shown in Figure 8. For this projection, the same linear terrain gradients of wind speed were used as for the correction of model data (Nawri et al., 2012b,c). After removing elevation effects, the northwest slopes of Hofsjökull and Vatnajökull, as well as the mountains northeast of Blanda (see Figure 1), are the main interior regions characterised by terrain induced speed-up in excess of that in other regions at the same height above mean sea level. However, these regions are difficult to access. Relative to the elevated interior regions, wind speed along the coast increases by the projection to mean sea level. The highest wind speeds there are found over exposed peninsulas, most notably Skagi, Melrakkaslétta, Langanes, and Snæfellsnes, particularly around Gufuskálar. High winds are also found along the south coast of Reykjanes, along the southernmost part of the island (between Landeyjar and Meðallandssveit), as well as around Höfn. The lowest winds for a given terrain elevation are found north and northeast of Vatnajökull.

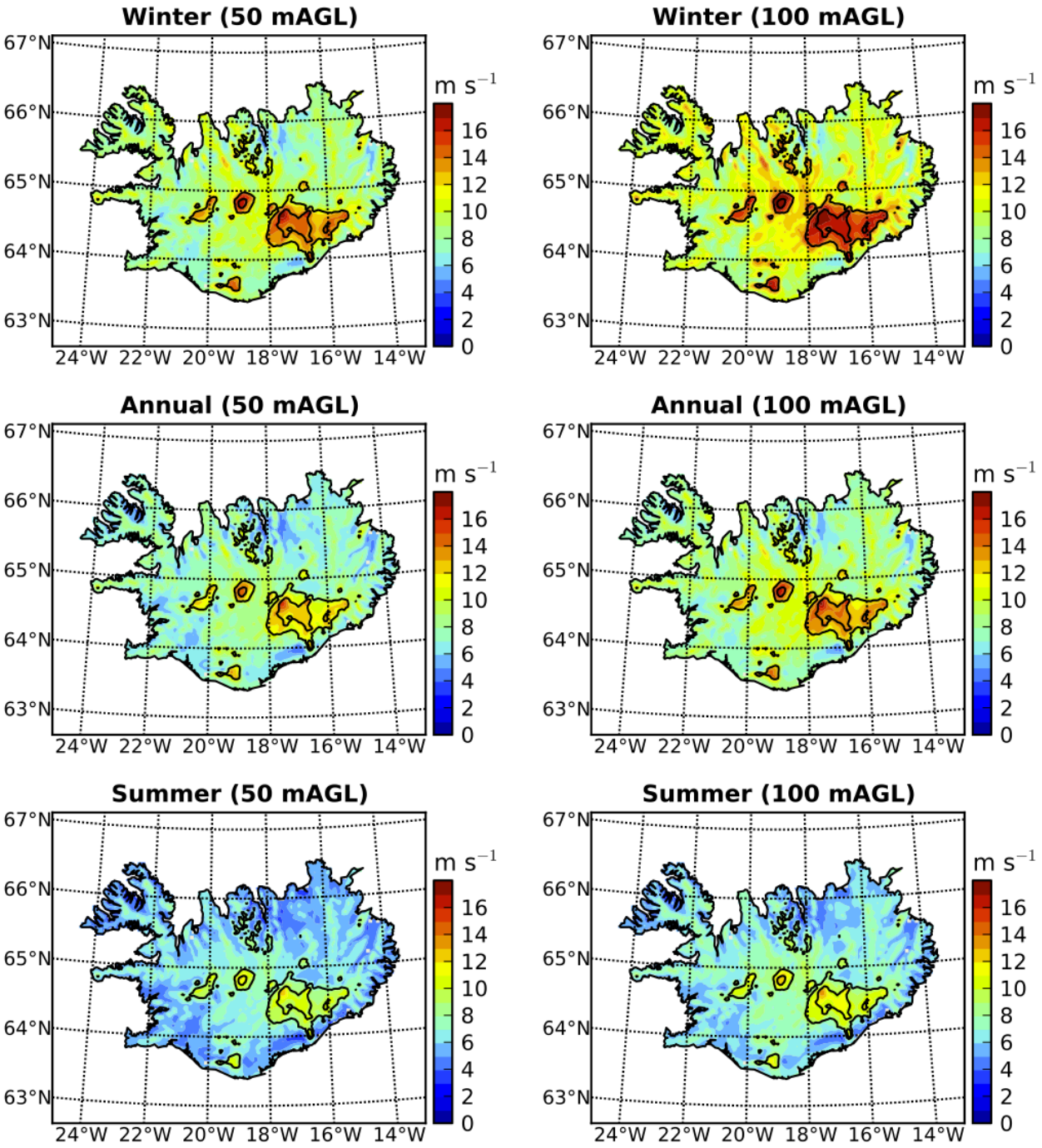


*Figure 7. Annual, winter (DJF), and summer (JJA) averages of wind speed at 50 and 100 m above ground level, based on corrected WRF model data. Terrain elevation contour lines are drawn at 1000 and 1500 mASL.*

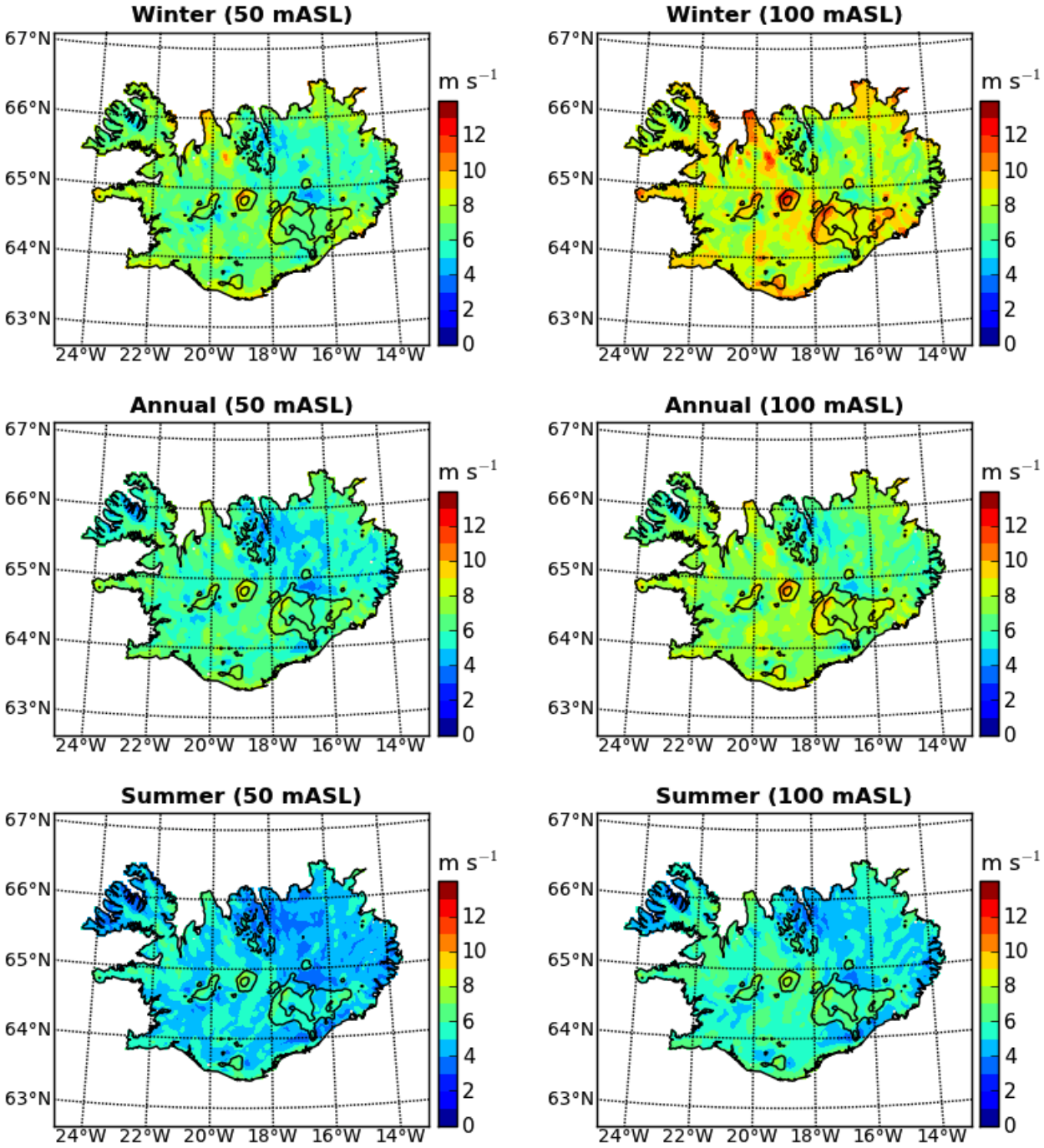


*Figure 8. Annual, winter (DJF), and summer (JJA) averages of wind speed projected to 50 and 100 m above mean sea level, based on corrected WRF model data. Terrain elevation contour lines are drawn at 1000 and 1500 mASL.*

Two locations with the same average wind speeds may have very different wind speed distributions. At one location, predominantly low wind speeds, on average, may be compensated by extreme winds during occasional severe storms, whereas at the other location wind speeds fluctuate more closely around the average. In the former case, the average available power may be considerably lower than in the latter case, due to the higher occurrence of wind speeds below the cut-in limit, and above the rated speed. Based on Weibull statistics, the shape of the wind speed distribution is described by parameter $k$. For $k = 1$ the distribution is exponential, with the highest probability at zero (calms), which is generally not representative of atmospheric conditions. For $k = 2$, wind speed has a Rayleigh distribution, with the most frequent (modal) wind speeds below the average wind speed. Over flat terrain, this is a common situation, implying that the two horizontal vector components are uncorrelated in time, and are each normally distributed, with zero mean and the same variance (Beckmann, 1964). For values of $k$ around 3.5, the Weibull distribution is close to a normal distribution, for which the modal and average wind speed coincide. As shown in Figure 9, the shape parameter across Iceland varies between 1.2 and 3.6, with the highest values, indicative of normal distributions, in winter and at high elevations.

Mean wind speed is related to the shape parameter, $k$, through the gamma function with argument $x = 1 + 1/k$ (see (2)). However, despite its spatial range of values, the effect of the shape parameter on mean wind speed is negligible, since $\Gamma(1 + 1/k)$ fluctuates by only a few percent across the island. For annual time-series at 50 mAGL, it varies between 0.886 and 0.925. On the other hand, mean cubed speed, or average power density, is significantly affected by variations in $k$. It is related to the shape parameter through the gamma function with argument $1 + 3/k$ (see (3)). For annual time-series at 50 mAGL, $\Gamma(1 + 3/k)$ varies between 0.976 and 2.737 across the island.

For real positive arguments, the gamma function has one (numerically determined) minimum at $x_0 = 1 + 3/k_0 = 1.46163$ (Wrench, 1968). For a given scale parameter, $A$, mean cubed speed attains its minimum value for $k = k_0 = 6.499$. Since across Iceland, the shape parameter is well below this value, average power density, for a given scale parameter, invariably decreases with increasing $k$. However, the percentage of wind speeds within the useable range between cut-in and cut-out speed increases with the shape parameter. The percentage of below cut-in speeds (see (4)) decreases with increasing scale parameter, and also decreases with increasing shape parameter, if the scale parameter is greater than the cut-in speed. Across Iceland, with minimum values of $A$ around 4 m s$^{-1}$ (not shown), this is the case. The percentage of above cut-out speeds increases with the scale parameter, but decreases with the shape parameter, since with a maximum value of around 18 m s$^{-1}$, $A$ is significantly below the cut-out speed. Although an increase in the shape parameter, with constant scale parameter, invariably reduces average power density, it may contribute to an increase in average available power. This ambiguity in the relationship between the averages of wind speed, power density, and available power needs to be taken into account when evaluating the wind energy potential of a given location. As discussed further in Section 6, an example of this is given by a comparison between the wind climate and the actual wind energy potential of two of the test sites, for which the annual wind speed distributions at 50 mAGL were shown in Figure 2.

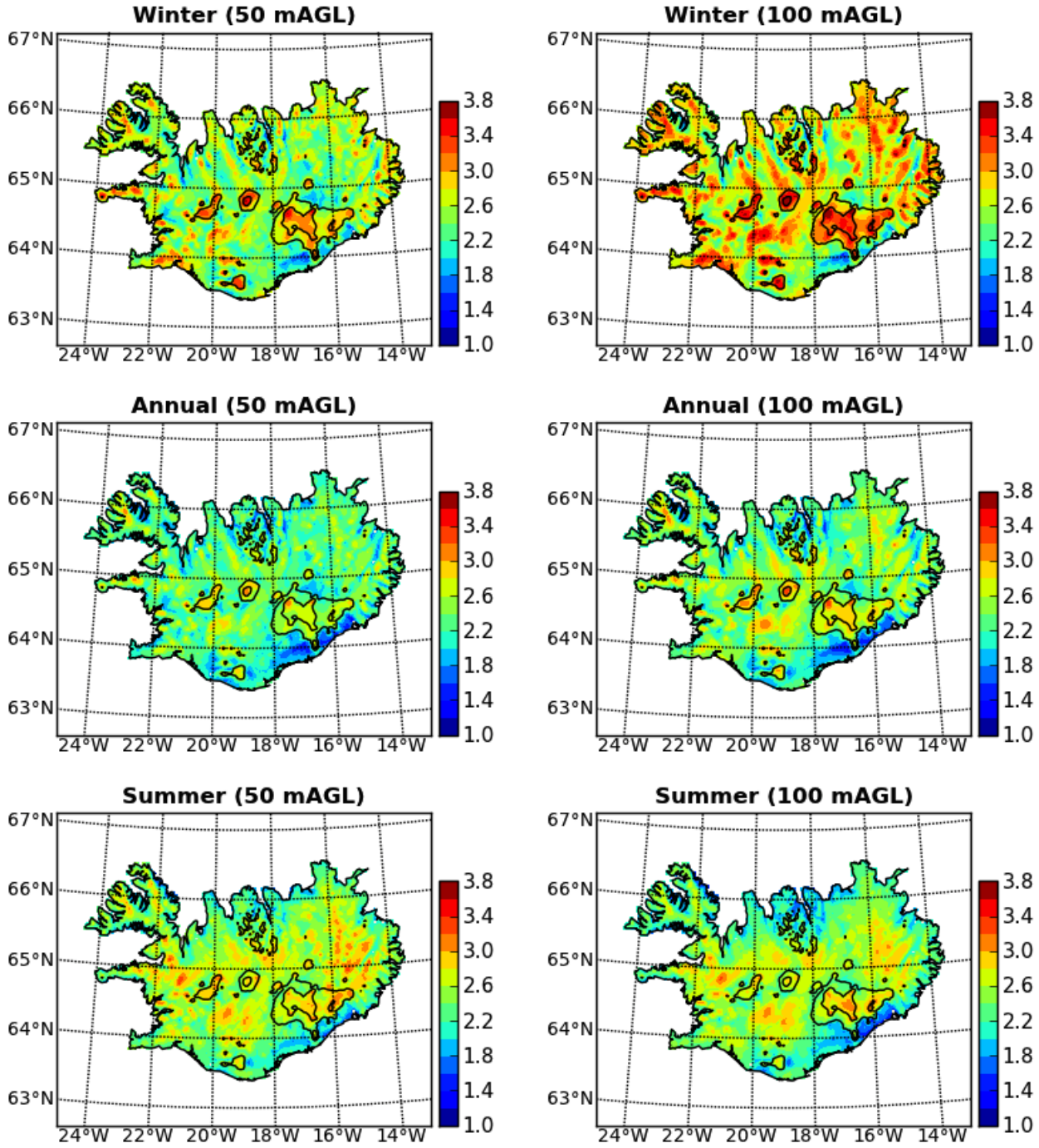


*Figure 9. Weibull shape parameter, k, for wind speed at 50 and 100 mAGL, and for all wind directions, based on corrected WRF model data. Terrain elevation contour lines are drawn at 1000 and 1500 mASL.*

## 5.2 Wind power density

Annual, winter, and summer averages of wind power density at 50 and 100 mAGL, based on the corrected WRF model data, are shown in Figure 10. As mentioned previously, regions in Iceland above 1000 mASL are primarily glaciers. Due to the combined effects of high terrain and low surface roughness, average power density over glaciers is about twice as high as over intermediate terrain between 500 – 1000 mASL. However, since these regions are not accessible for wind energy production, values above 1000 mASL are masked in the figures, to allow for a more nuanced scaling at low values. Since power density depends on the cube of wind speed, the relative seasonal and spatial variability is significantly larger than that for average wind speed. Compared with summer, average power density in winter is increased throughout Iceland by a factor of 2.0 – 5.5, with the largest increases on the lower slopes of Vatnajökull, along the complex coastline of the Westfjords, and over the low-lying areas in the northeast. For comparison, average wintertime wind speeds only increase by a factor of 1.2 – 1.8, relative to summer (see again Figure 7). In any given season, there are also considerable spatial differences in average wind power density. Relative to the average power density within 10 km of the coast, power density across Iceland varies between 50 – 450%. The largest reduction relative to the near-coastal average occurs in low-lying regions of the southwest and northeast. At intermediate elevations of 500 – 1000 mASL, independent of the distance to the coast, power density is within 200 – 250% of the near-coastal average. Again, for comparison, the spatial variability of wind speed throughout the year is between 75 and 225% of the average wind speed within 10 km of the coast. Natural temporal and spatial variability of wind speed, as well as measurement and simulation errors, are amplified when considering power density. An accurate and detailed assessment of local wind conditions is therefore essential.

Average wind power density at 50 and 100 mAGL, based on NORA10 data, is shown in Figure 11. To allow for a more nuanced scaling at low values, power densities in excess of 2000 W $m^{-2}$ are masked in the figures. Over the ocean, differences compared with the WRF model simulations are small (see again Figure 6). Over the land, differences are somewhat larger, partly due to differences in spatial resolution. Many of the terrain features responsible for local increases or decreases in wind speed or power density are not properly resolved in the downscaled reanalyses. Spatial variability in the NORA10 data is therefore significantly smaller than in the WRF model simulations. However, wintertime average wind power density, at low elevations up to 500 mASL, is within the same range of 250 – 750 W $m^{-2}$ as for the corrected WRF model data. At intermediate elevations of 500 – 1000 mASL in the interior, wintertime NORA10 power density is within 750 – 1250 W $m^{-2}$, which is between the values for the original and corrected WRF model data. In other seasons, differences between WRF model data and NORA10 are smaller. Throughout the year, the NORA10 values are between those of the original and corrected WRF model simulations.

In addition to seasonal and spatial variability, differences in average wind speed or power density also exist for different wind directions. On the large scale, without local terrain-induced effects, directional variability is usually due to the passage of fronts associated with cyclonic storm systems, causing sudden changes in wind speed and direction. Near the coast, the sharp transition in surface roughness between ocean and land may cause differences between the intensity of onshore and offshore winds. In the presence of elevated terrain, there may be dynamically induced differences in the intensity of horizontally or vertically deflected flow, or between upslope and downslope winds.

Differences in average wind power density at 50 and 100 mAGL between winds from the northerly and southerly 30-degree sector, based on the corrected WRF model data, are shown in Figure 12. The largest differences of $\pm$ 4 kW m$^{-2}$ occur in winter, and are associated with the three main glaciers, Langjökull, Hofsjökull, and Vatnajökull, where stronger winds occur on lee than on windward slopes. For surface wind speeds, this leeward speed-up has already been discussed by Nawri et al. (2012b). Along the coast in winter, power density of onshore wind is higher by 500 – 1000 W m$^{-2}$ than that of offshore wind. In summer, differences between the power density of onshore and offshore winds, based on WRF model data, are small and unsystematic.

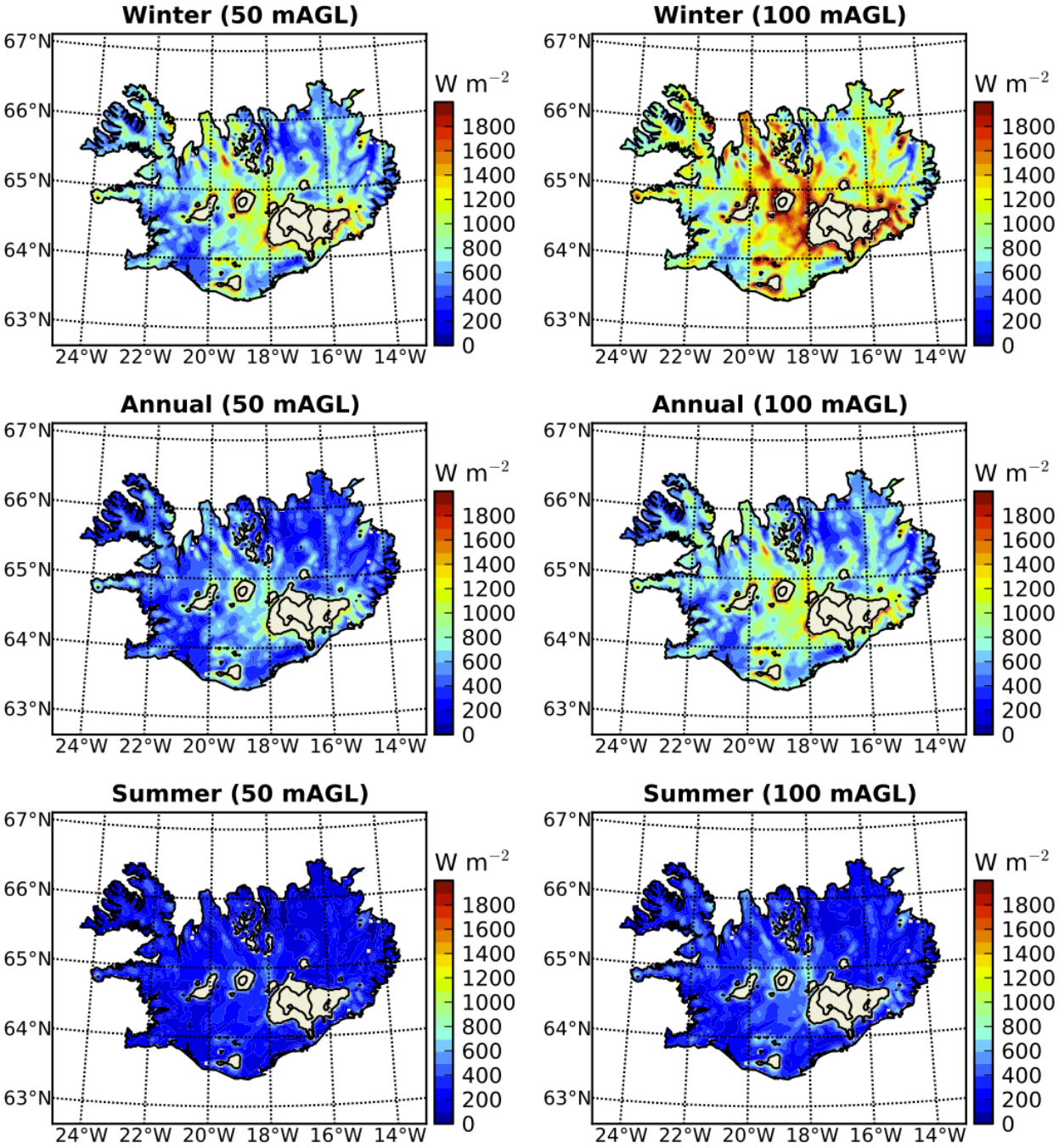


*Figure 10. Annual, winter (DJF), and summer (JJA) averages of wind power density at 50 and 100 mAGL, based on corrected WRF model data. Terrain elevation contour lines are drawn at 1000 and 1500 mASL. Values above 1000 mASL are masked.*

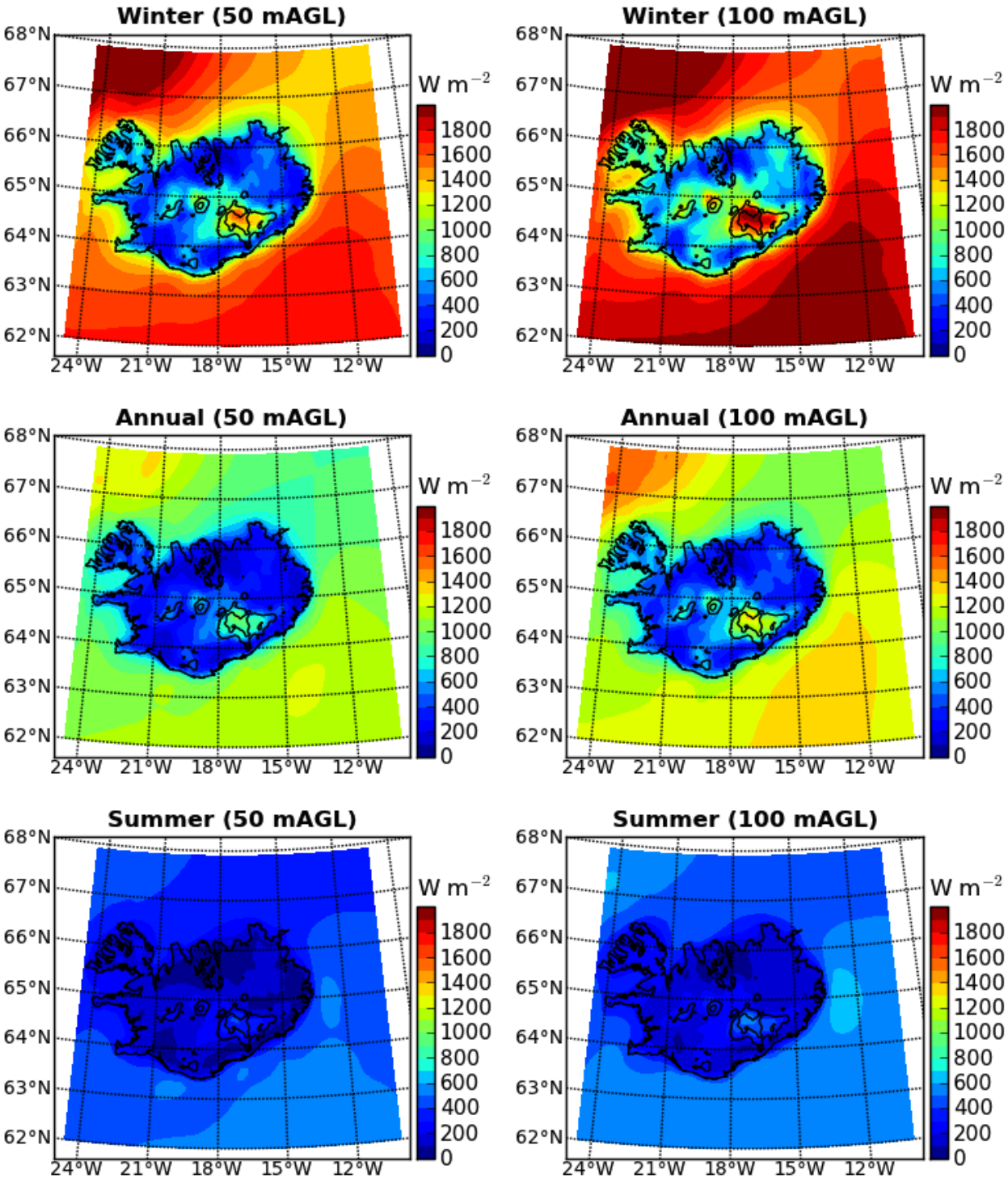


*Figure 11. Annual, winter (DJF), and summer (JJA) averages of wind power density at 50 and 100 mAGL, based on NORA10 data. Terrain elevation contour lines are drawn at 1000 and 1500 mASL. Values in excess of 2000 W m$^{-2}$ are masked.*

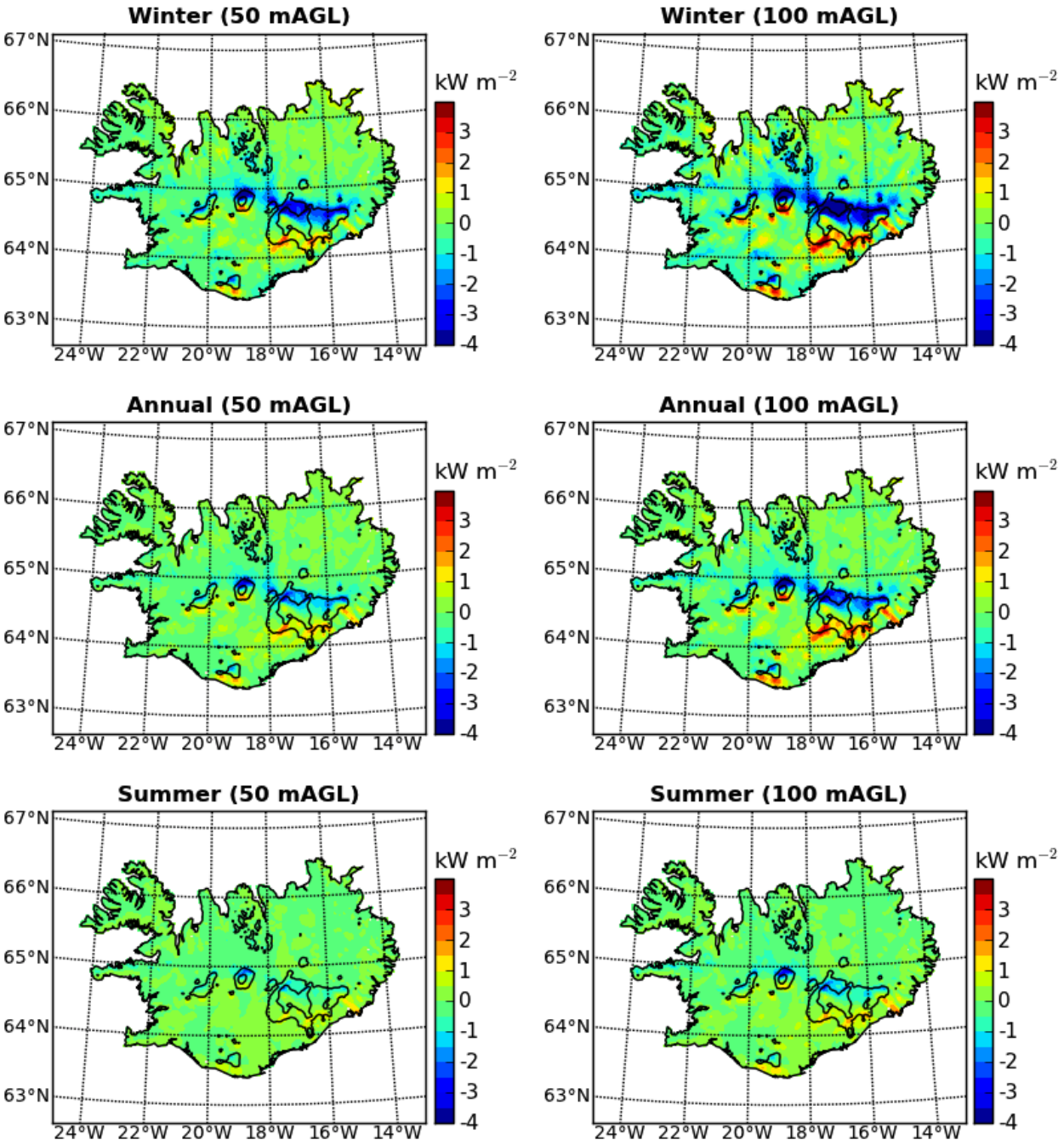


*Figure 12. Differences in annual, winter (DJF), and summer (JJA) averages of wind power density at 50 and 100 mAGL between winds from the northerly and southerly 30-degree sector, based on corrected WRF model data. Terrain elevation contour lines are drawn at 1000 and 1500 mASL.*

# 6 Test sites

In this section, a brief overview is given of the wind energy potential of the 14 test sites selected for this study (see Figure 1). Detailed maps of average power density are shown in the appendix. The test sites fall into two groups: 10 locations near the coast, chosen for their accessibility and relatively strong winds considering their low height above mean sea level (see again Figure 8); and 4 inland locations, near some of the largest hydro- and geothermal power plants in the country. Due to their proximity to preexisting industrial sites, the latter locations are already accessible by regular roads, despite being situated on higher terrain. There is also established electric grid access. Additional impact from the installation of wind turbines at these sites, as far as nature conservation and tourism are concerned, are minimal. Seismic activity cannot be excluded anywhere in Iceland, but all test sites are away from major avalanche paths, and include several square kilometres of flat land. Even tall turbines installed at these locations are not anticipated to interfere with aviation.

The results were obtained through high-resolution WAsP modelling, with a regular horizontal grid-spacing of 100 m, based on corrected grid-point time-series from the WRF model. As described in Section 3.1, and in more detail in Troen and Petersen (1989), the WAsP method works by generalising the input data at one point within a given domain, and exporting the generalised wind climate to other locations. In all 14 domains, the surface roughness length over land is specified as 3 cm, whereas over water, it is set to zero. For each site, two scenarios for different WRF model grid points are determined. Ideally, the generalisation of the input data would result in the same resource maps regardless of the location of the model grid point. However, in some regions, considerable differences do exist, despite small differences between the input data at the two grid points. This is indicative of the limitations of the parameterised description of boundary-layer processes, which is the basis for the WAsP method, at least over the complex terrain of many parts of Iceland. In the appendix, the resource maps for both scenarios at each test site are shown graphically. For an easier comparison, Tables 3 and 4 list the most relevant wind-related properties of each region, based on the wind conditions at 55 mAGL. Turbine specific quantities are calculated for the Enercon E44. The values are spatial averages over that part of the domain within the indicated range of terrain elevation, and excluding lakes. Additionally, averages were taken between the scenarios for each of the two model grid points. The primary wind direction is determined by considering only wind speeds within the useable range between cut-in and cut-out speed. At all sites, and for all wind direction sectors, differences between the regional average histogram and the histograms at individual grid points are less than 3%. The indicated primary wind directions therefore apply throughout each domain. High wind direction variability is detrimental to efficient wind energy production, as it requires a frequent reorientation of the rotor. That in itself requires energy, and might also result in some strong winds to be missed. Therefore wind direction constancy is defined here as the combined percentage of wind directions in the three most frequent 30-degree sectors. As a baseline, with a homogeneous distribution of wind directions, any three sectors would contain 25% of the values. High wind direction constancy can be the result of orographic channelling, as in the Búrfell region, or of the constancy of the large-scale prevailing winds, as on Skagi. Below cut-in and above cut-out speeds are determined based on the corresponding Weibull distribution. The highest downtime due to weak winds can be expected at Höfn, with a below cut-in speed occurrence of 15% throughout the year, and 29% in summer (see Table 3). The highest downtime due to strong winds would result on Skagi, with 3% above cut-out speeds annually, and 7% throughout the year.

As indicated in Section 5.1, an interesting comparison can be made between the wind energy potential and the actually produced wind energy on Hellisheiði and Skagi. Based on the annual wind conditions at 55 mAGL, Hellisheiði has an average power density of 1600 W $m^{-2}$, compared with 2530 W $m^{-2}$ on Skagi (see Table 4). Therefore, purely based on atmospheric conditions, Skagi has a 58% higher wind energy potential than Hellisheiði. However, to be able to fully exploit a given wind energy potential, the cut-out speed and rated power of the chosen turbine must be sufficiently high. The saturation point of power production is reached at the rated speed. Beyond that, efficiency is deliberately reduced to protect the turbine. At the cut-out speed and above, wind energy potential is lost completely to average available power, whereas these high winds weigh heavily in averages of power density. In the case of Skagi, these technical limitations clearly come into play. Despite the higher values of average power density, the average available power for the Enercon E44 of 480 kW is 11% lower than that on Hellisheiði, with an average available power of 540 kW. This is primarily the result of the higher proportion of above cut-out speeds, together with a small loss from a higher proportion of below cut-in speeds (see again Figure 2). Much of the power density at above-rated speeds is also lost by the reduced efficiency within that range. The average efficiency of power generation is defined here as the ratio between average available power, and average power density multiplied by the area swept by the rotor blades. As listed in Table 4, the efficiency on Hellisheiði is about twice as high as on Skagi. Generally, based on the annual wind conditions at 55 mAGL, and for the Enercon E44, efficiency is between 12% for Skagi, with the best wind energy potential, and 32% for Fljótsdalsheiði, with low wind energy potential. Wind conditions on Iceland are characterised by a strong seasonal cycle, with wintertime wind speeds larger by typically 50 – 70% than in summer, and average wintertime power densities typically between 2 – 5 times as high as in summer. Wintertime increases in the actual energy production are typically between 50 – 150% of the summer averages, and are timed well with the demands for increased lighting during the winter.

Table 5 contains some of the quantities listed in Tables 3 and 4, for the annual wind conditions at 67 mAGL, and with turbine specific quantities calculated for the Vestas V80. For a 22% increase in hub height, average power density typically increases by 8 – 10%. With an additional 82% increase in rotor diameter, or an increase in the area swept by the rotor blades by a factor of 3.3, average available power typically increases by a factor of 2.5 – 2.7. Despite the increase in hub height, the actually generated power does not increase proportional to the square of the rotor diameter, since the efficiency of larger turbines is reduced. As for the Enercon E44, the lowest efficiency is found for the wind conditions on Skagi, reduced even further for the Vestas V80 due to the 3 m $s^{-1}$ lower cut-out speed, and 1 m $s^{-1}$ higher cut-in speed. Still, the benefit from installing a medium-size turbine such as the Vestas V80, rather than a small turbine such as the Enercon E44, would be an increase in the generated power by more than a factor of 2.3 at all test sites.

*Table 3. Winter (DJF) / annual / summer (JJA) values of primary wind direction (PWD), wind direction constancy (WDC), average wind speed, below cut-in speed occurrence (BCI), and above cut-out speed occurrence (ACO), based on the wind conditions at 55 mAGL, and for the Enercon E44 turbine. Percentage values of winter average wind speeds relative to summer are given in parentheses.*

| | Height [mASL] | PWD [deg] | WDC [%] | Speed [m $s^{-1}$] | BCI [%] | ACO [%] |
|---|---|---|---|---|---|---|
| Blanda | 450 – 550 | 150 / 150 / 180 | 54 / 48 / 43 | 13.7 (161%) / 11.2 / 8.5 | 4 / 6 / 8 | 4 / 1 / 0 |
| Búrfell | 200 – 400 | 60 / 60 / 60 | 61 / 60 / 54 | 11.6 (149%) / 10.0 / 7.8 | 5 / 7 / 8 | 2 / 0 / 0 |
| Fljótsdalsheiði | 600 – 700 | 240 / 270 / 300 | 38 / 34 / 34 | 11.2 (165%) / 8.9 / 6.8 | 4 / 7 / 8 | 0 / 0 / 0 |
| Gufuskálar | 5 – 100 | 90 / 60 / 60 | 46 / 50 / 55 | 13.3 (158%) / 10.8 / 8.4 | 2 / 5 / 10 | 1 / 0 / 0 |
| Hellisheiði | 300 – 400 | 60 / 60 / 180 | 45 / 40 / 41 | 13.0 (143%) / 11.4 / 9.1 | 2 / 3 / 4 | 1 / 0 / 0 |
| Höfn | 5 – 100 | 0 / 0 / 210 | 49 / 45 / 48 | 10.7 (181%) / 8.7 / 5.9 | 8 / 15 / 29 | 1 / 1 / 0 |
| Landeyjar | 5 – 60 | 120 / 120 / 120 | 41 / 46 / 49 | 12.2 (137%) / 10.8 / 8.9 | 4 / 7 / 10 | 1 / 1 / 0 |
| Langanes | 5 – 100 | 210 / 120 / 120 | 39 / 35 / 38 | 12.0 (167%) / 9.8 / 7.2 | 3 / 7 / 14 | 0 / 0 / 0 |
| Meðallandssveit | 5 – 40 | 330 / 90 / 90 | 37 / 37 / 41 | 11.5 (116%) / 11.2 / 9.9 | 5 / 5 / 7 | 1 / 1 / 0 |
| Melrakkaslétta | 5 – 100 | 180 / 90 / 90 | 38 / 33 / 42 | 11.7 (156%) / 9.6 / 7.5 | 3 / 6 / 8 | 0 / 0 / 0 |
| Mýrar | 5 – 20 | 60 / 60 / 60 | 51 / 50 / 43 | 11.9 (153%) / 10.0 / 7.8 | 3 / 5 / 8 | 0 / 0 / 0 |
| Skagi | 5 – 100 | 120 / 120 / 60 | 52 / 58 / 62 | 15.3 (156%) / 12.2 / 9.8 | 2 / 6 / 12 | 7 / 3 / 1 |
| Snæfellsnes | 5 – 150 | 60 / 60 / 30 | 47 / 46 / 37 | 11.4 (156%) / 9.7 / 7.3 | 5 / 8 / 15 | 1 / 0 / 0 |
| Þorlákshöfn | 5 – 100 | 60 / 60 / 240 | 47 / 42 / 36 | 12.1 (155%) / 10.3 / 7.8 | 3 / 5 / 9 | 0 / 0 / 0 |

*Table 4. Winter (DJF) / annual / summer (JJA) values of average power density (APD), average available power (AAP), and efficiency of power generation, based on the wind conditions at 55 mAGL, and for the Enercon E44 turbine. Percentage values of winter averages relative to summer are given in parentheses.*

| | APD [W $m^{-2}$] | AAP [kW] | Efficiency [%] |
|---|---|---|---|
| Blanda | 2990 (460%) / 1610 / 650 | 510 (159%) / 450 / 320 | 11 / 19 / 32 |
| Búrfell | 2010 (394%) / 1230 / 510 | 520 (179%) / 440 / 290 | 17 / 23 / 38 |
| Fljótsdalsheiði | 1470 (525%) / 740 / 280 | 490 (245%) / 360 / 200 | 22 / 32 / 46 |
| Gufuskálar | 2370 (339%) / 1410 / 700 | 590 (179%) / 470 / 330 | 16 / 22 / 31 |
| Hellisheiði | 2210 (295%) / 1600 / 750 | 630 (158%) / 540 / 400 | 19 / 22 / 35 |
| Höfn | 1750 (449%) / 1070 / 390 | 460 (256%) / 340 / 180 | 17 / 21 / 31 |
| Landeyjar | 2140 (233%) / 1620 / 920 | 550 (153%) / 470 / 360 | 17 / 19 / 26 |
| Langanes | 1850 (402%) / 1130 / 460 | 570 (219%) / 440 / 260 | 20 / 26 / 37 |
| Meðallandssveit | 1810 (151%) / 1630 / 1200 | 520 (121%) / 500 / 430 | 19 / 20 / 23 |
| Melrakkaslétta | 1690 (367%) / 1030 / 450 | 570 (204%) / 440 / 280 | 22 / 28 / 41 |
| Mýrar | 1670 (363%) / 1040 / 460 | 540 (193%) / 430 / 280 | 21 / 27 / 40 |
| Skagi | 4400 (299%) / 2530 / 1470 | 550 (149%) / 480 / 370 | 8 / 12 / 17 |
| Snæfellsnes | 1690 (331%) / 1150 / 510 | 500 (200%) / 400 / 250 | 19 / 23 / 32 |
| Þorlákshöfn | 1870 (353%) / 1240 / 530 | 580 (200%) / 470 / 290 | 20 / 25 / 37 |

Whether based on the turbine-specific characteristics of the Enercon E44 at 55 mAGL, or the Vestas V80 at 67 mAGL, of those sites considered here, a wind farm installed on Hellisheiði would effectively produce the most energy per turbine annually, as well as during the winter. This is the result of a combination of a high wind energy potential, as measured by power density, together with a particular wind speed distribution, which allows the wind energy potential to be extracted efficiently. Additional advantages of the site are the proximity to the second largest power plant in Iceland, the proximity to the capital area of greater Reykjavík, and sufficient space for tens of turbines over essentially flat terrain. Meðallandssveit, with the second highest average available power among the test sites, could be considered for another wind farm in the south, to cover low-wind periods on Hellisheiði, especially in summer, when average available power in Meðallandssveit is the highest. The turbine-independent wind energy potential on Skagi by far exceeds that of all other test sites. Among the sites in the northern part of the country, it also has the highest average available power. However, to be able to extract the high wind energy potential more efficiently, a turbine with a higher rated power, and especially with a higher cut-out speed would be required.

*Table 5. Annual values of wind direction constancy (WDC), average wind speed, below cut-in speed occurrence (BCI), above cut-out speed occurrence (ACO), average power density (APD), and average available power (AAP), based on the wind conditions at 67 mAGL, and for the Vestas V80 turbine. Percentage increases relative to the values at 55 mAGL, and for the Enercon E44, are given in parentheses.*

| | WDC [%] | Speed [m $s^{-1}$] | BCI [%] | ACO [%] | APD [W $m^{-2}$] | AAP [kW] | Efficiency [%] |
|---|---|---|---|---|---|---|---|
| Blanda | 48 | 11.5 (103%) | 9 | 3 | 1740 (108%) | 1130 (251%) | 13 |
| Búrfell | 61 | 10.3 (103%) | 11 | 1 | 1340 (109%) | 1140 (259%) | 17 |
| Fljótsdalsheiði | 34 | 9.2 (103%) | 11 | 0 | 810 (109%) | 980 (272%) | 25 |
| Gufuskálar | 51 | 11.1 (103%) | 9 | 2 | 1530 (109%) | 1180 (251%) | 15 |
| Hellisheiði | 41 | 11.8 (104%) | 5 | 1 | 1730 (108%) | 1360 (252%) | 16 |
| Höfn | 45 | 9.0 (103%) | 21 | 2 | 1170 (109%) | 890 (262%) | 15 |
| Landeyjar | 46 | 11.2 (104%) | 10 | 2 | 1770 (109%) | 1190 (253%) | 13 |
| Langanes | 35 | 10.2 (104%) | 11 | 1 | 1240 (110%) | 1140 (259%) | 18 |
| Meðallandssveit | 37 | 11.6 (104%) | 10 | 2 | 1780 (109%) | 1190 (238%) | 13 |
| Melrakkaslétta | 33 | 10.0 (104%) | 10 | 0 | 1130 (110%) | 1110 (252%) | 20 |
| Mýrar | 50 | 10.3 (103%) | 9 | 0 | 1150 (111%) | 1100 (256%) | 19 |
| Skagi | 58 | 12.6 (103%) | 9 | 6 | 2730 (108%) | 1170 (244%) | 9 |
| Snæfellsnes | 46 | 10.1 (104%) | 13 | 1 | 1260 (110%) | 1000 (250%) | 16 |
| Þorlákshöfn | 43 | 10.6 (103%) | 9 | 1 | 1360 (110%) | 1170 (249%) | 17 |

# 7 Conclusions

To be able to determine to what extent wind energy production in Iceland is viable, the annual averages of wind power density and available power obtained in this study need to be compared with the wind resources of other countries, as well as with the capacity of domestic hydro- and geothermal power plants.

According to the European Wind Atlas published by Risø National Laboratory (Troen and Petersen, 1989), the highest wind power class in Western Europe, not including Iceland, covers the western and northern coast of Ireland, the whole of Scotland, and the northwestern tip of Denmark. It is characterised by annual average wind power density at 50 mAGL of $> 250$ W m$^{-2}$ over sheltered terrain, $> 700$ W m$^{-2}$ along the open coast, and $> 1800$ W m$^{-2}$ on top of hills and ridges. Referring back to Figure 6 for a large-scale overview, as well as to the more detailed analyses in Section 6 and the appendices, it is clear that Iceland is well within that wind power class, and therefore highly competitive within the Western European context. Annual wind conditions are therefore not a limiting factor for wind energy production.

Commercial electricity production in Iceland is already almost entirely based on renewable resources, with currently around 73% from hydropower, 27% from geothermal power plants, and only a negligible amount from fossil fuel (see the annual statistics published by the National Energy Authority (Orkustofnun) at http://www.nea.is/the-national-energy-authority/energy-statistics/generation-of-electricity/).

The Hellisheiði geothermal power plant, with 303 MW installed electric capacity, is the largest geothermal power plant in Iceland, and the second largest in the world (see the description by Landsvirkjun of all commercial power stations in Iceland at http://www.landsvirkjun.com/Company/PowerStations/). One Enercon E44 wind turbine installed on the plateau in the vicinity of the power plant, at terrain elevations of 300 – 400 mASL, would produce around 540 kW on average throughout the year, or 0.18% of the produced geothermal power. One Vestas V80 wind turbine would produce around 1360 kW annually, or 0.45%. On higher terrain with elevations of 400 – 500 mASL, the average available wind power produced by one Enercon E44 increases to around 570 kW (0.19%), and to around 610 kW (0.20%) at elevations above 500 mASL. For one Vestas V80, the average available power increases to around 1420 kW (0.47%) at 400 – 500 mASL, and to around 1490 kW (0.49%) above 500 mASL. Even on Hellisheiði, with the highest wind energy production (for either the Enercon E44 or the Vestas V80) among the sites analysed here, a substantial wind farm of at least 200 Vestas V80 would be required to produce the same amount of energy as the local geothermal power plant. This would make it one of the largest onshore wind farms in the world, comparable in the number of turbines to the Fantanele-Cogealac wind farm in Romania, which covers an area of 12 by 6 km (see the description by the CEZ Group at http://www.cez.cz/en/cez-group/media/press-releases/4051.html). More than 500 Vestas V80 on Hellisheiði would be required to produce the same amount of energy as the Fljótsdalur hydropower plant, which is the largest power plant in Iceland, with an installed electric capacity of 690 MW. However, only a modest wind farm would be required to match Laxá I, the smallest hydropower plant in Iceland, with 5 MW electric capacity, and Bjarnarflag, the smallest geothermal power plant in Iceland, with 3 MW electric capacity. A wind farm consisting of 15 Enercon E44 turbines, or 6 Vestas V80 turbines installed on Hellisheiði would produce more power throughout the year than

the two small power plants together. For the same power output, the number of required turbines could be reduced by increasing the rotor size or hub height.

Therefore, considering the low environmental impact from the installation of wind turbines, compared with the lasting or permanent impact especially from hydropower dams, wind power should be considered as a serious option for renewable energy production, especially in a country such as Iceland, with high wind energy potential, and a low population density.

# A Resource maps

This appendix contains maps of average wind power density at 55 mAGL, for the 14 test sites (see Figure 1). The results were obtained through WAsP modelling, with a regular horizontal grid-spacing of 100 m, based on two corrected grid-point time-series for each site from the WRF model. A comparison between the two scenarios gives the range of possible values, and a measure of the uncertainty of the results within a given region.

At any location, average wind energy potential varies on a seasonal time-scale, as well as with wind direction within any given season. Therefore, two figures are shown for each site: 1) annual average wind power density for two significant wind direction sectors; 2) annual, winter (DJF), and summer (JJA) averages of wind power density for all wind directions.

In all these figures, the position of the generating WRF model grid point is indicated by a white dot with red edge. The dashed grid lines are spaced at 2 km. Terrain elevation contour lines are drawn in black, and labelled in metres above mean sea level. Boundaries between land and lakes are indicated by white lines, whereas coastlines are indicated by black-and-white lines.

## A.1 Blanda

The domain for the WAsP analysis covers the northern part of Blöndulón lake in northern Iceland, artificially created by the dam of the Blanda hydropower plant installed at the beginning of the deep and narrow Blöndudalur river valley, continuing northwestwards to the coast. Several smaller lakes are located northwest of Blöndulón, and a flat area extends towards the north. The first WRF model grid point (GP1) is located at 19.66177°W, and 65.24368°N. The elevation range on the plain above the river valley is 450 – 550 mASL. There is no significant terrain sheltering on the plateau, but the small hills have a local speed-up effect of about 1 kW $m^{-2}$ in winter. The surface type of the land area is characterised by rocks and grass, without any tall vegetation. The wintertime speed-up effect over the lake amounts to about 500 W $m^{-2}$. The average power density on the main island in the lake is between that over flat terrain, and over hill tops. Aside from the hydroelectric dam, there are no tall manmade structures within the domain. Access to the area is via Mountain Route F35.

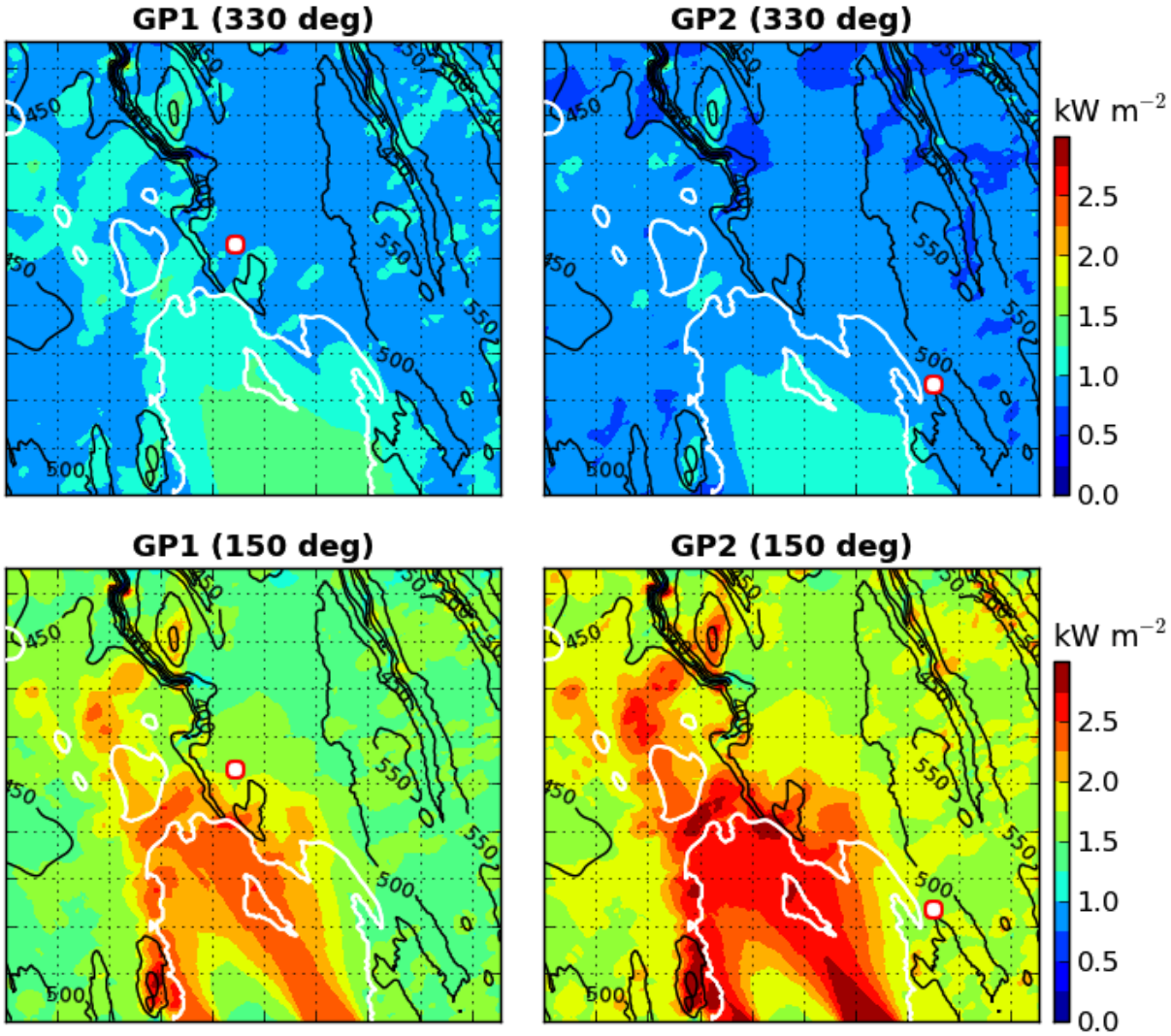


*Figure 13. Annual mean wind power density at 55 mAGL within the Blöndulón region, for two different wind directions, and for each of the two WRF model grid points (GPs).*

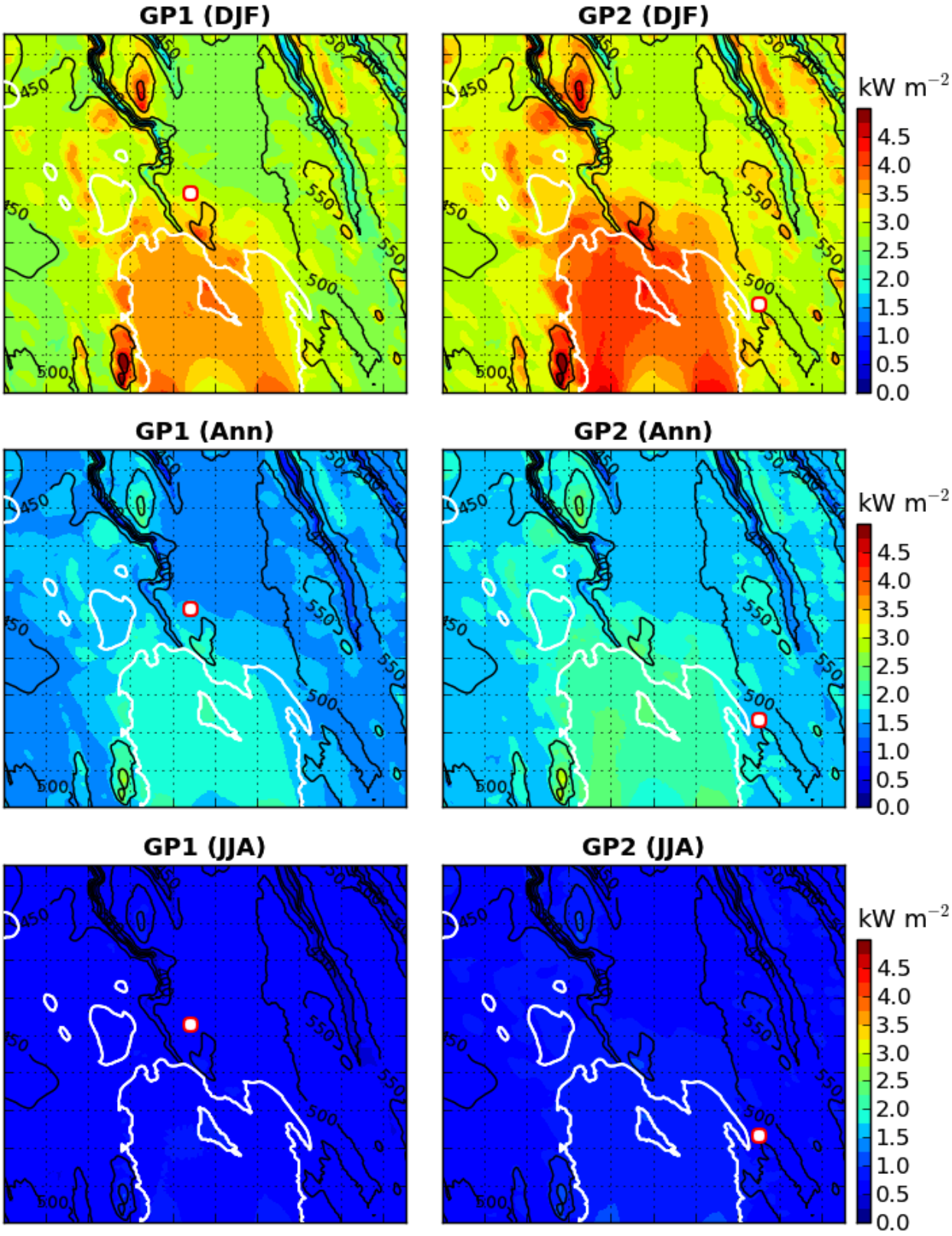


*Figure 14. Annual, winter (DJF), and summer (JJA) averages of wind power density at 55 mAGL within the Blöndulón region, for each of the two WRF model grid points (GPs).*

## A.2 Búrfell

The domain for the WAsP analysis covers a section of the Þjórsá river valley northeast and southwest of Búrfell hill in southwest Iceland. The first WRF model grid point (GP1) is located at 19.77802°W, and 64.10781°N. The terrain elevation on the valley floor is around 200 mASL. Towards the northwest, terrain slopes up to around 500 mASL within the domain. Towards the southeast corner, the terrain on the slopes of Hekla volcano reaches elevations of about 1000 mASL. On the valley floor, Búrfell is the only major hill, with a local speed-up effect of about 2 kW $m^{-2}$ in winter. The surface type of the land area is characterised by rocks and grass, without any tall vegetation. Aside from the hydropower plant north of Búrfell, there are no tall manmade structures within the domain. The area is accessible either via Route 26 or Route 32.

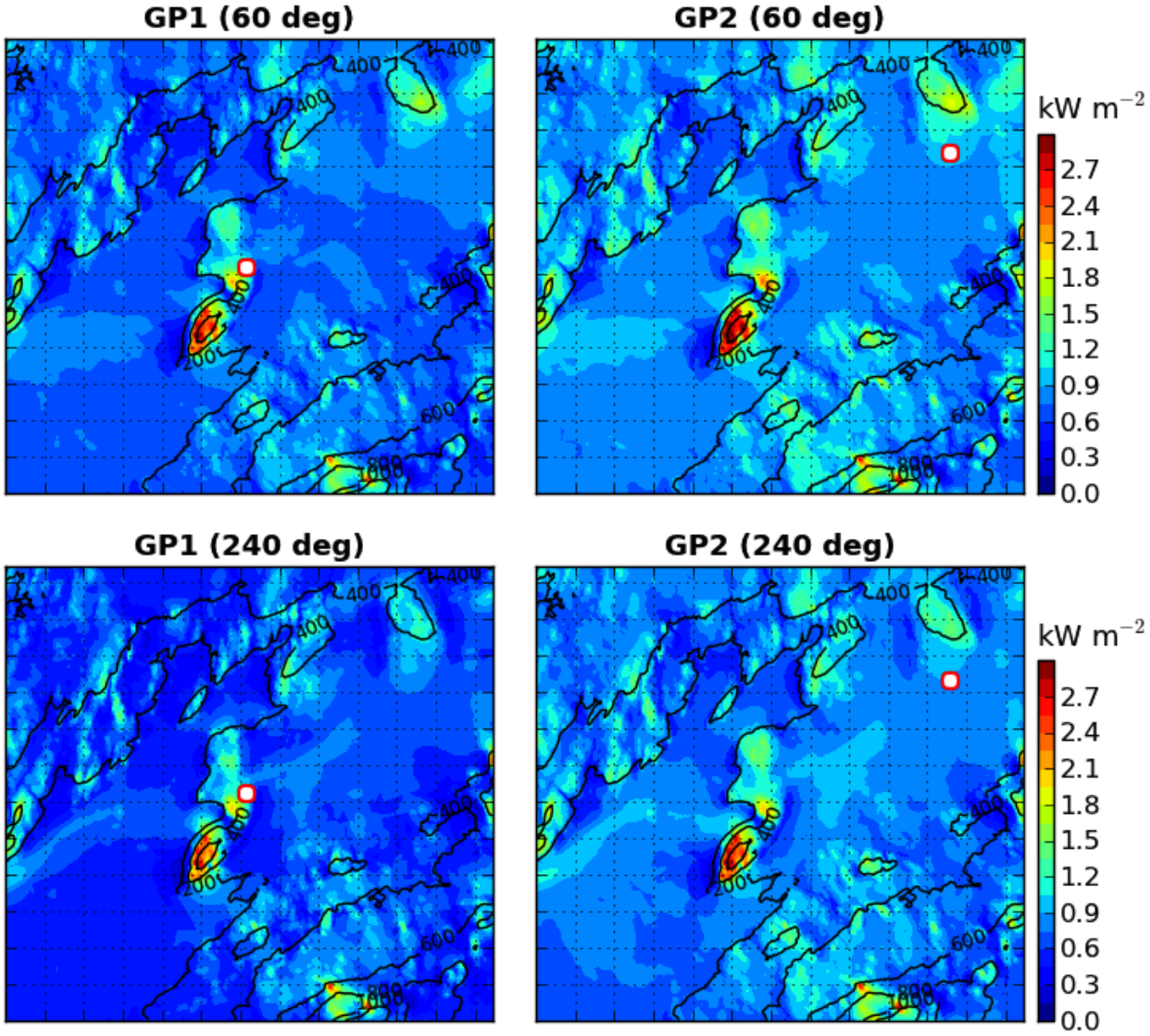


*Figure 15. Annual mean wind power density at 55 mAGL within the Búrfell region, for two different wind directions, and for each of the two WRF model grid points (GPs).*

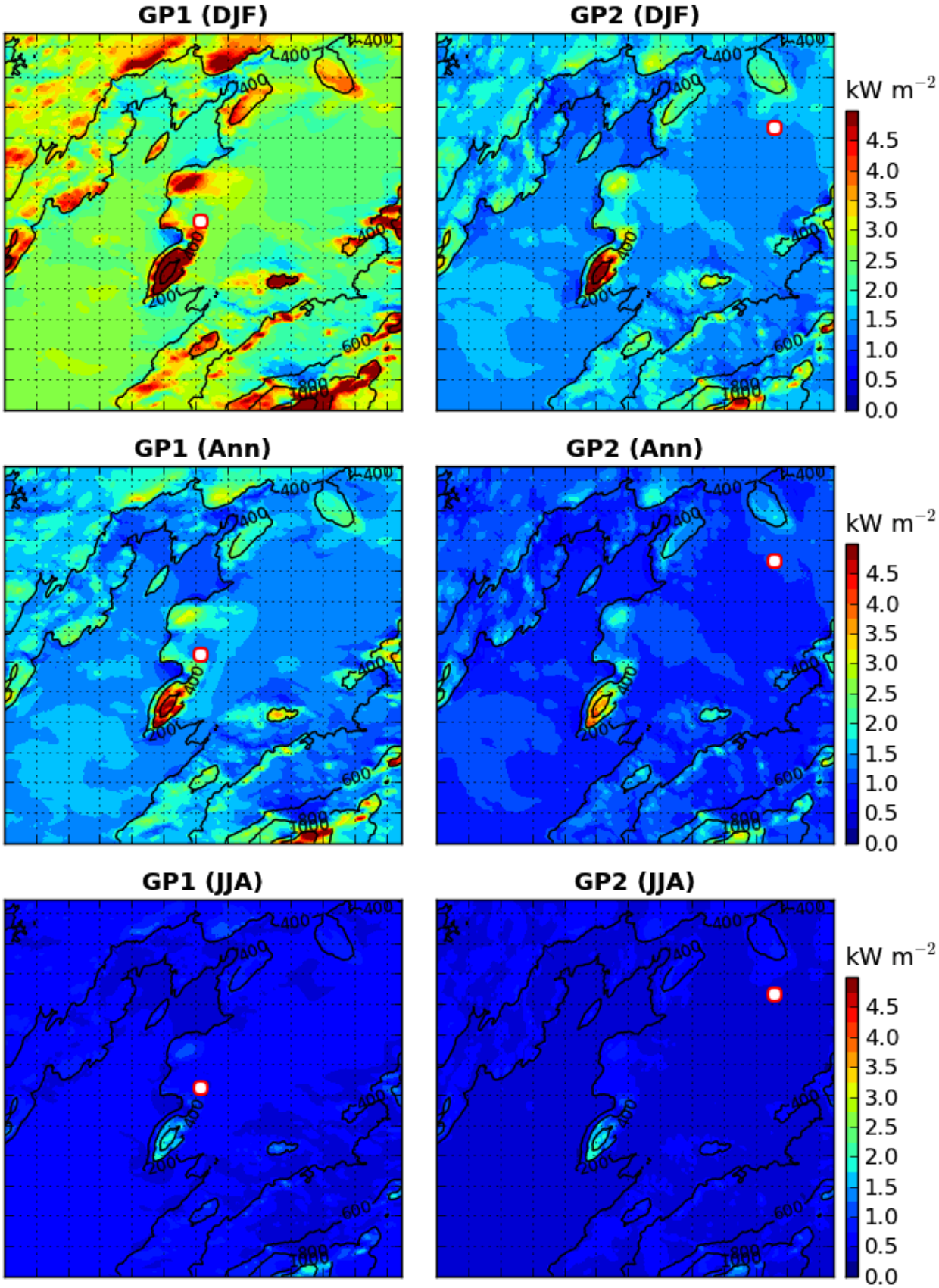


*Figure 16. Annual, winter (DJF), and summer (JJA) averages of wind power density at 55 mAGL within the Búrfell region, for each of the two WRF model grid points (GPs).*

## A.3 Fljótsdalsheiði

The domain for the WAsP analysis covers the central part of a highland plateau between the Jökuldalur and Fljótsdalur river valleys in eastern Iceland. The first WRF model grid point (GP1) is located at 15.14998°W, and 65.12013°N. The elevation range on the plateau is 600 – 700 mASL, without significant sheltering or speed-up effects. The surface type of the land area is homogeneous grassland, without any tall vegetation. The Fljótsdalur power plant is at the northern end of Hálslón lake, at the foot of Kárahnjúkar mountain, just outside the southwest corner of the domain. There are no tall manmade structures within the domain. Access to the southern part of the area is via Mountain Route F910.

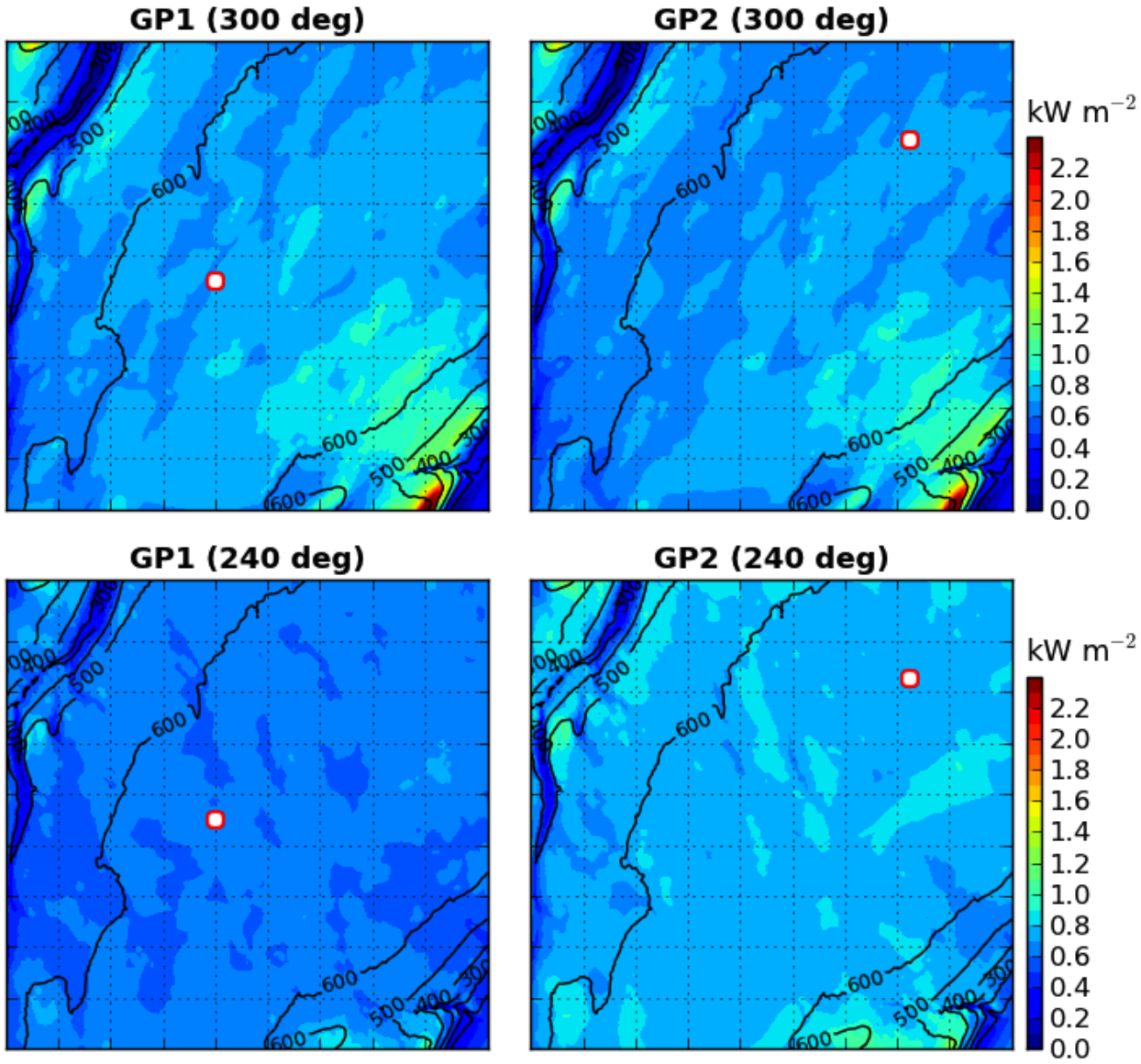


*Figure 17. Annual mean wind power density at 55 mAGL within the Fljótsdalsheiði region, for two different wind directions, and for each of the two WRF model grid points (GPs).*

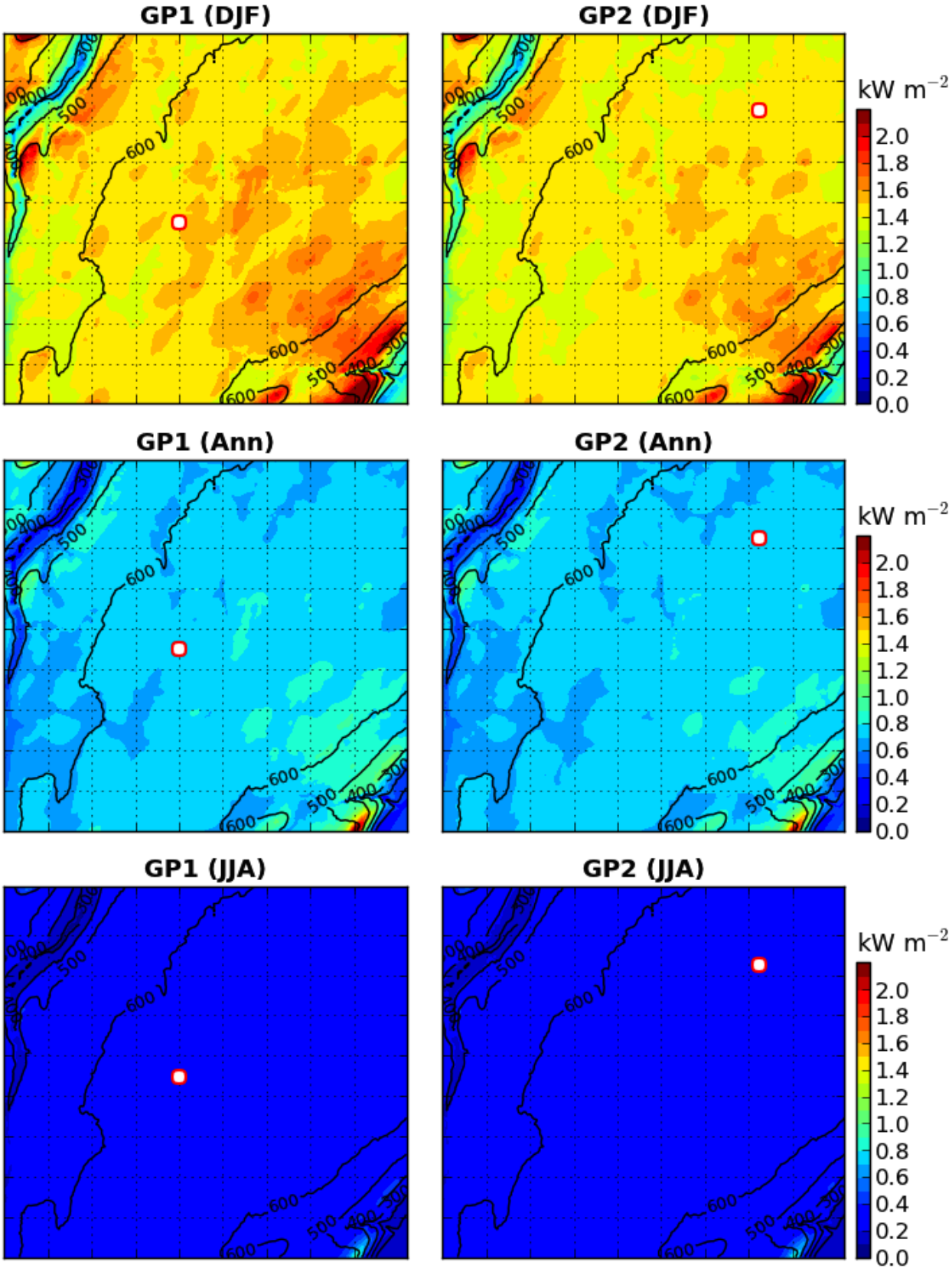


*Figure 18. Annual, winter (DJF), and summer (JJA) averages of wind power density at 55 mAGL within the Fljótsdalsheiði region, for each of the two WRF model grid points (GPs).*

## A.4 Gufuskálar

The domain for the WAsP analysis covers a section of the coast at the western tip of Snæfellsnes peninsula in western Iceland. The village of Hellissandur is near the northeast corner, and village of Rif (including a small airport) is just outside the northeast edge of the domain. The first WRF model grid point (GP1) is located at 23.93852°W, and 64.90002°N. Terrain elevation is below 120 mASL throughout most of the domain, without significant sheltering or speed-up effects. Towards the southeast corner, the terrain on the slopes of Snæfellsjökull rises rapidly, associated with local speed-up effects of about 2 kW $m^{-2}$ in winter. Compared with these terrain-related effects, the speed-up towards the coast is minor. The surface type of the land area is characterised by rocks and grass, without any tall vegetation. An abandoned LORAN-C station, including a 412 m tall longwave radio mast, is situated at GP1. The mast is now used by the National Broadcasting Service (RÚV). The area is accessible via Route 574.

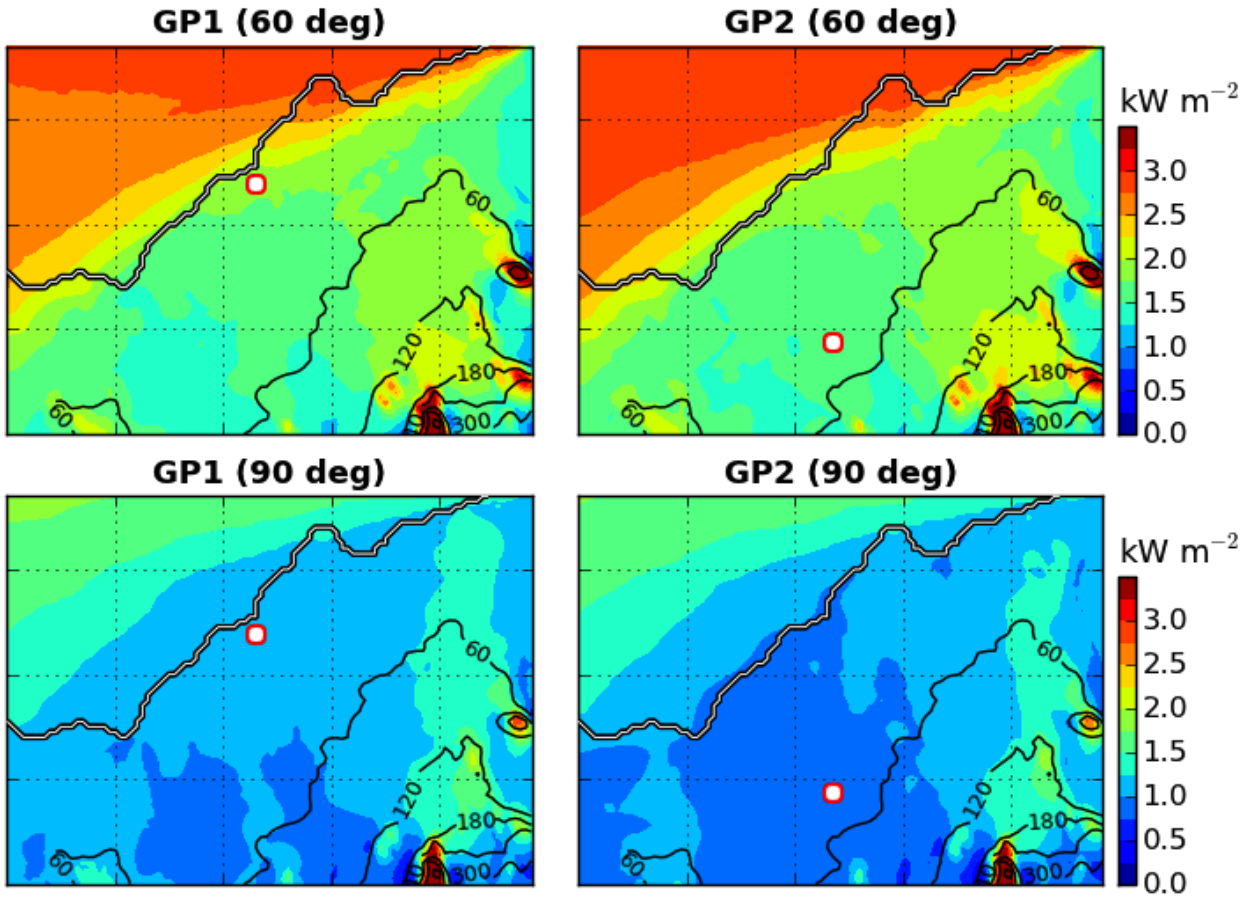


*Figure 19. Annual mean wind power density at 55 mAGL within the Gufuskálar region, for two different wind directions, and for each of the two WRF model grid points (GPs).*

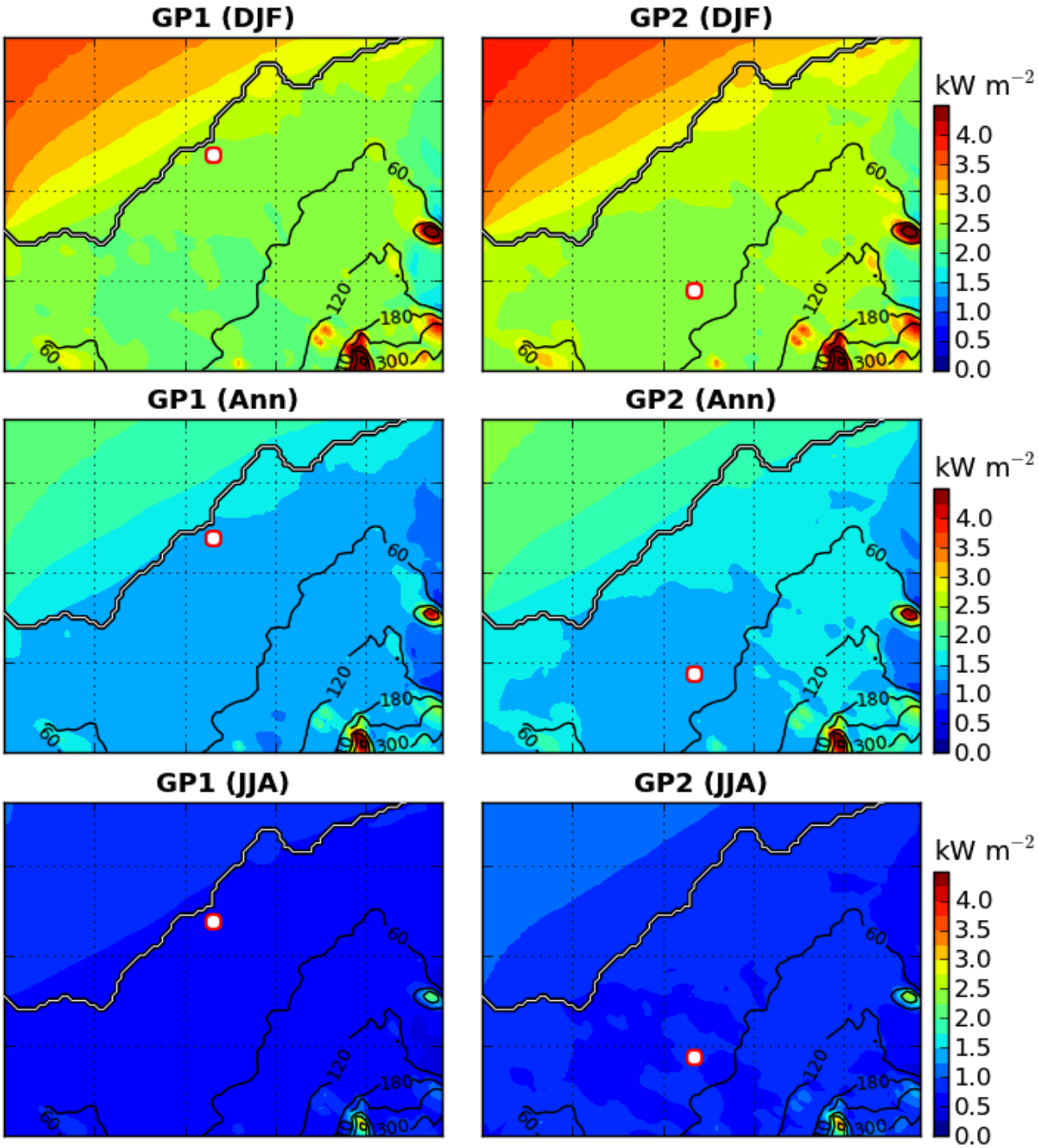


*Figure 20. Annual, winter (DJF), and summer (JJA) averages of wind power density at 55 mAGL within the Gufuskálar region, for each of the two WRF model grid points (GPs).*

## A.5 Hellisheiði

The domain for the WAsP analysis covers at its centre the elevated plateau of Hellisheiði in south-west Iceland, together with several of the surrounding higher peaks. The first WRF model grid point (GP1) is located at 21.25460°W, and 64.01540°N. The elevation range on the plateau is 300 – 400 mASL. The hills south of the plateau reach 500 mASL, with local speed-up effects of around 2 kW $m^{-2}$ in winter. The hills in the north reach up to 700 mASL, with local speed-up effects of around 3 kW $m^{-2}$. The surface type of the land area is characterised by rocks and grass, without any tall vegetation. Aside from the geothermal power plant near the western edge of the domain, there are no tall manmade structures. Route 1, the main road around Iceland, passes through the middle of the domain. The nearest residential area is the town Hveragerði, at the foot of the plateau in the eastern half of the domain. The capital area of greater Reykjavík is about 35 km towards the northwest.

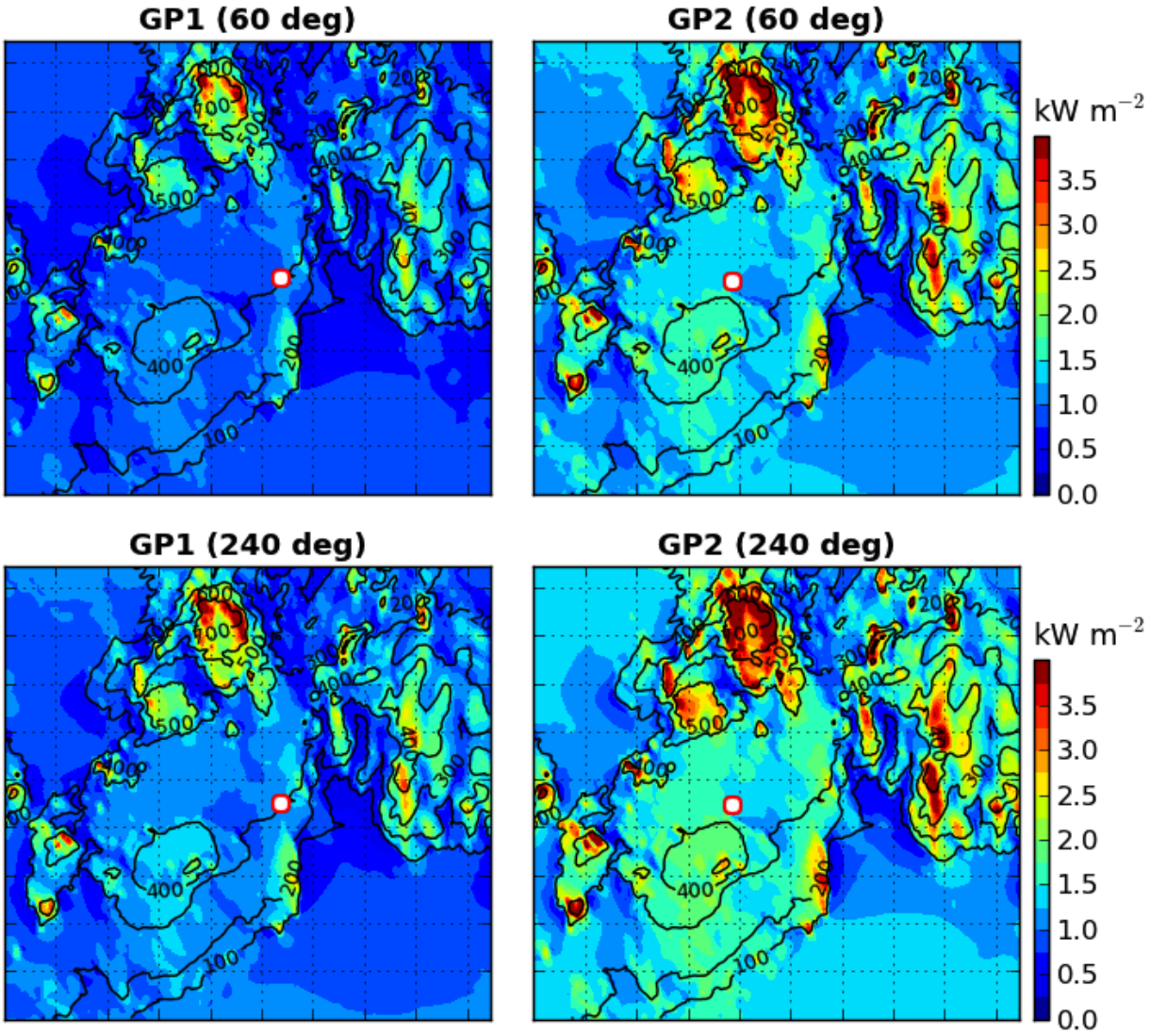


*Figure 21. Annual mean wind power density at 55 mAGL within the Hellisheiði region, for two different wind directions, and for each of the two WRF model grid points (GPs).*

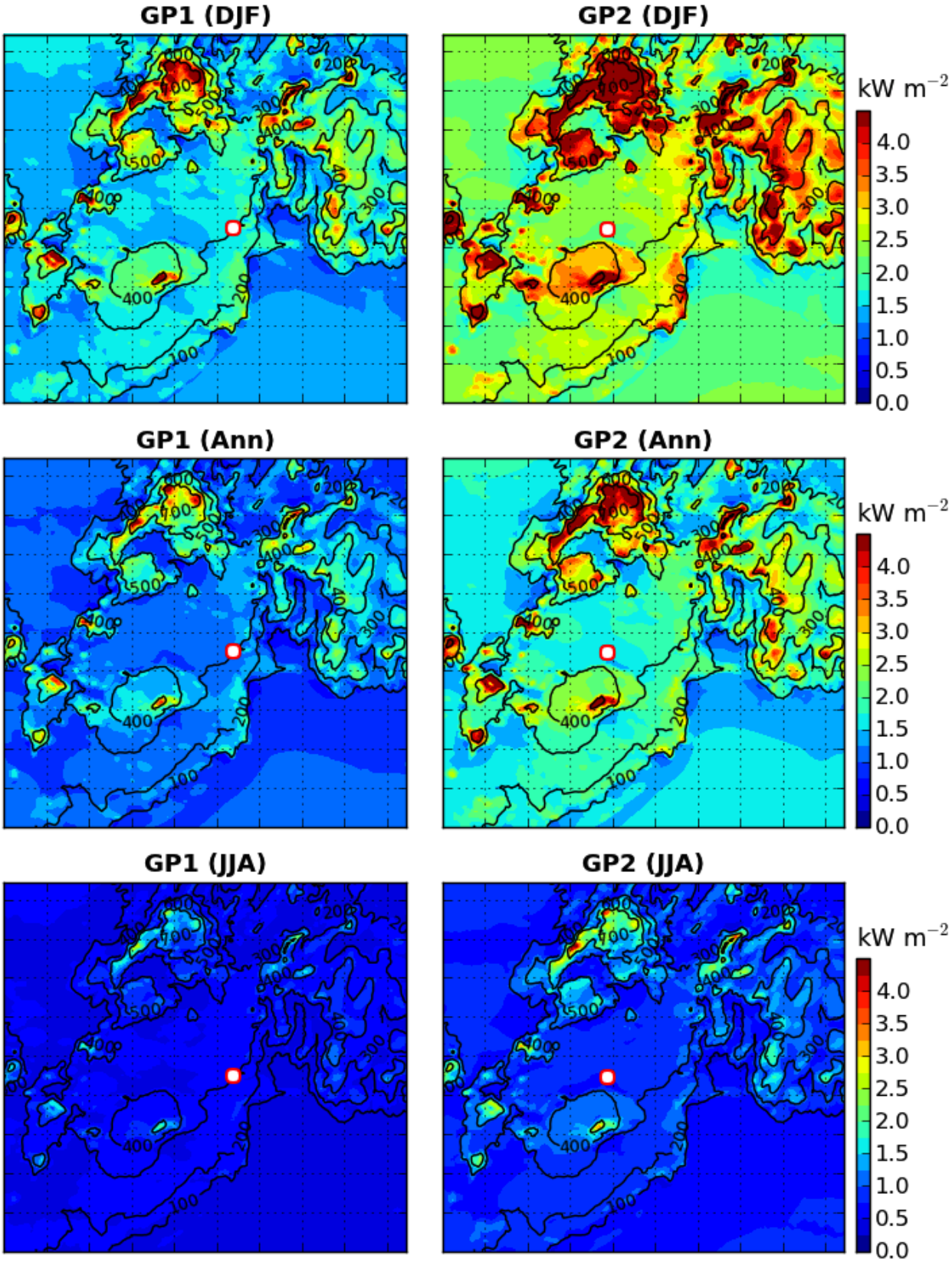


*Figure 22. Annual, winter (DJF), and summer (JJA) averages of wind power density at 55 mAGL within the Hellisheiði region, for each of the two WRF model grid points (GPs).*

## A.6 Höfn

The domain for the WAsP analysis covers the Hornafjörður area along the southeast coast, with the residential areas of Höfn and Nesjahverfi in the eastern half. The first WRF model grid point (GP1) is located at 15.36731°W, and 64.23226°N. Terrain elevation is below 100 mASL throughout most of the domain, without significant sheltering or speed-up effects. Towards the northeast corner of the domain, the terrain rises rapidly, associated with local speed-up effects of 3 – 4 kW $m^{-2}$ in winter. Compared with these terrain-related effects, the speed-up towards the coast is minor. Outside of urban areas, there are only a few individual buildings within the domain. The surface type of the land area is homogeneous grassland, without any tall vegetation. The area is accessible via Route 1.

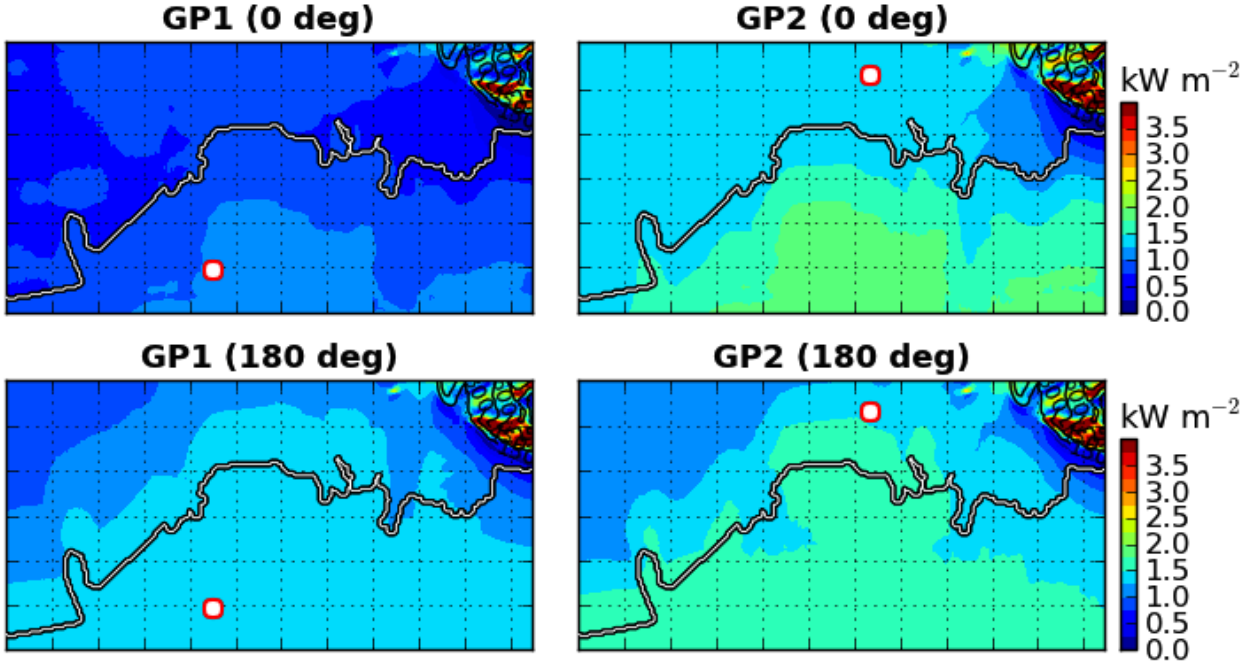


*Figure 23. Annual mean wind power density at 55 mAGL within the Höfn region, for two different wind directions, and for each of the two WRF model grid points (GPs).*

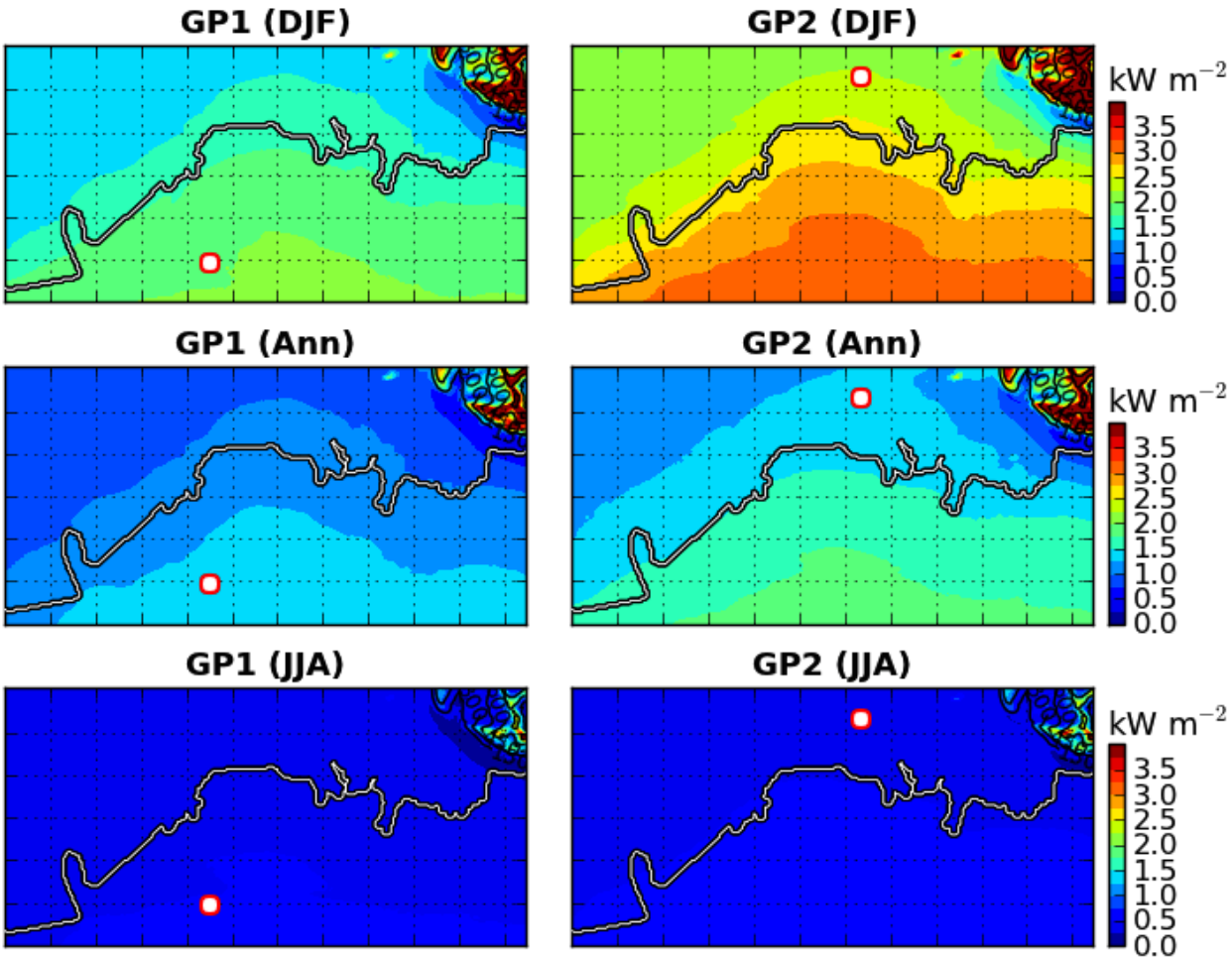


*Figure 24. Annual, winter (DJF), and summer (JJA) averages of wind power density at 55 mAGL within the Höfn region, for each of the two WRF model grid points (GPs).*

## A.7 Landeyjar

The domain for the WAsP analysis covers the Vestmannaeyjar archipelago south of the main island, and a section of the main coastline towards the west of Eyjafjallajökull volcano. The first WRF model grid point (GP1) is located at 20.13433°W, and 63.54062°N. Excluding the slopes of the volcano, terrain elevation is below 60 mASL on the mainland, without significant sheltering or speed-up effects. The hills on the smaller islands are associated with local speed-up effects of around 2 kW $m^{-2}$ in winter, but are unlikely to be available for the installation of wind turbines. Within the coastal zone on the mainland, the speed-up towards the ocean is about 1 kW $m^{-2}$ in winter. There are a few individual buildings throughout the domain, but no concentrated urban area. The surface type of the land area is characterised by farmland, without significant groups of tall vegetation. The area is accessible by a network of roads branching off Route 1.

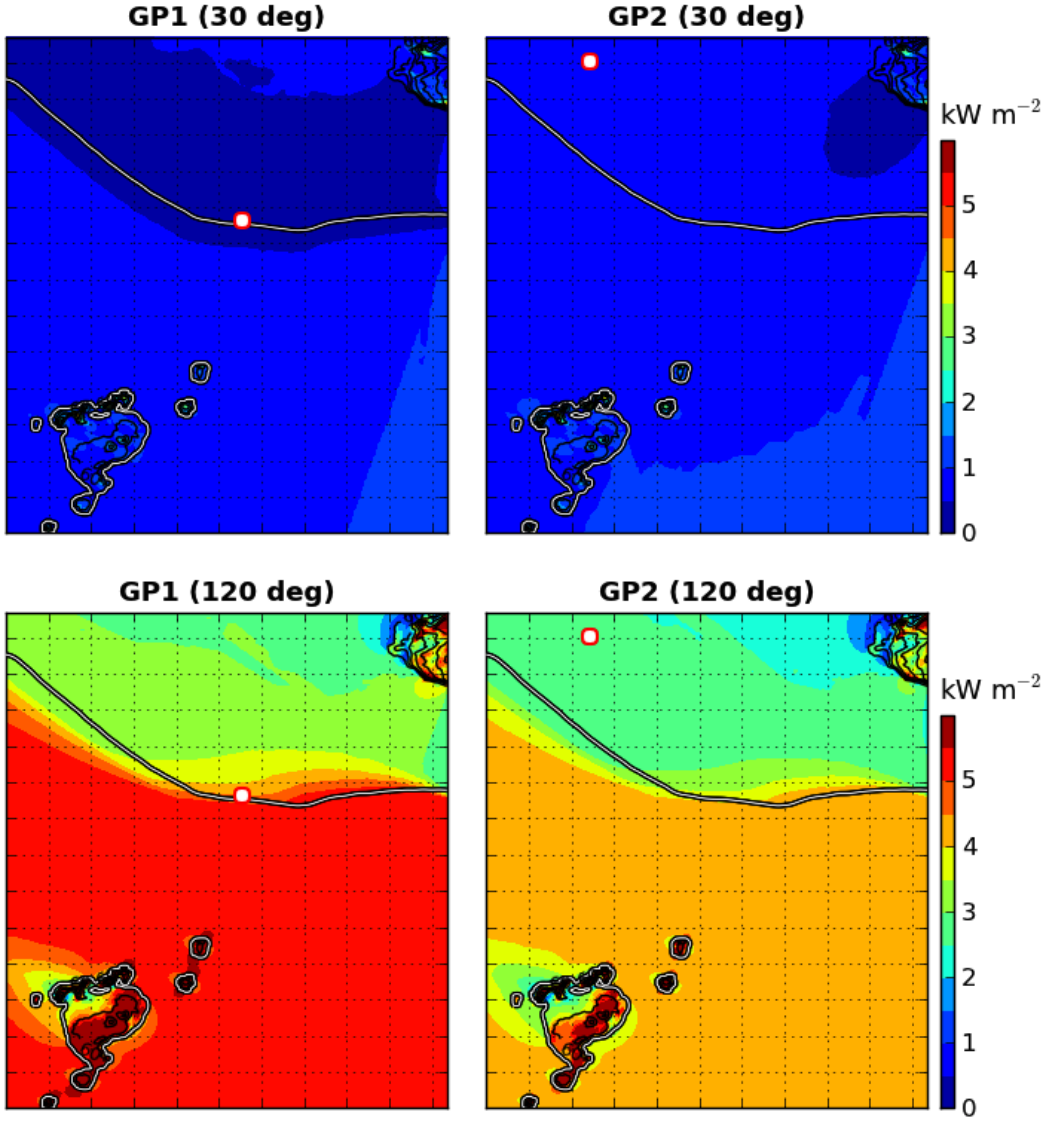


*Figure 25. Annual mean wind power density at 55 mAGL within the Landeyjar region, for two different wind directions, and for each of the two WRF model grid points (GPs).*

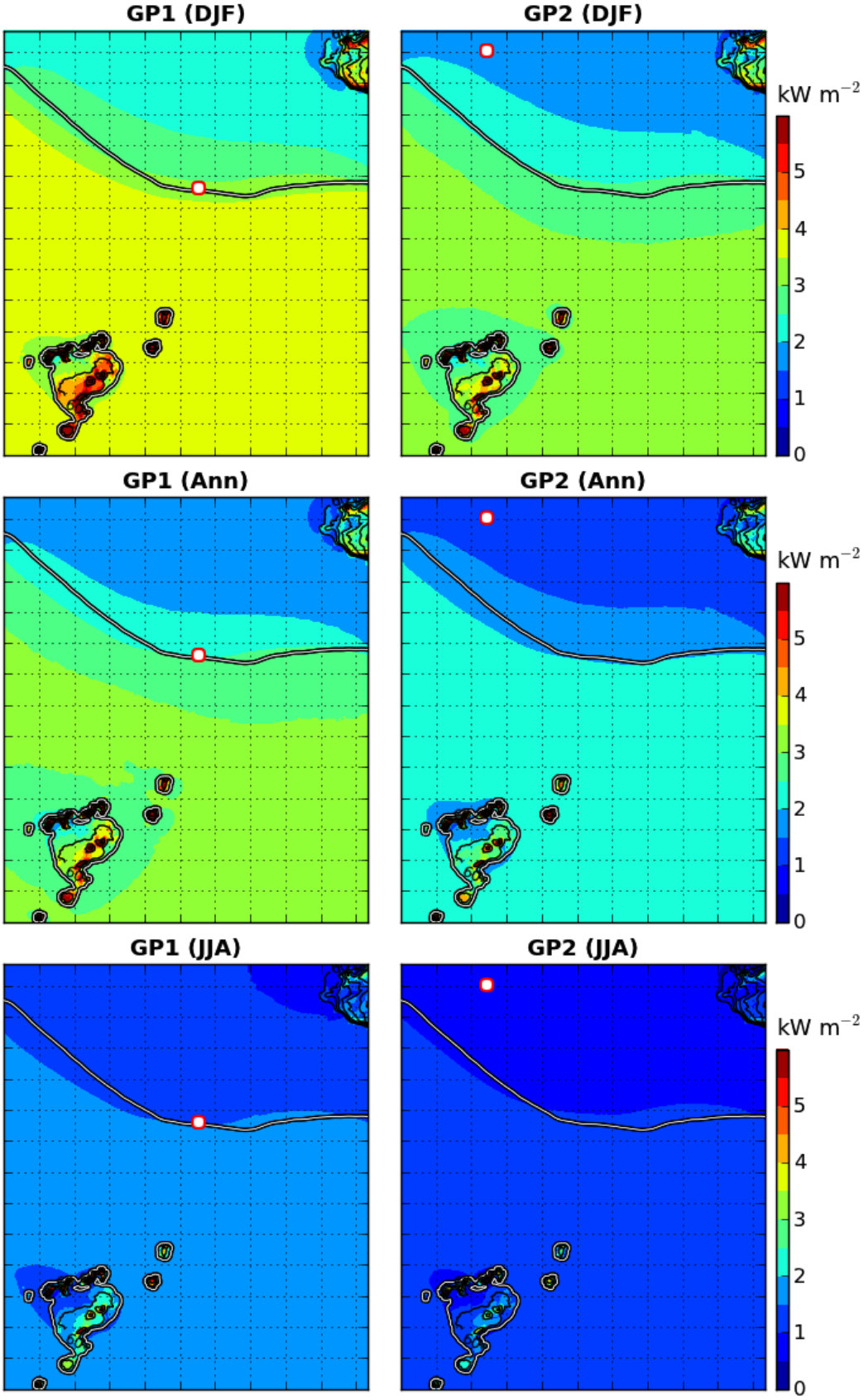


*Figure 26. Annual, winter (DJF), and summer (JJA) averages of wind power density at 55 mAGL within the Landeyjar region, for each of the two WRF model grid points (GPs).*

## A.8 Langanes

The domain for the WAsP analysis covers Lónafjörður, and the southwest part of Langanes peninsula in northeast Iceland. The first WRF model grid point (GP1) is located at 15.27662°W, and 66.24009°N. Away from the coast, towards the south and east, the terrain rises to about 200 mASL. The elevated terrain is associated with both local sheltering and speed-up effects of around 500 W $m^{-2}$ in winter, which is similar to the speed-up towards the coast. The village and small airport of Þórshöfn are situated in the centre of the domain. Outside this urban area, there are only a few individual buildings. The surface type of the land area is characterised by rocks and grass, without any tall vegetation. The area is accessible via Routes 85 and 869.

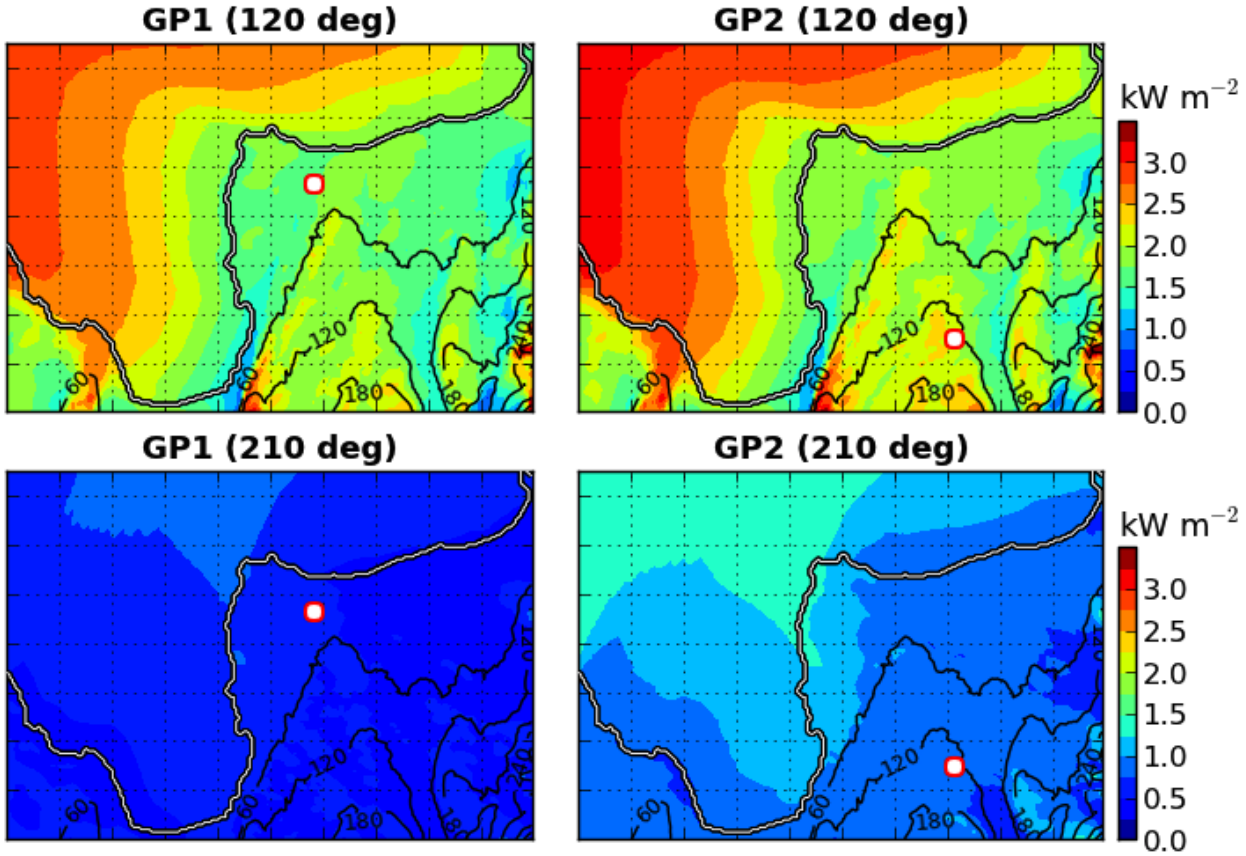


*Figure 27. Annual mean wind power density at 55 mAGL within the Langanes region, for two different wind directions, and for each of the two WRF model grid points (GPs).*

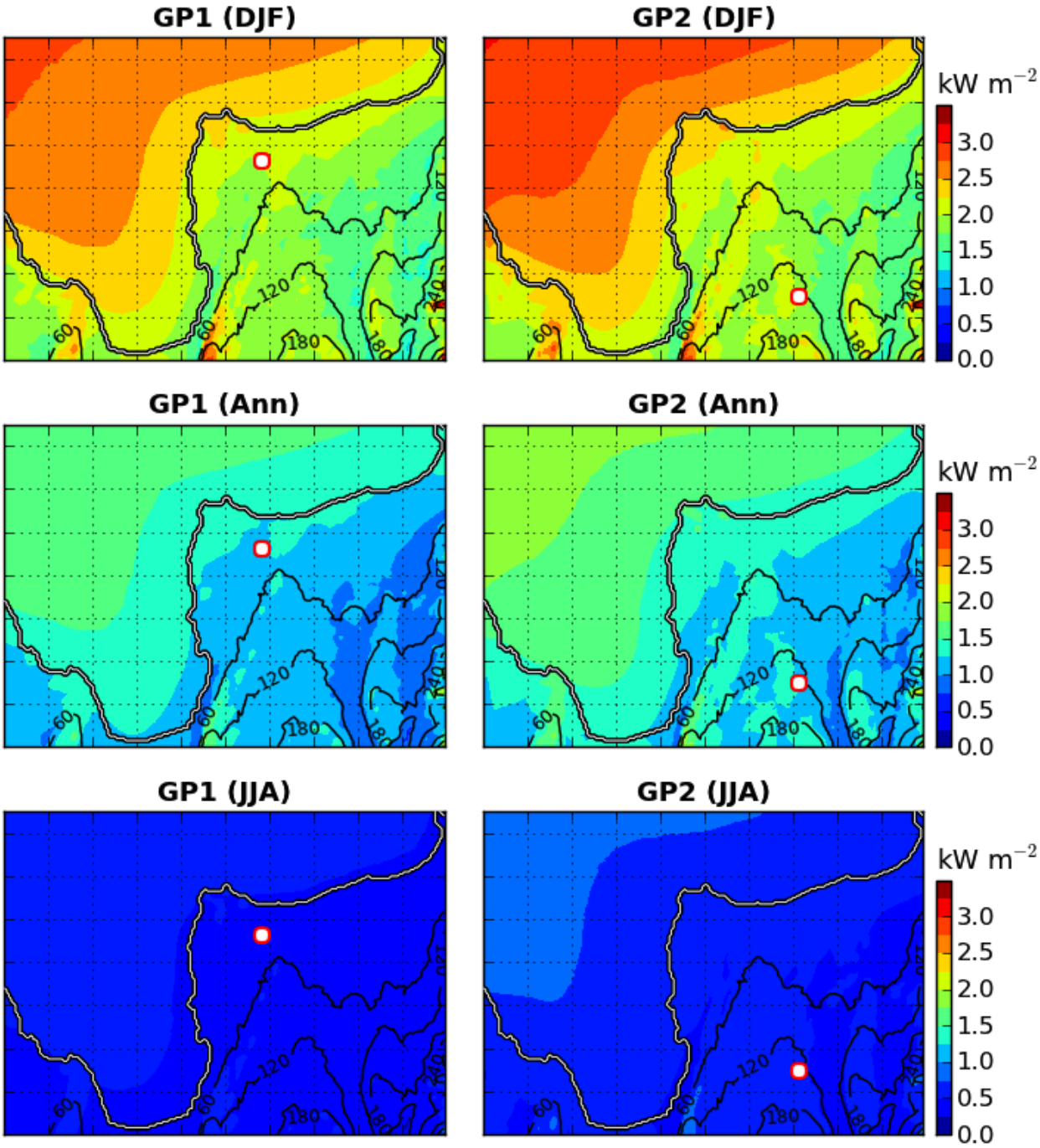


*Figure 28. Annual, winter (DJF), and summer (JJA) averages of wind power density at 55 mAGL within the Langanes region, for each of the two WRF model grid points (GPs).*

## A.9 Meðallandssveit

The domain for the WAsP analysis covers a section of the south coast east of Katla volcano, and south of the village Kirkjubæjarklaustur. The first WRF model grid point (GP1) is located at 18.13947°W, and 63.56192°N. Terrain elevation is below 40 mASL throughout most of the domain, without significant sheltering or speed-up effects. Within the coastal zone, the speed-up towards the ocean is around 1.5 kW $m^{-2}$ in winter. There are a few individual buildings throughout the domain, but no concentrated urban area. The surface type of the land area away from the coast is characterised by farmland, without significant groups of tall vegetation. A sandy beach extends for about 5 km from the coast. The area is accessible via Route 204 branching off Route 1.

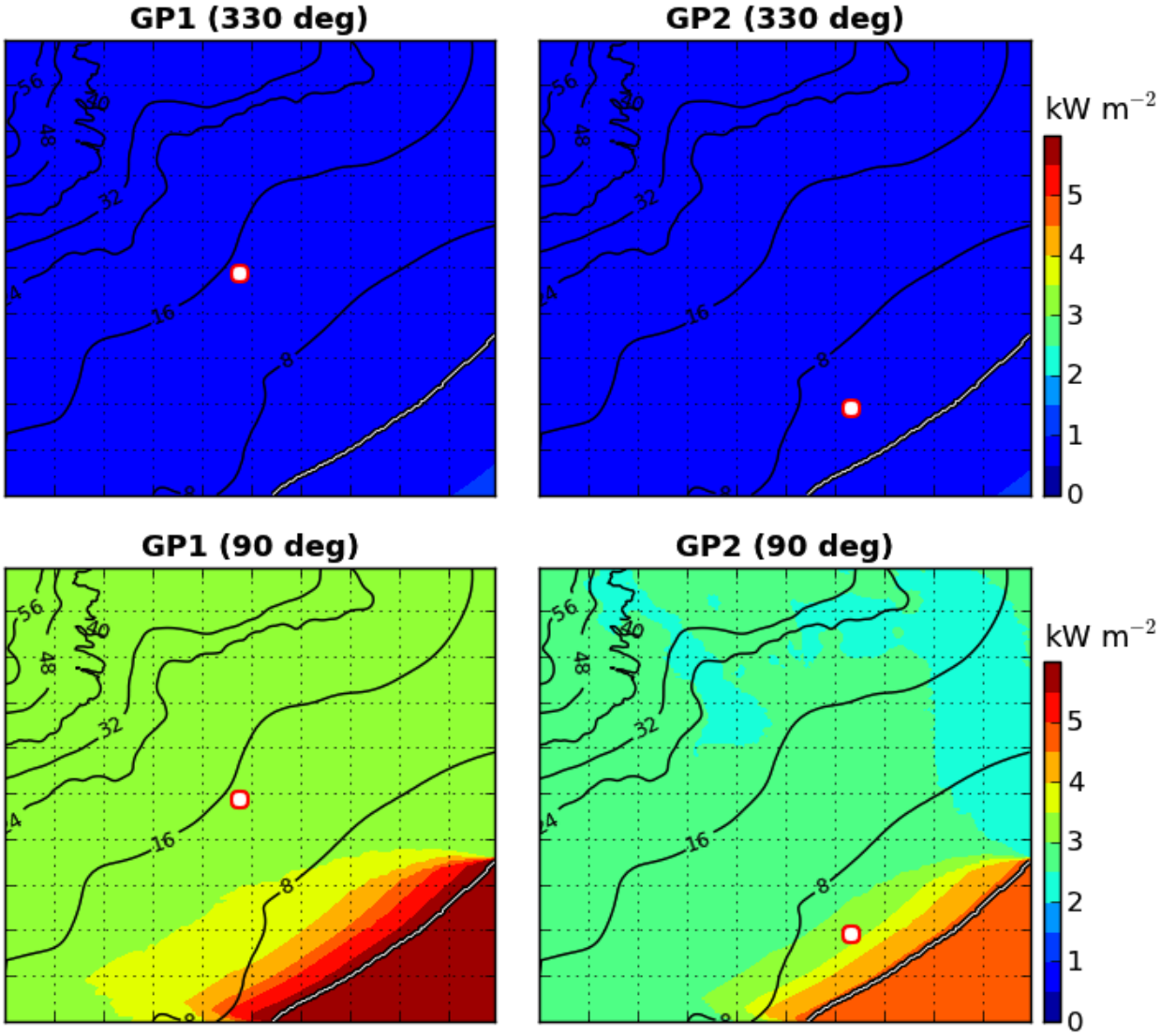


*Figure 29. Annual mean wind power density at 55 mAGL within the Meðallandssveit region, for two different wind directions, and for each of the two WRF model grid points (GPs).*

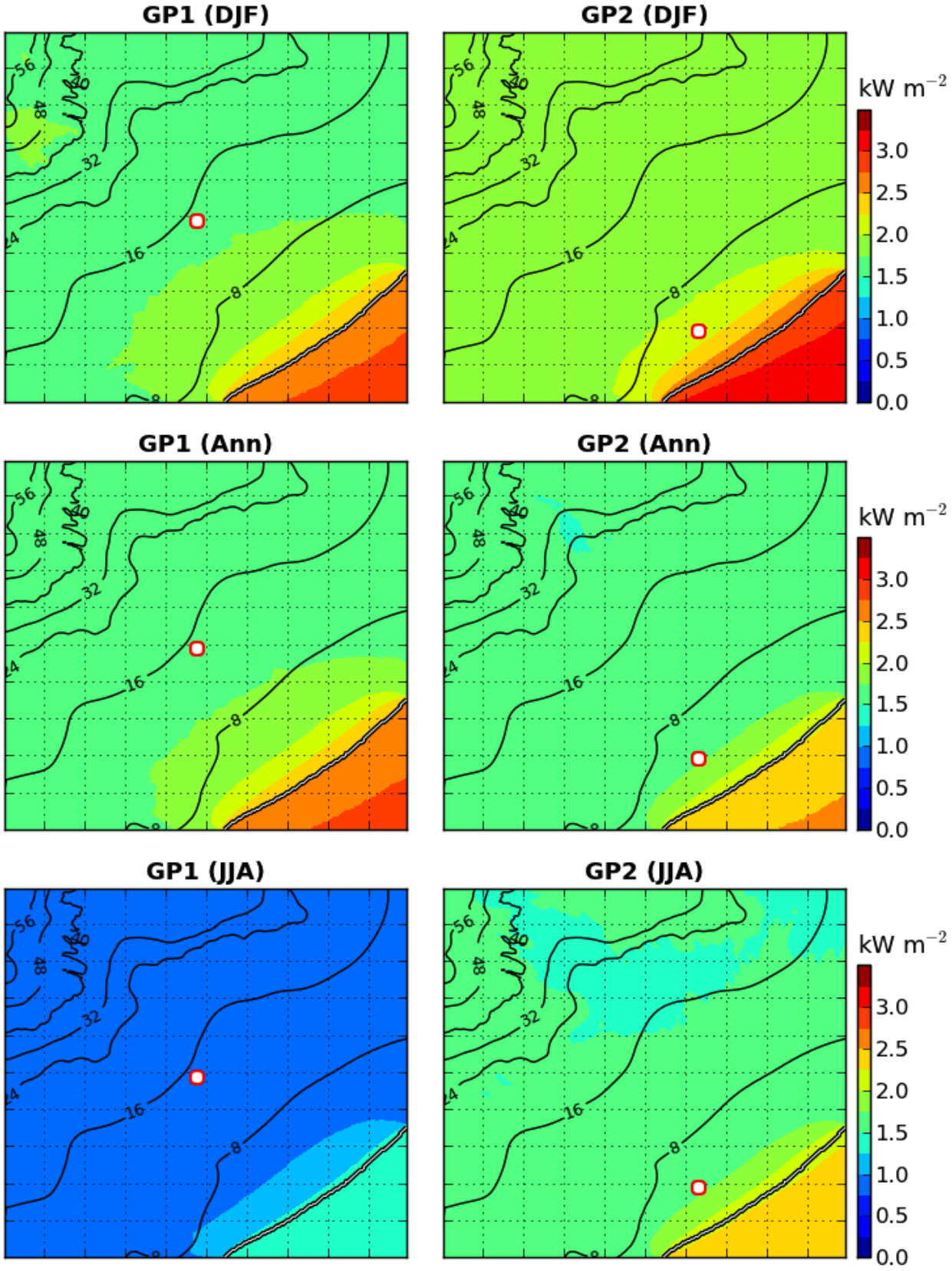


*Figure 30. Annual, winter (DJF), and summer (JJA) averages of wind power density at 55 mAGL within the Meðallandssveit region, for each of the two WRF model grid points (GPs).*

## A.10 Melrakkaslétta

The domain for the WAsP analysis covers the northeastern tip of Melrakkaslétta peninsula in northeast Iceland. The village Raufarhöfn is situated just outside the eastern edge of the domain. The first WRF model grid point (GP1) is located at 16.20084°W, and 66.40083°N. Away from the coast, towards the south, the terrain rises to about 120 mASL. The elevated terrain is associated with both local sheltering and speed-up effects of around 250 W $m^{-2}$ in winter, which is about half the speed-up towards the coast. There are a few individual buildings throughout the domain, but no concentrated urban area. At low elevations in the northeast, there are several small lakes. The surface type of the land area is characterised by rocks and grass, without any tall vegetation. Along the coast, the area is accessible via Route 870.

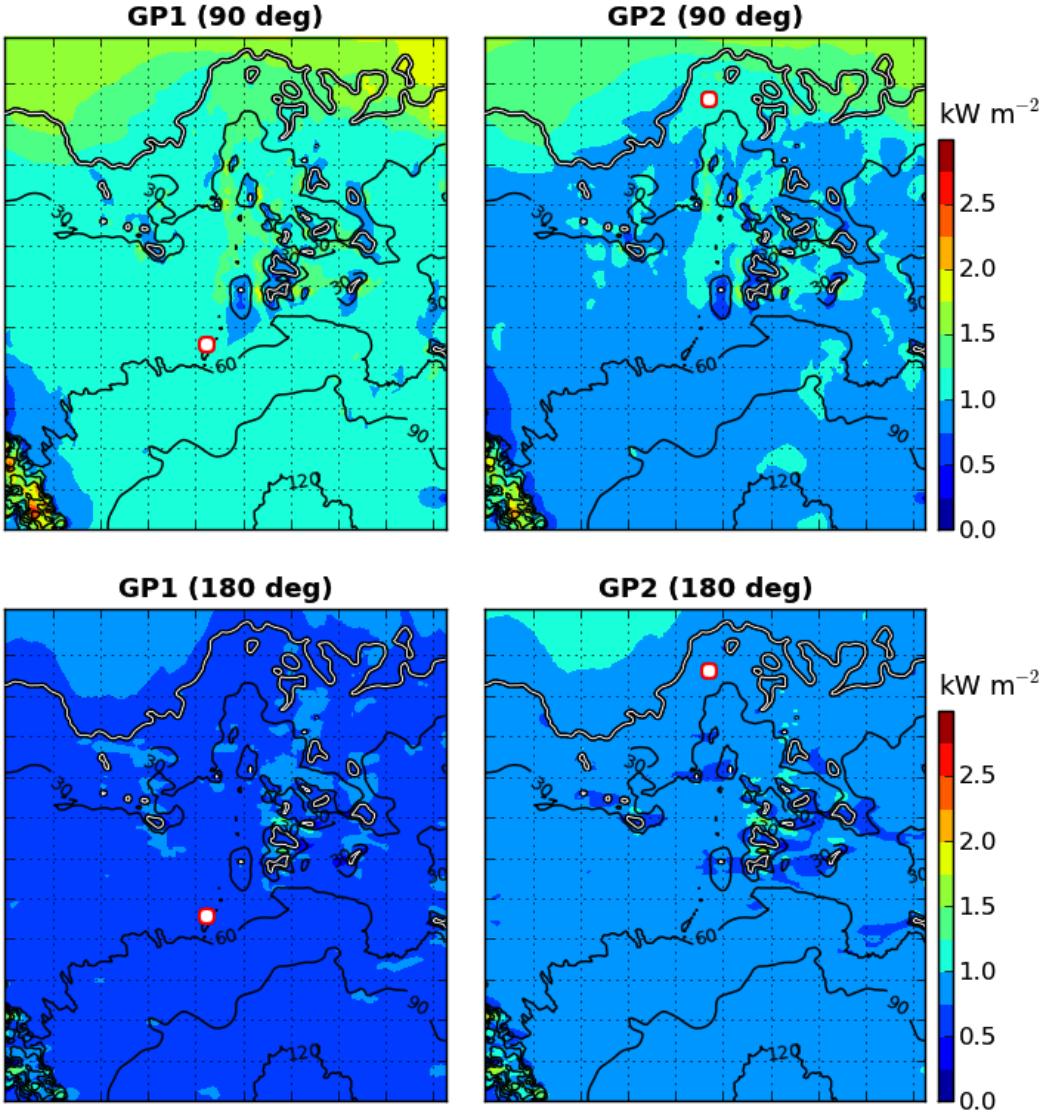


*Figure 31. Annual mean wind power density at 55 mAGL within the Melrakkaslétta region, for two different wind directions, and for each of the two WRF model grid points (GPs).*

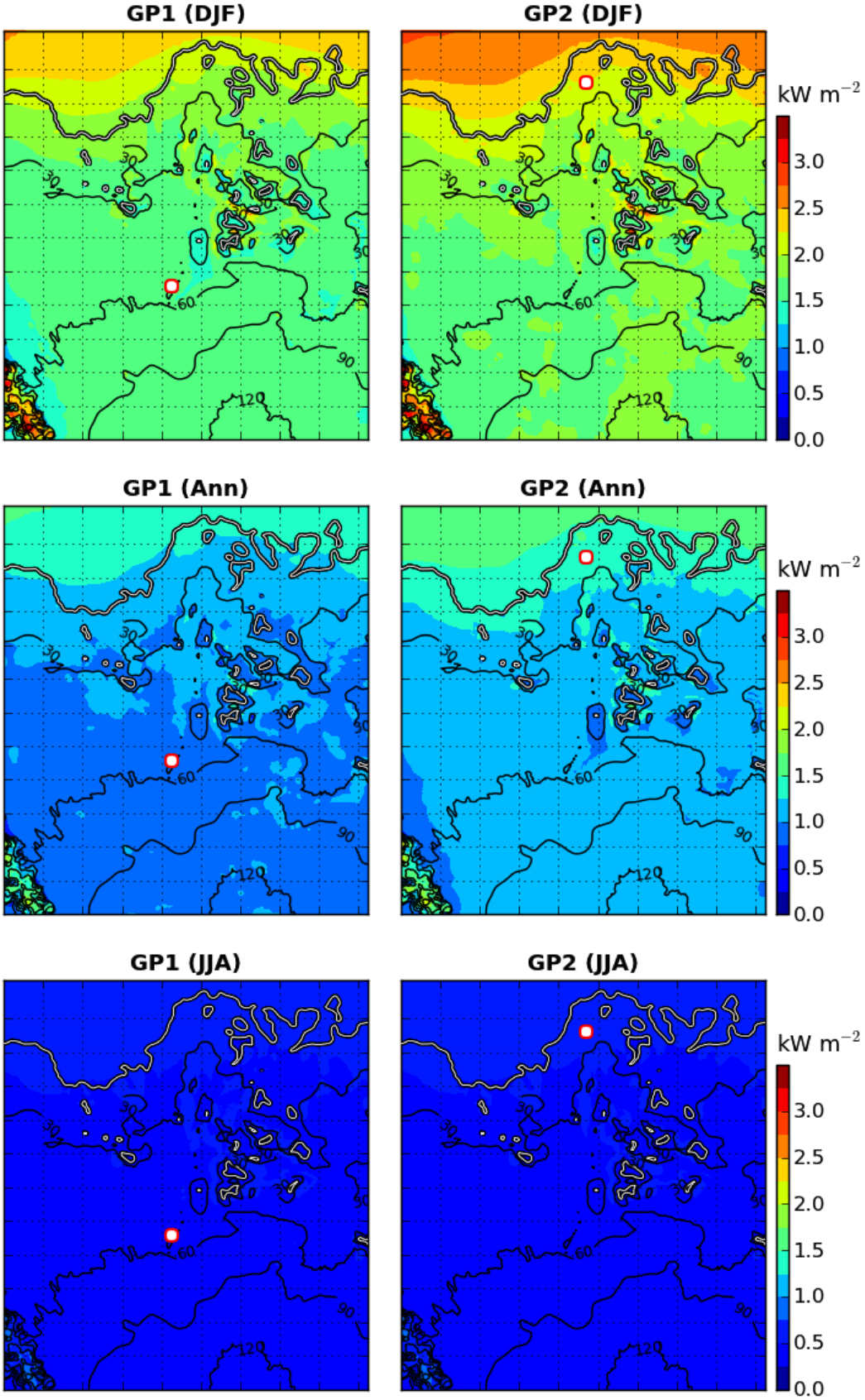


*Figure 32. Annual, winter (DJF), and summer (JJA) averages of wind power density at 55 mAGL within the Melrakkaslétta region, for each of the two WRF model grid points (GPs).*

## A.11 Mýrar

The domain for the WAsP analysis covers the southern part of the land area north of Borgarfjörður in western Iceland. The town Borgarnes is situated just outside the eastern edge of the domain. The first WRF model grid point (GP1) is located at 22.10437°W, and 64.48763°N. Terrain elevation is below 20 mASL throughout most of the domain, without significant sheltering or speed-up effects. There is however a gradual increase in average power density towards the coast. There are a few individual buildings throughout the domain, but no concentrated urban area. As the name suggests, the area is characterised by moorland with several small lakes, and without any tall vegetation. It is accessible via Routes 533 and 534.

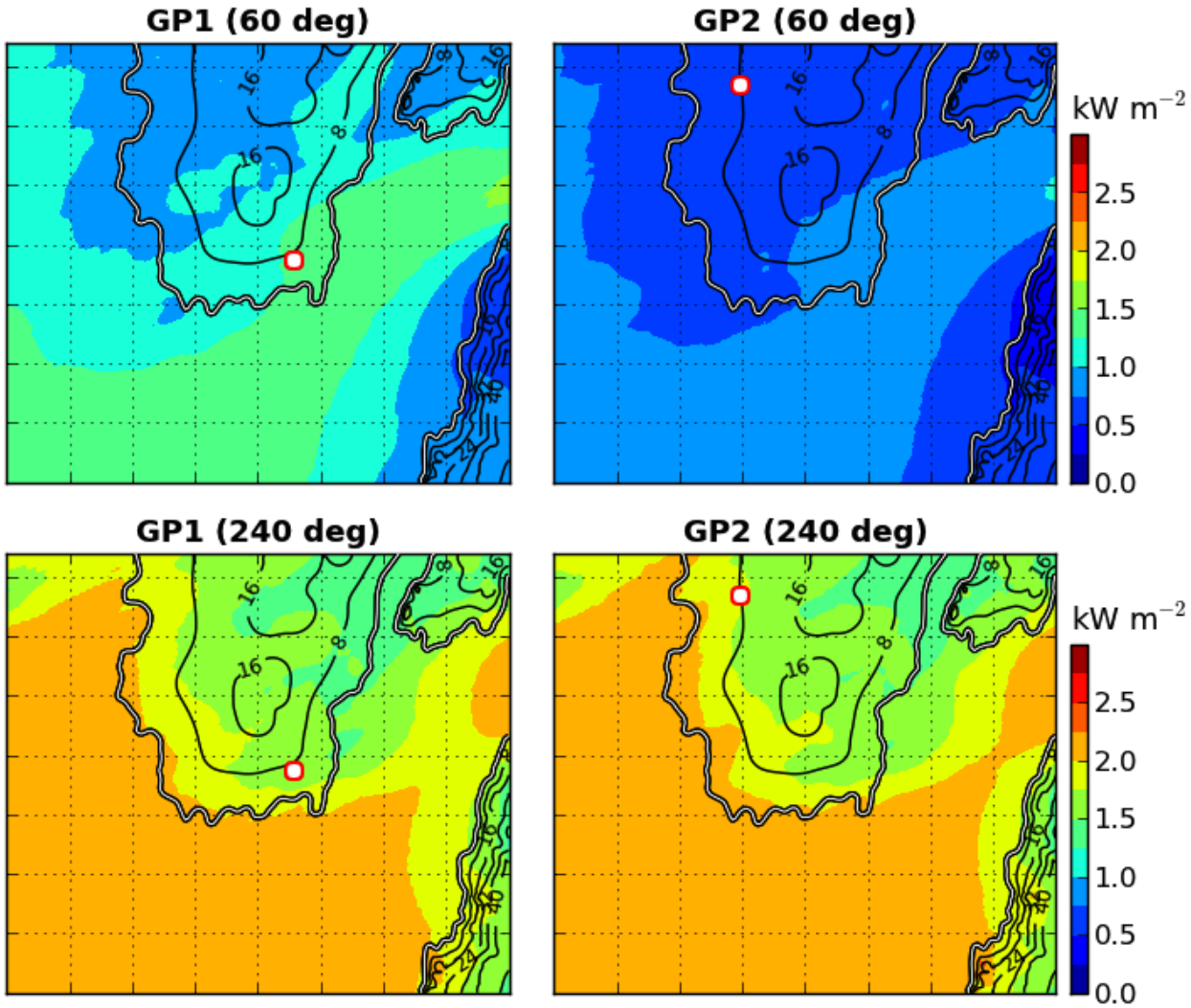


*Figure 33. Annual mean wind power density at 55 mAGL within the Mýrar region, for two different wind directions, and for each of the two WRF model grid points (GPs).*

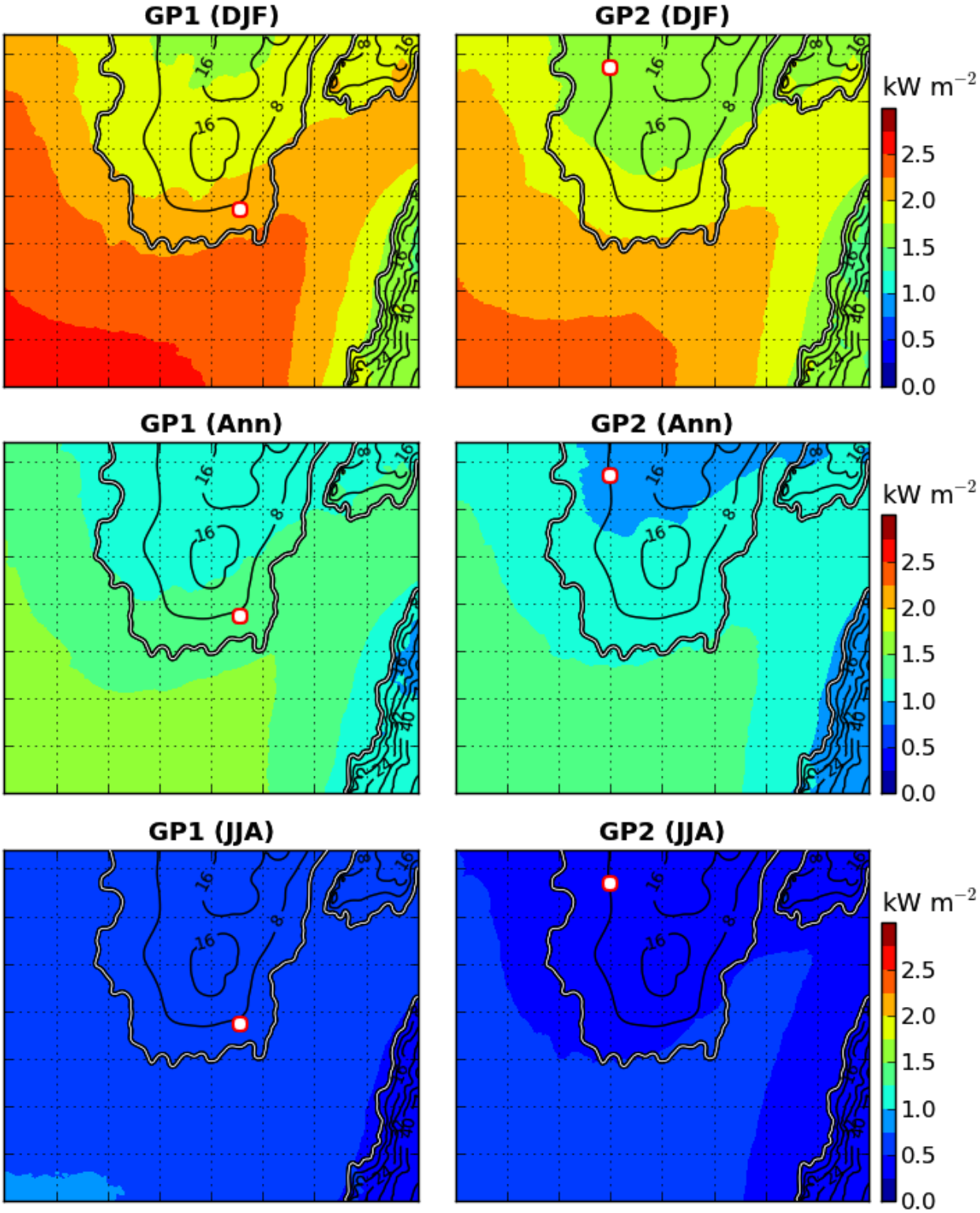


*Figure 34. Annual, winter (DJF), and summer (JJA) averages of wind power density at 55 mAGL within the Mýrar region, for each of the two WRF model grid points (GPs).*

## A.12 Skagi

The domain for the WAsP analysis covers the tip of Skagi peninsula in northern Iceland. The first WRF model grid point (GP1) is located at 20.20412°W, and 66.08346°N. Away from the coast, towards the south, the terrain rises to about 120 mASL. Terrain elevation is below 100 mASL throughout most of the domain. Individual hills are associated with both local sheltering and speed-up effects of around 2 kW $m^{-2}$ in winter, which is similar to the speed-up towards the coast. There are several small lakes throughout the domain, and a few individual buildings along the coast, but no concentrated urban area. The surface type of the land area is characterised by rocks and grass, without any tall vegetation. Along the coast, the area is accessible via Route 740.

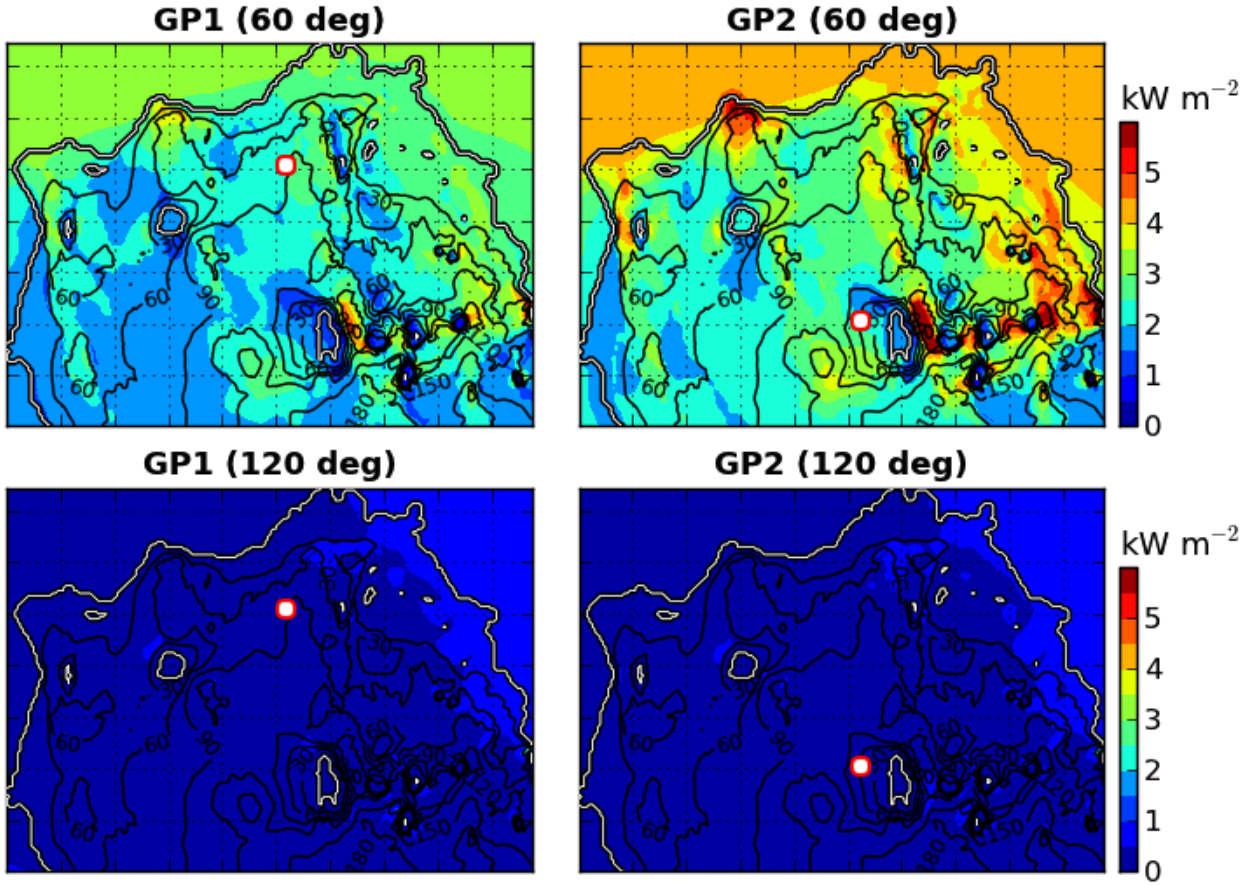


*Figure 35. Annual mean wind power density at 55 mAGL within the Skagi region, for two different wind directions, and for each of the two WRF model grid points (GPs).*

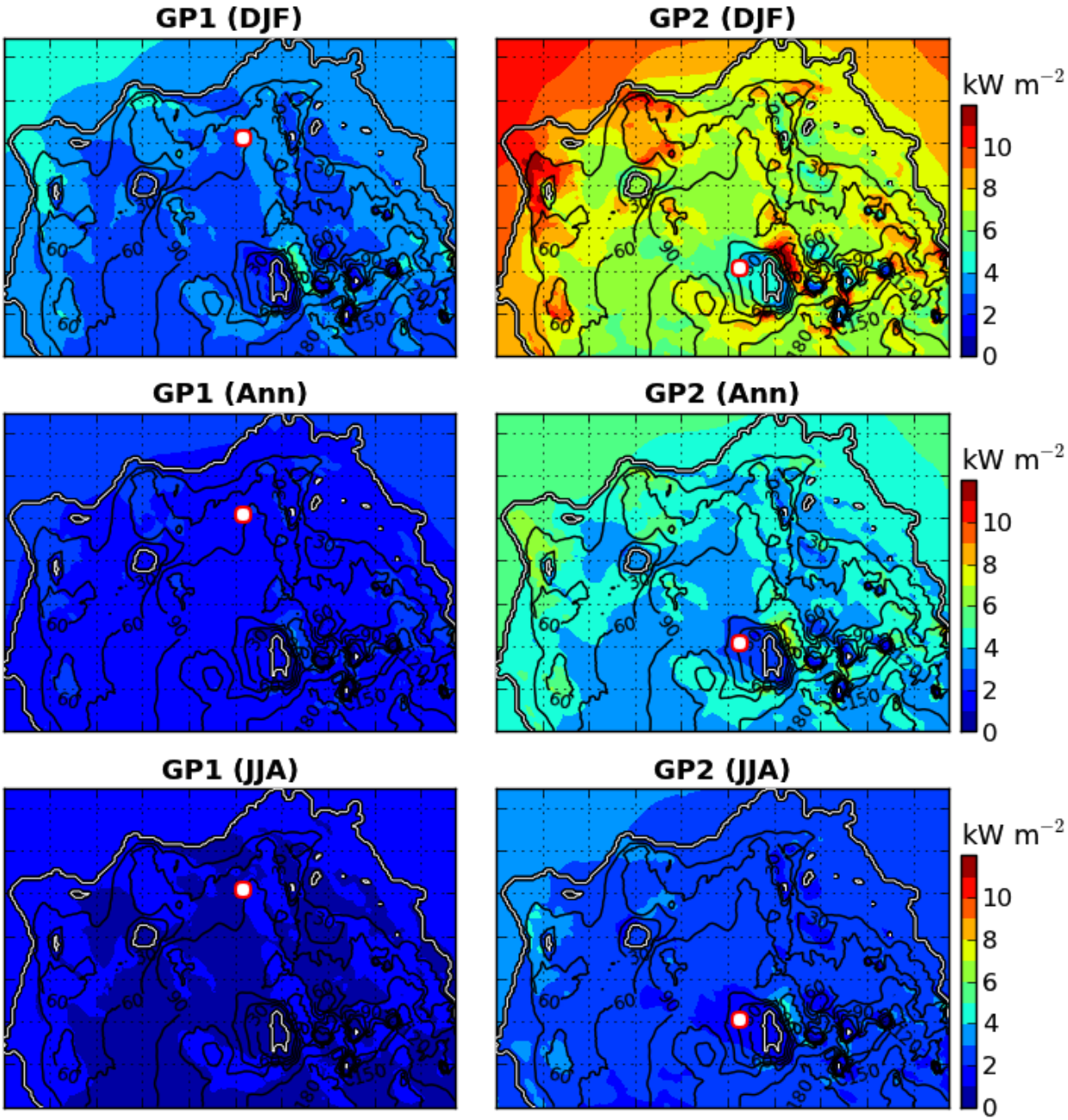


*Figure 36. Annual, winter (DJF), and summer (JJA) averages of wind power density at 55 mAGL within the Skagi region, for each of the two WRF model grid points (GPs).*

## A.13 Snæfellsnes

The domain for the WAsP analysis covers a section of the southern coast of Snæfellsnes peninsula in western Iceland. The first WRF model grid point (GP1) is located at 22.90054°W, and 64.79463°N. Terrain elevation is below 150 mASL throughout most of the domain, without significant sheltering or speed-up effects. Towards the north, the terrain rises rapidly, associated with local speed-up effects of 4 – 7 kW $m^{-2}$ in winter. Compared with these terrain-related effects, the speed-up towards the coast is negligible. The surface type of the land area is characterised by rocks and grass, without any tall vegetation. There are a few individual buildings throughout the domain, but no concentrated urban area. The area is accessible via Route 54.

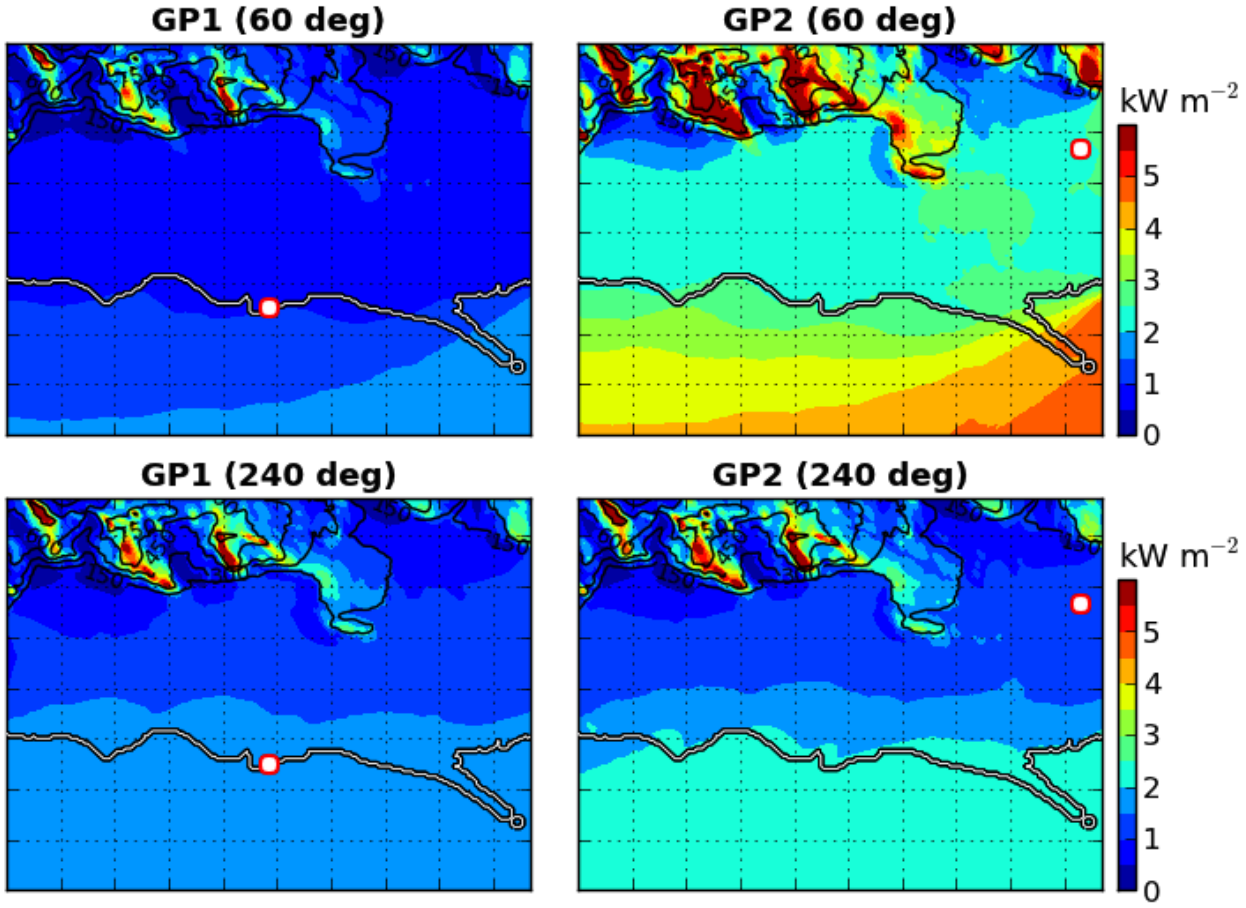


*Figure 37. Annual mean wind power density at 55 mAGL within the Snæfellsnes region, for two different wind directions, and for each of the two WRF model grid points (GPs).*

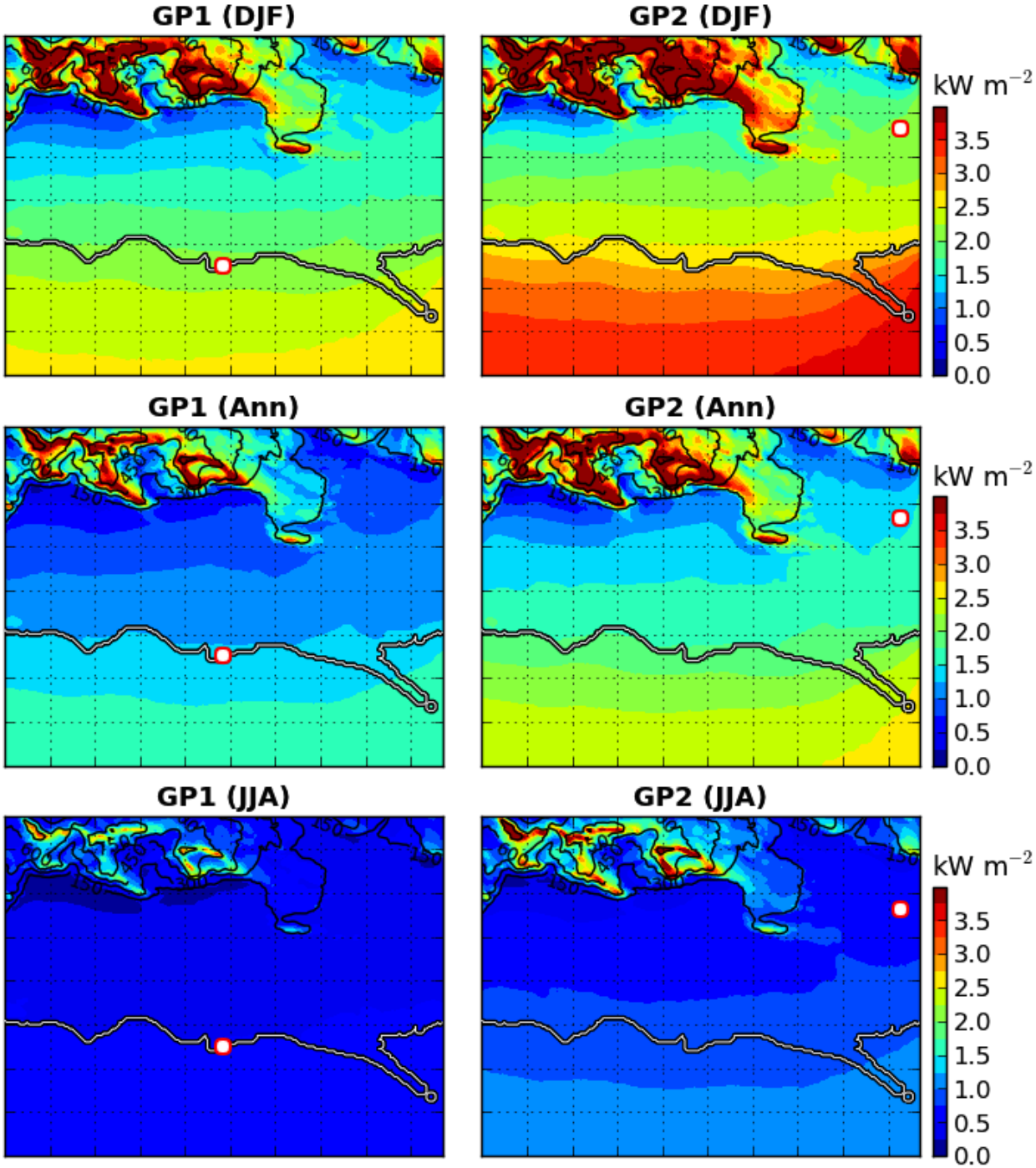


*Figure 38. Annual, winter (DJF), and summer (JJA) averages of wind power density at 55 mAGL within the Snæfellsnes region, for each of the two WRF model grid points (GPs).*

## A.14 Þorlákshöfn

The domain for the WAsP analysis covers a section of the southern coast of Reykjanes peninsula, with the town Þorlákshöfn in the southeastern part. The first WRF model grid point (GP1) is located at 21.48786°W, and 63.85021°N. Terrain elevation is below 100 mASL within the coastal zone, without significant sheltering or speed-up effects. Towards the north, the terrain rises rapidly, associated with local speed-up effects of around 500 W $m^{-2}$ in winter, which is similar to the speed-up towards the coast. The surface type of the land area is characterised by rocks and grass, without any tall vegetation. Outside the urban area, there are only a few individual buildings within the domain. The area is accessible via Route 380 in the north, and Route 427 along the coast.

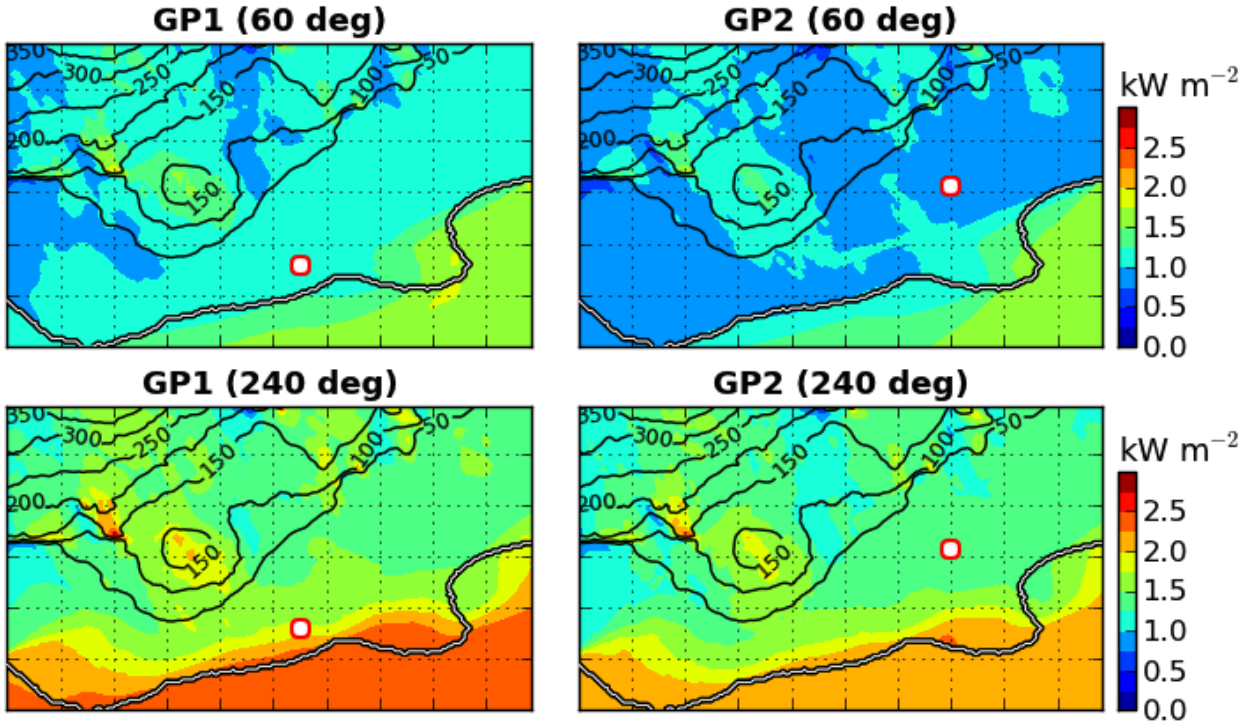


*Figure 39. Annual mean wind power density at 55 mAGL within the Þorlákshöfn region, for two different wind directions, and for each of the two WRF model grid points (GPs).*

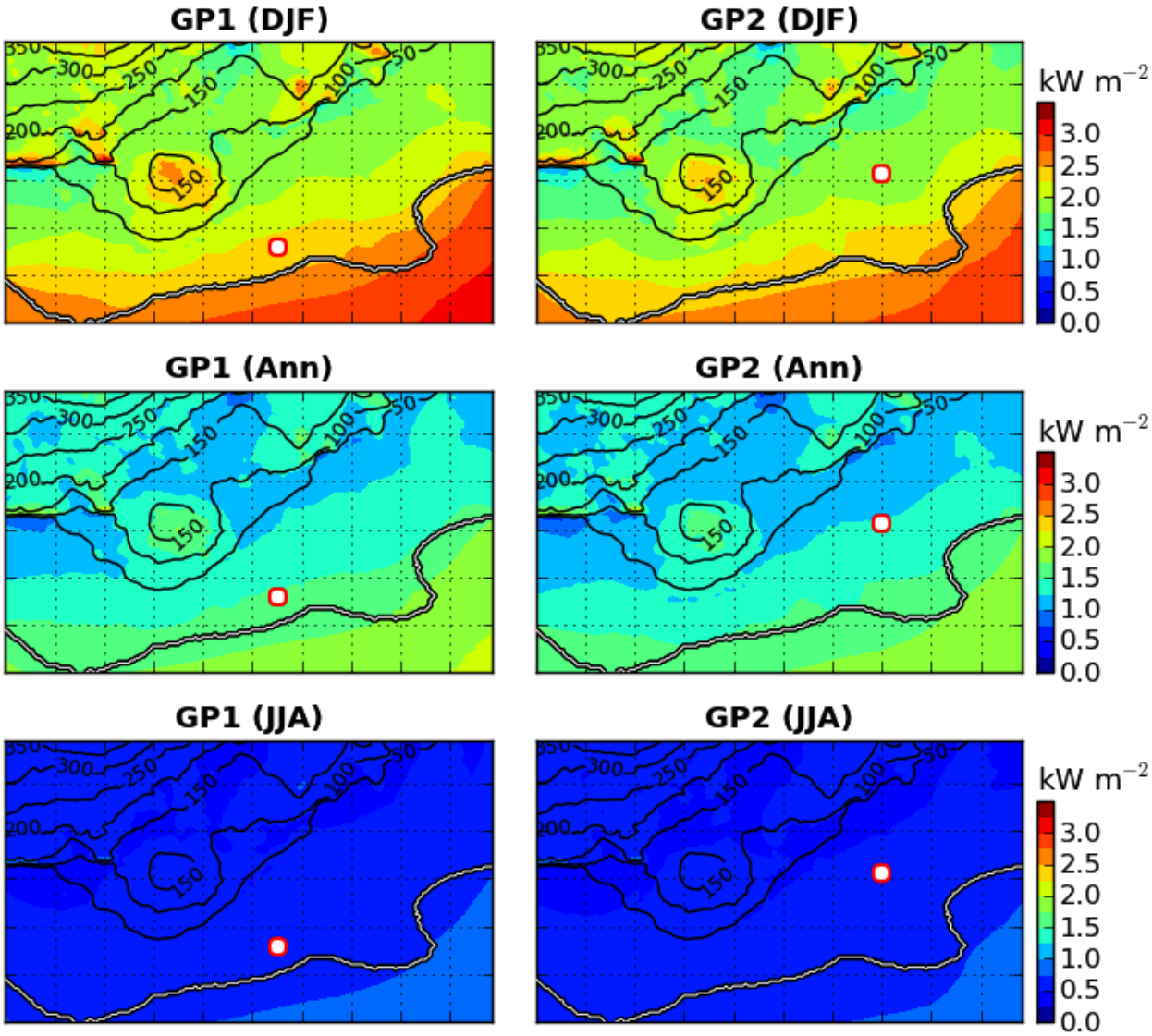


*Figure 40. Annual, winter (DJF), and summer (JJA) averages of wind power density at 55 mAGL within the Þorlákshöfn region, for each of the two WRF model grid points (GPs).*

# References


Andersson, E. and Thépaut, J. N. (2008). ECMWF's 4D-Var data assimilation system – the genesis and ten years in operations. *ECMWF Newsletter*, 115:8–12.

Beckmann, P. (1964). Rayleigh distribution and its generalizations. *Radio Science Journal of Research NBS/USNC-URSI*, 68D(9):927–932.

Betz, A. (1966). *Introduction to the Theory of Flow Machines*. Pergamon Press, Oxford, UK, 281 pp.

Björnsson, H., Guðmundsson, S., and Pálsson, F. (2005). Glacier winds on Vatnajökull ice cap, Iceland, and their relation to temperatures of its lowland environs. *Annals Glaciol.*, 42:291–296.

Courtier, P. (1997). Dual formulation of four-dimensional variational assimilation. *Quart. J. Roy. Meteor. Soc.*, 123:2449–2461.

Einarsson, M. Á. (1976). *Veðurfar á Íslandi*. Iðunn, Reykjavik, Iceland.

Einarsson, M. Á. (1984). Chapter 7: Climate of iceland. In van Loon, H., editor, *Climates of the Oceans*, volume 15 of *World Survey of Climatology*, pages 673–697, Amsterdam, Netherlands. Elsevier.

Hanna, E., Jónsson, T., and Box, J. E. (2004). An analysis of Icelandic climate since the Nineteenth Century. *Int. J. Climatol.*, 24:1193–1210.

Hennessey, J. P. (1977). Some aspects of wind power statistics. *J. Appl. Meteorol.*, 16(2):119–128.

Morgan, E. C., Lackner, M., Vogel, R. M., and Baise, L. G. (2011). Probability distributions for offshore wind speeds. *Energy Convers. Man.*, 52:15–26.

Nawri, N., Björnsson, H., Jónasson, K., and Petersen, G. N. (2012a). Empirical terrain models for surface wind and air temperature over Iceland. Report VÍ 2012-009, Icelandic Meteorological Office, Reykjavik, Iceland.

Nawri, N., Björnsson, H., Jónasson, K., and Petersen, G. N. (2012b). Evaluation of WRF mesoscale model simulations of surface wind over Iceland. Report VÍ 2012-010, Icelandic Meteorological Office, Reykjavik, Iceland.

Nawri, N., Björnsson, H., Jónasson, K., and Petersen, G. N. (2012c). Statistical correction of WRF mesoscale model simulations of surface wind over Iceland based on station data. Report VÍ 2012-011, Icelandic Meteorological Office, Reykjavik, Iceland.

Nawri, N., Björnsson, H., Jónasson, K., and Petersen, G. N. (2012d). Surface wind and air temperature over Iceland based on station records and ECMWF Operational Analyses. Report VÍ 2012-008, Icelandic Meteorological Office, Reykjavik, Iceland.

Reistad, M., Breivik, O., Haakenstad, H., Aarnes, O. J., Furevik, B. R., and Bidlot, J.-R. (2011). A high-resolution hindcast of wind and waves for the North Sea, the Norwegian Sea, and the Barents Sea. *J. Geophys. Res.*, 116:C05019.

Rögnvaldsson, Ó., Ágústsson, H., Einarsson, E. M., Ólafsson, H., Björnsson, H., and Sveinsson, Ó. G. B. (2007). Stöðuskýrsla vegna fyrsta árs RÁV verkefnisins. Technical report, Reiknistofa í veðurfræði, Reykjavik, Iceland.

Rögnvaldsson, Ó., Ágústsson, H., and Ólafsson, H. (2011). Aflræn niðurkvörðun veðurs innan LOKS verkefnisins. Technical report, Reiknistofa í veðurfræði, Reykjavik, Iceland.

Seguro, J. V. and Lambert, T. W. (2000). Modern estimation of the parameters of the Weibull wind speed distribution for wind energy analysis. *J. Wind Eng. Ind. Aerodyn.*, 85:75–84.

Skamarock, W. C., Klemp, J. B., Dudhia, J., Gill, D. O., Barker, D. M., Duda, M. G., Huang, X.-Y., Wang, W., and Powers, J. G. (2008). A description of the Advanced Research WRF Version 3. NCAR Technical Note NCAR/TN-475+STR, National Center for Atmospheric Research, Boulder, Colorado, USA.

Troen, I. and Petersen, E. L. (1989). *European Wind Atlas*. Risø National Laboratory, Roskilde, Denmark.

Undén, P., Rontu, L., Järvinen, H., et al. (2002). HIRLAM-5 Scientific Documentation. Technical report, Swed. Meteorol. Hydrol. Inst., Norrköping, Sweden.

Uppala, S. M., Kållberg, P. W., Simmons, A. J., et al. (2005). The ERA-40 re-analysis. *Q. J. R. Meteorol. Soc.*, 131:2961–3012.

Wrench, J. W. (1968). Concerning two series for the gamma function. *Math. Comput.*, 22:617–626.